5-9-2014

Advanced Simulation of Wave Reflection: Theory and Applications for Subsurface Imaging

Zhao Zhao
University of Connecticut - Storrs, pete741999@gmail.com

Advanced Simulation of Wave Reflection: Theory and Applications for Subsurface Imaging

Zhao Zhao, PhD

University of Connecticut, 2014

Abstract

This Ph. D. dissertation focuses on the numerical simulation of physical wave propagation in time domain focusing on the wave reflection simulation and their relationship with the inner structure imaging. First of all, this dissertation studies the wave phenomena from a systematic perspective.

Secondly, a series of wave propagation simulation methods are developed. These methods include the finite difference time domain method (FDTD), pseudospectral time domain (PSTD) method and multi-region (MR) method. The advantages and disadvantages of these methods are discussed. The novel efficient recursive integration perfectly matched layer is used as the absorbing boundary condition.

The third, a novel directional Kirchhoff integration is introduced and developed in this dissertation. The novel directional Kirchhoff integration makes the multi-region PSTD method into the directional multi-region PSTD method. A case study is shown to prove that the directional multi-region PSTD method is valid in the full waveform simulation while keeping all the computational efficiencies of the traditional multi-region PSTD method.

The fourth, a novel model subtraction method is introduced in detail. The purpose of the introduction of the model subtraction is to apply the directional multi-region PSTD method in some real reflection model simulation. A case study is illustrated to show that the model subtraction is the ideal method to apply the directional multi-region method into the simulation of a reflection model. Combined with the pre-stack Kirchhoff time migration and stack techniques, the model subtraction method with directional multi-region PSTD algorithm is proved to be able and efficient in the inner structure imaging studies.

The fifth part of this dissertation is the discussion of interferometry technique and its utilization into some geological fracture imaging. Interferometry technique transfers the wave field obtained by a transmission model into a virtual reflection wave field. It is especially useful in subsurface borehole radar survey because it is very easy to target the area of research interests. A 3D case study is provided to show that the interferometry method is efficient in fracture detection. Based on the synthetic model results, the simulation and migration results suggest some vital clue in subsurface fracture detection and characterization.

Advanced Simulation of Wave Reflection: Theory and Applications for Subsurface Imaging

B. S., Beijing University, 1996

M. S., University of Tokyo, 2001

A Dissertation

Submitted in Partial Fulfillment of the

Requirements for the Degree of Doctor of Philosophy

at the

University of Connecticut,

2014

APPROVAL PAGE

Doctor of Philosophy Dissertation

Advanced Simulation of Wave Reflection: Theory and Applications for Subsurface Imaging

Presented by

Zhao Zhao, M. S.

Major Advisor_____

Dr. Lanbo Liu

Associate Advisor_____

Dr. Benjamin E. Barrowes

Associate Advisor_____

Dr. John W. Lane

Associate Advisor_____

Dr. Vernon F. Cormier

University of Connecticut, 2014

Acknowledgement

My dissertation partially came from years of research which has been done since I came to University of Connecticut in fall 2007, and partially came from my working experiences when I came to Ion, Geophysical as a geophysicist. I have worked with a plenty of people whose contributions were assorted to my research so that I can accomplish my dissertation. It is my greatest pleasure to express my gratitude to them in my acknowledgement.

In the first place, I would express my greatest appreciation to my major advisor, Dr. Lanbo Liu. I would like to record my gratitude for his supervision, advice, and guidance throughout this work. Whenever I confronted difficulties during the research, Dr. Lanbo Liu can always provide the pertinent advice and help me to solve the problems in efficiently manner with his rich experience and truly scientist intuition. His strong enthusiasm on both work and life keeps on encouraging me to challenging myself and reach my goal. By working under his guidance, I found a lot of fun on the research of numerical modeling and medical imaging. All the knowledge I learned from him will definitely become one of the most precious treasures throughout my life.

I gratefully acknowledge Dr. Benjamin E. Barrowes for his support, supervision and crucial advice, which made him a backbone of this research and so to this thesis. His involvement with his brilliance has widely broaden my horizon that I benefit from, for now and future.

I especially want to express my gratitude to Dr. Vernon F. Cormier and Dr. John. W. Lane. What they taught in the courses have greatly enlightened me and contributed to my thesis. The knowledge acquired from the course by Dr. V. F. Cormier stimulated my great interests on the reflection model research and the inner structure imaging of a certain physical body. In addition, I strongly appreciate that they spend their precious time to be my Ph.D. degree advisory committee members.

In addition to thanks owe to my Ph.D. degree advisory committee members, I would like to extend my thanks to my colleagues in Ion Geophysical. Sr. David Shope, Sr. Kevin Ragsdale, Sr. Thomas Cheriyan (now Total E&P, USA), Dr. David Brookes, Sr. Darrell Armentrout, Dr. Jianyong Bai, Dr. Yunong Qi, Dr. Qiong Wu, Dr. Tony Feng and a lot of other colleagues. I learned the modern imaging techniques, for example, Kirchhoff migration, reverse time migration and 3D tomography from them to make my dissertation much more resourceful. I want to thank Ion Geophysical here also. Ion Geophysical kindly supports me for paying part of my tuition, and in allowing me to use the computation facilities. Without the help from Ion Geophysical, it is difficult for me to complete this dissertation on time.

Many thanks go to my current and previous co-workers. They were very helpful and informative. I especially thank Kuang He, Zijian Liu, Yongping Chen, Januka Attanayake, Hao Xie, Linhui Zhang and Lei Fu for their first-hand help in my daily work. I will cherish the memory that we studied, worked and had fun together forever.

Table of Contents

List of Abbreviations

1D	One-Dimensional
2D	Two-Dimensional
3D	Three-Dimensional
ABC	Absorbing Boundary Conditions
CPU	Central Processing Unit
CWP	Center for Wave Phenomena
DFN	Discrete Fracture Network
DFT	Discrete Fourier Transform
DKI	Directional Kirchhoff Integration
E	Electric field
EM	Electromagnetic
FDTD	Finite Difference Time Domain
FFT	Fast Fourier Transform
GPR	Ground Penetrating Radar
H	Magnetic field
HPC	High Performance Computing

J Electric current density

KM Kirchhoff Migration

MR Multi-Region

MS Model Subtraction

PML Perfectly Matched Layers

PSTD Pseudospectral Time Domain

PSTM Pre-Stack Time Migration

RI Recursive Integrated

RIPML Recursive Integrated PML

RMSD Root Mean Square Deviation

RTM Reverse-time Migration

SNR Signal Noise Ratio

SU Seismic Unix

T/S Total Scatter

WIVS Wave Interferometry Virtual Source

List of Figures

Figure 3.5 Comparison of time traces of EM wave from single-region PSTD and DKI/MR/PSTD method for all receivers. Left: PSTD results; center: DKI/MR/PSTD results; right: NRMSD differences.

Figure 3.6 Memory usage variation with the calculation time window length according to different variable types in MR/PSTD. Black line：total memory usage; red line ： time variable memory usage; blue line: 3D and 2D memory usage.

Figure 4.1 A 2D slice of the 3D reflection model in X-Z plane at Y=64. Yellow plus: receivers, white plus: source, color bar: dielectric constant scale.

Figure 4.2 Sub-region setup as for the model in Fig. 4.1. A 2D slice of the 3D sub-region setup at Y=64; white rectangular frame: human body sub-region; white crosses: DKI surface; yellow crosses: virtual total scatter surface (T/S).

Figure 4.3 Illustration of the basic idea of the model subtraction method. (a) human body model setup; (b): Free space model setup.

Figure 4.4 Illustration of the traces obtained using the model subtraction method. (a): traces of the human body model setup; (b): traces of the free space model setup, in fact the DKI/TS artifacts; (c): traces after subtracting free space model traces from human body model traces; (d): traces obtained using a single-region method.

Figure 4.5 Illustration of the 2D slice, of the 3D flat incident wave reflection model. The horizontal direction: x, the vertical direction: z.

Figure 4.6 Illustration of the waveform obtained at (375,128,256). Red line: waveform obtained using the block model; green line: waveform obtained using the free space model, in fact the DKI/TS artifacts; blue line: waveform obtained after the model subtraction.

Figure 4.7 Illustration of the 2D slice of determined reflection plane at the plane of Y=128.

Figure 4.8 Illustration of the 3D heterogeneous human body model and the imaged surface after model subtraction at Y=116.

Figure. 4.9 A 2D slice of the 3D human body model in meters. At the plane of y=128 in grid number and 0.512m in meters.

Figure 4.10 Comparisons of the model subtracted trace gather and model subtracted migration gather at the source No. 7. Left: model subtracted trace gather; right: migrated trace gather after Kirchhoff PSTM.

Figure. 4.11 Comparisons of the model subtracted trace gather and model subtracted migration gather at the source No. 40. Left: model subtracted trace gather; right: migrated trace gather after Kirchhoff PSTM.

Figure 4.12 The final model subtracted image. As the source and receiver line is put as Y=1.5m, no image right of this line is available.

Figure 4.13 DKI image obtained using the DKI trace gathers with out model subtraction. No image is available at the region right to the source and receiver line, Y=1.5m.

Figure 5.1 A 3D model used in this thesis. A family of fractures is embedded into a uniform media. B0 – B5 are holes for borehole radar.

Figure 5.2 Illustration of a forward modeling at nt = 400 with the source at the depth of 20m, 200 in the grid number.

Figure 5.3 B4 and B2 one source transmission simulation gathers obtained using the staggered-grid PSTD method. Source at depth = 20m, and all receivers along B4 and B2 are illustrated.

Figure 5.4 Illustration of the natural sources of the simulation. The source signal is Ez, and receiver signal recorded in Ex.

Figure 5.5 The comparison of the simulated single-hole, multi-offset reflection in B4 for the source at depth of 20.1m (left) and the virtual reflection by interferometry with the virtual source at the depth of 20.1m (right).

Figure 6.1 Comparisons of the virtual reflection and the Kirchhoff PSTM results. Left: virtual reflection trace gather; right: migrated trace gather after a Kirchhoff PSTM.

Figure 6.2 B4-B0 stacked migration trace gather, stacked migration trace gather of B4 to show the image between B0 to B4. Left: B4-B0 stacked migration using the WIVS approach; right: B4-B0 stacked migration using the true reflection model.

Figure 6.3 Left: B4-B0 stacked migration trace gather; right: B2-B0 stacked migration trace gather, stacked migration trace gather of B2 to show the image between B0 to B2.

Figure 6.4 2D slice of the original model and merged migrated image comparison. 100 MHz Ricker wavelet in Ez along the B0 source line, and Ex component recorded along B4 and B2 in receivers.

Figure 6.5 Original model and merged migrated image comparison. 100 MHz Ricker wavelet in Ez as sources along B0 line, and Ey data recorded in receivers along B4 and B2 lines.

Figure 6.6 Original model and merged migrated image comparison. 100 MHz Ricker wavelet in Ez as sources along B0 line, and Ez data recorded in receivers along B4 and B4 lines.

Figure 6.7 Original model and Merged migrated image comparison. 100 MHz Ricker wavelet in Ex as sources along B0 line, and Ex data recorded in receivers along B4 and B2 lines.

Figure 6.8 Original model and Merged migrated image comparison. 100 MHz Ricker wavelet in Ex as sources along B0 line, and Ey data recorded in receivers along B4 and B2 lines.

Figure 6.9 Original model and Merged migrated image comparison. 100 MHz Ricker wavelet in Ex as sources along B0 line, and Ez data recorded in receivers along B4 and B2 lines.

Figure 6.10 Original model and Merged migrated image comparison. 100 MHz Ricker wavelet in Ey as sources along B0 line, and Ex data recorded in receivers along B4 and B2 lines.

Figure 6.11 Original model and Merged migrated image comparison. 100 MHz Ricker wavelet in Ey as sources along B0 line, and Ey data recorded in receivers along B4 and B2 lines.

Figure 6.12 Original model and Merged migrated B4-B0-B2 image comparison. 100 MHz Ricker wavelet in Ey as sources along B0 line, and Ez data recorded in receivers along B4 and B2 lines.

Figure 6.13 Sketch of the bedrock well field on the Storrs campus of Univ. of Connecticut to show the relative positions of two wells (SIMA1 and SIMA2) in which bore hold radar data were collected.

Figure 6.14 Comparisons of fracture images using mono-static, migrated mono-static and stacked migration image of WIVS approach. Left: mono-static data; center: migrated mono-static data; right: stacked migration image of WIVS approach.

List of Tables

Chapter 1. Introduction

In many theoretical and practical problems, the forward modeling of the wave propagations is always the most important and basic step of the research. Waves are a kind of very common phenomenon in not only the academic and industrial problems, but also in our daily life. The importance of wave is due to that the waves not only carry out the source information, but also takes the information of the media out. For examples, some geophysicists use GPR survey data to explore the shallow subsurface (Liu and Li, 2001; Liu and Guo, 2003), and use borehole radar to imagine the velocity and/or attenuation distribution, characterize hydrological system or monitor mass transport within cross-well (Liu and Quan, 1998; Zhou, Liu and Lane, 2001, Lane et al., 2001; Liu et al., 2004). The seismologists use the received seismic waves by seismometers to reconstruct the inner structure of the Earth (Aki and Richards, 2001; Cormier and Richards, 1997; Cormier, 1985; Fukao et al., 2003) so we can make hypotheses that there should exist some discontinuity interfaces which divide the Earth into core, mantle and crust; In addition, some other scientists use the acoustic wave equation to study the sound propagation for civil or military purposes. (Papadopoulous and Don, 1991; Albert, 2001; Liu and Albert, 2006). The examples of wave propagation are numerous. Obviously the wave is a very important, non-destructive, valid and efficient physical tool for physical and geophysical study of the inner structure of certain object.

In general, three different types of the physical waves have been studied and applied in different real problems. They are the acoustic wave, the electromagnetic (EM) wave and the elastic or seismic wave. Among all of the three typical physical waves, the EM wave can be representative in that the EM wave can travel in any medium even in the vacuum. (Balanis, 1989). The medium is not a necessary condition for EM wave propagation, but this is not true for the mechanical

waves such as the seismic wave and the acoustic wave (Sheriff and Geldart, 1995; Aki and Richard, 2001). That's why the EM wave is most extensively used in real physical problems. The utilization of EM radar has a very wide range from biomedical engineering, civil engineering, remote sensing and the geological subsurface structure detection. In following chapters, the EM wave equations are used to show how some advanced numerical methods and algorithms are developed, and some new techniques are developed to make contribution to the numerical simulation and inner structure imaging. Although the methods and algorithms discussed in this dissertation are based on the EM wave, they can also be applied to the acoustic and seismic wave propagation and applications with similar effort.

The EM wave equation was derived from Maxwell's equations, which is named after the famous English physicist J.C. Maxwell. In 1873, Dr. Maxwell published one of the greatest papers in history "A Treatise on Electricity and Magnetism", which marks the culmination of classical physics. In his paper, Maxwell united some past physicists' important contributions together to a complete EM theory by building a simultaneous four equations, which is so called "Maxwell's equations" (Balanis, 1989; Kraus and Fleisch, 1999). Maxwell's equations mainly describe how the electric current generates a magnetic field, and the varying magnetic field generates eddy electric field, i.e., the electric field and magnetic field are coupled together; both of the two fields propagate from the source as a wave, which is known as "EM wave" or "EM field".

With the building of Maxwell's equations more than a century ago, the search of solution for electromagnetic wave propagation phenomena has become one of the most important issues in academia and industry (Taflove, 1995). However, the numerical solution of Maxwell's equations remained a big challenge until the last a couple decades. The main reason is that the fast development of computing technology mainly happened in the recent decade.

Before the emergence of advanced computer facilities, the popular method for modeling wave propagation is the ray-tracing method (Cerveny, 1977; Zeng et al, 1995; Cai and McMechan, 1995). The main principle of ray tracing method is the geometric optics. When a ray hits an interface between two different media it will reflect and/or transmit via Snell's law. The basic assumption of ray-tracing method is that the source has a very high frequency, for example visible light wave with a narrow frequency range of about 1014 to 1015 Hz (Hecht and Zajac, 1973; Kraus and Fleisch, 1999). Therefore the ray-tracing method is not ideal for solving medium and low frequency source problems. Another big shortcoming of the ray-tracing method is that it is not easy to handle the problems that comprise complicated media, for example caustics issue is a bitter challenge to ray-tracing method. Moreover, the amplitudes that obtained ray-tracing method compute are a quite rough approximation, much less accurate than those by numerical method (Cerveny, 1977; Taflove, 1994; Cai and McMechan, 1997).

In general, nowadays ray-tracing method and numerical modeling methods are the two most popular methods for solving wave propagation phenomena problem, but these two methods are based on quite different mechanisms for searching the solutions. If the media are not complicated, for example, all the interfaces are horizontal or spherical and all the layers are isotropic, then the ray-tracing method can be an efficient and fast way to solve the wave propagation problem (Cerveny, 1977). But in most cases the media are complicated the interface maybe not be flat but hilly or even physical property with randomness, then ray-tracing method might not be able to handle with those problems straightforward. The wave field in reality includes not just a few rays but many rays and some of them even mixed together such as caustics phenomenon, and it is a very difficult job for ray tracing method to process so many rays in the whole field but it is much easier for numerical method to simulate the whole field.

The numerical modeling method can produce the whole field for all the related physical components, which include both electric fields and magnetic fields. However the numerical modeling method has a much higher requirement on computational facilities such as CPU speed and available memory volume compared to that for the ray-tracing method. The numerical modeling method was not practical several decades ago because the computation facilities were not advanced enough to handle such intensive computation. With the emergence and development of advanced computing technology, nowadays so called the high performance computing (HPC), the capabilities of numerical method for solving Maxwell's equations becomes more and more powerful (Taflove, 1994). One milestone of numerical method for the solution of Maxwell's equations was made by K. Yee (1966). In his paper K. Yee proposed his scheme for finite-difference time-domain (FDTD) method: spatially staggered grids mesh for electric field and magnetic field, and temporally staggered time marching step for alternatively updating electric field and magnetic field in time. Several decades later Yee's scheme for FDTD is still one of the most popular numerical methods for solutions of the EM wave equation (Taflove, 1994), and it has been widely used for modeling EM wave propagation (Berenger, 1994; Chew and Weedon, 1994). However, Yee's FDTD has its disadvantages. The first disadvantage is that it requires at least ten to twenty grids per wavelength to keep the calculation accurate and stable, and its limited accuracy has the 2nd order by 1st order difference scheme. The other main disadvantage is that the traditional FDTD method updates the electric field and magnetic field by an explicit scheme (Yee, 1966), which limits the time step subject to the Courant-Friedchs-Levy (CFL) constraint to minimize numerical dispersion (Taflove, 1994). These are the two drawbacks that limit the efficiency of Yee's FDTD method. In the following sections the dissertation briefly describes the pseudospectral time-domain (PSTD) method (Witte, 1989; Liu, 1997; Xiao, Liu and Cormier, 1998; Cormier, 2000). In general, five or six grids per wavelength are good enough for the PSTD method to keep the algorithm stable and accurate. It is a big advantage especially in the large scale three-dimensional (3D) problems. When we try to simulate the real 3D problem, the

memory cost is proportional to the total grid numbers which is increasing at a speed of N^3. Obviously the PSTD method is much superior to the FDTD method in saving the memory cost drastically. However, the computation time and memory cost can still be intensive, when we try to simulate the wave propagation in some large-scale and high frequency physical problems. Some other simulation methods were designed to improve the efficiency in computation time and memory cost.

Multi-region (MR) method, which was first introduced by Johnson and Rahmat-Samii, (1997), was designed to simulate the physical problem which has a relatively large computation domain and relatively small scatters with highly improved efficiencies in computation time and memory cost. MR method is a hybrid simulation method using a combination of Kirchhoff integration and the traditional FDTD and/or PSTD method. Based on the time domain Schelkunoff surface equivalence principle, MR methods divide the whole computation domain into a series of small sub-regions to enclose the small scatters. Inside of each sub-region, a traditional FDTD or PSTD method can be used to simulate the EM wave propagation. However outside the sub-regions, the EM wave propagation is simulated using the Kirchhoff integration. MR method was proved to be a valid and efficient method in EM wave simulation (Johnson and Rahmat-Samii, 1997, Coleman, 2005, Bernardi et al.., 2002).

Among all the forward modeling problems, the full waveform simulation of a reflection model has its unique importance. The full waveform simulation of a reflection model is closely related to the inner structure imaging. Most of the forward modeling methods are closely related to the final purpose of understanding the inner structure of a certain physical object. The range could be very wide from the research of a human body in biomedical engineering, the P or S wave global tomography in modern seismology, the ice crevasse detection in remote sensing, and the geological structure imaging in oil and gas industry. Theoretically the forward modeling can be

done using the traditional FDTD and PSTD methods, but in many practical problems it can be extremely difficult in both computational resource limitation and data acquisition. This dissertation is focusing on the hybrid method to simulate the wave propagation for some difficult reflection models. The results are imaged with the pre-stack Kirchhoff migration to prove that the hybrid methods are not only accurate, high efficient but also robust and compatible with the modern inner structure techniques.

For contributing to this area, this dissertation presented three novel techniques of the forward modeling to facilitate the research of some realistic reflection model: directional Kirchhoff integration (DKI) multi-region (MR) pseudospectral time domain (PSTD) method, model subtraction (MS) method and the combination of interferometry, virtual reflection and migration technique. All the three techniques have been applied and involved with profound theoretical and practical significance. Chapter 2 of this dissertation will be the introduction to some modern geophysical simulation theories. Chapter 3 is an introduction to the DKI/MR method with a case study to show how the DKI/MR method can offer accurate simulation results with much less computational cost in both computation time and memory cost. Chapter 4 will introduce the novel model subtraction method. A case study combined with DKI/MR method shows that the model subtraction is the best idea to extend the DKI/MR method into real reflection model simulation and all the high efficiencies in computation time and memory cost can be kept. The Kirchhoff PSTM offers good imaging results. Chapter 5 introduces the interferometry technique and 3D WIVS approach. A case study in fracture detection and characterization is provided in Chapter 5. The 3D WIVS approach turns the transmission model into a virtual reflection model. It facilitates the field work in real geophysical data acquisition. Chapter 6 is going on with the imaging work based on the research of Chapter 5. Kirchhoff PSTM and stack techniques are applied to the simulated results. The results are good evidences in that the interferometry and WIVS approach

are ideal techniques in fracture detection and characterization. Chapter 7 is the final summary of the whole dissertation.

The recursive integrated (RI) Perfect Matched Layer (PML) absorbing boundary condition (ABC) is used throughout this Ph.D. dissertation as the numerical modeling boundary conditions (Drossaert and Giannopoulos, 2007). The principal advantage of this ABC is that it can be very suitable for parallel HPC computing and easy for coding the algorithm. Compared to the Berenger's PML ABC (Berenger, 1994), RIPML ABC can save much programming codes, memory cost and performs better for most diverse media conditions. The fundamental philosophies of the two different ABCs are almost the same.

Chapter 2. Maxwell's Equations, PSTD Method and Kirchhoff Integration

2.1 Introduction

Numerical modeling of electromagnetic wave propagation is an important part of geophysical studies. To solve the real-world problem with consideration of irregular interface and free surface, the introduction of pseudospectral time domain (PSTD) method has been proved to be effective and efficient in suppressing the numerical differentiation of the stairway like approximation of studies (Witte, 1989; Liu, 1997; Cormier, 2000). Previous studies have proved that the setup of perfectly matched layers (PML) is reputed as the most efficient absorbing boundary conditions (ABC) (Berenger, 1994; Drossaert and Giannopoulos, 2007). As the basis of this research, this chapter is trying to focus on the investigation of the combination of stretched coordinates and PML, and the discussion is associated with the staggered grid PSTD method.

2.2 Fourier Transform (FT) and Inverse Fourier Transform (IFT)

Fourier transform, named after the French mathematician Joseph Fourier (Lathi, 1998), is an integral transform that re-expresses a function in terms of sinusoidal basis functions, *i.e.* as a sum or integral of sinusoidal functions multiplied by some coefficients or "amplitudes". The standard Fourier transform can be expressed as Equation 2.1, (Porat, 1997)

$$F(\omega) = \int_{-\infty}^{\infty} f(t) e^{-i\omega t} dt \tag{2.1}$$

Inverse Fourier transform is the opposite operation of Fourier transform, and it can be written as (Porat, 1997)

$$f(t) = \int_{-\infty}^{\infty} F(\omega) e^{i\omega t} d\omega \tag{2.2}$$

If both sides of above equation are differential to time t, then it can be written as Equation 2.3

$$\begin{aligned} \frac{\partial f(t)}{\partial t} &= \frac{\partial}{\partial t} \int_{-\infty}^{\infty} F(\omega) e^{i\omega t} d\omega \\ &= \int_{-\infty}^{\infty} i\omega F(\omega) e^{i\omega t} d\omega \\ &= IFT\{i\omega \bullet FT[f(t)]\} \end{aligned} \tag{2.3}$$

So we can find that derivative of a function $f(t)$ with respect to time t can be obtained by inverse Fourier transform of product between that function's Fourier transform F(ω) and (iω). Actually, the function f can be not only the time function f(t), but also be spatial function f(**x**), and vector **x**= **x**(x,y,z,t). This property is very important in numerical modeling. The extensively used pseudospectral time domain (PSTD) method is based upon this property.

In general, Fourier transform is widely used to handle the time-frequency domain dataset. However Fourier transform is also valid for datasets in other domain, for instance, space-wavenumber domain. The principle is straightforward: substitute time variable t by spatial variable **x**, and substitute angular frequency ω by wavenumber k, then the above equations (2.4) are converted to (Witte, 1989; Liu, 1997)

$$\begin{aligned} F(k) &= \int_{-\infty}^{\infty} f(x) e^{-ikx} dx \\ f(x) &= \int_{-\infty}^{\infty} F(k) e^{ikx} dk \\ \frac{\partial f(x)}{\partial x} &= \int_{-\infty}^{\infty} ikF(k) e^{ikx} dk \end{aligned} \tag{2.4}$$

where wavenumber k is defined by

$$k = \frac{2\pi}{\lambda} \tag{2.5}$$

And λ is the wavelength. Consequently, the spatial variable **x** and wavenumber k become a Fourier transform pair, just like the relationship between t and ω. Usually, they are denoted as (Lathi, 1998)

$$\begin{aligned} t &\Leftrightarrow \omega \\ x &\Leftrightarrow k \end{aligned} \tag{2.6}$$

2.3 Fast Fourier Transform (FFT)

The fast Fourier transform (FFT) was introduced in 1965 by IBM researcher Dr. Jim Cooley and Princeton faculty member Dr. John Tukey. FFT was a major breakthrough in digital signal processing and applied science or engineering (Press *et al*., 1992; Porat, 1997). Before that, practical use of the discrete Fourier transform was limited to small-size problems with the data set relatively small. The difficulty in applying the Fourier transform to real problems is that, for an input sequence of length N, the number of arithmetic operations in direct computation of the DFT is proportional to N^2. For instance, if N=1000, then about a million operations are necessary to finish the transform. Provided N increases to 10,000, there will be one hundred million operations necessary to finish the transform. Only computers with very large memory and robust CPU are able to make the computation practical. Such a large amount of computation had prevented the applications of Fourier and inverse Fourier transforms in most applied science or engineering because the computer facilities were poor at that time. Cooley and Tukey's discovery proves that when N, the discrete Fourier transform (DFT) length, is a composite number (*i.e.*, not a prime), the DFT operation can be decomposed to a number of DFTs of shorter lengths. Their paper has

proved that the total number of operations necessary for the shorter DFTs is much less than the number required for direct computation of the length-N DFT. And each shorter DFTs, in turn, can be decomposed and performed by yet smaller DFTs. DFT is a recursive process and can be repeated until all DFTs are of prime lengths. Finally, the DFTs of prime lengths are computed directly. The total number of operations in this scheme depends on the factorization of N into prime factors, but in general the operation number is much smaller than N^2. In particular, when N is an integer power of 2, the number of operations is on the order of N*log2N. For large N this number can be smaller than N^2 by many orders of magnitude. This improvement makes the DFT a much more practical tool for digital signal processing. The algorithm discovered by Cooley and Tukey soon became known as the fast Fourier transform, or FFT. As a kind of DFT, FFT requires much less computation time and memory cost and is able to give the same result as DFT. Nowadays there is no doubt that FFT is one of the most highly developed areas of signal and image processing, and it has gained extensive application in both science and engineering area. All DFT used in this dissertation is FFT.

2.4 Pseudospectral Time Domain (PSTD) Scheme

In Yee's FDTD scheme, the finite difference method is used to approximate the spatial derivatives, so the accuracy of results are limited, *i.e*., 2nd order by 1st order finite difference through staggered grids. In order to keep accuracy and stability of the numerical simulation, it usually takes at least 10 grids per wavelength (Liu, 1997). Consequently FDTD method needs a lot of memory in computing large-scale problem, especially in a 3D case. However the achievable accuracy is not satisfactory as expected. From the computational point, Fourier transform methods, especially the FFT methods are well suitable to this task. The pioneering work of spectral method for wave propagation was investigated as early as 1970s (Kreiss and Oliger, 1972; Orzag, 1980; Gazdag, 1981; Kosloff and Baysal, 1982), they examined the modeling of the

seismic or acoustic wave equation with transform methods, in their method they used the Fourier transform and Inverse Fourier transform to replace the spatial derivatives. The technique that they used is called "Pseudospectral Time-Domain" (PSTD) method, and they found that the PSTD method can get much higher accuracy than traditional FDTD given same grid density, but needs much more computational time and double memory.

In the past two decades, the similar works on EM wave have pioneered using the Fourier transform method for EM wave modeling (Witte, 1989; Liu, 1997; Xiao et al. 1998). For example, Q.H. Liu (1997) wrote that PSTD can use at less as two grids per wavelength but FDTD method requires 10-20 grids per wavelength, thus the PSTD method is more efficient than FDTD. In addition, the PSTD method is ideal for parallel computing of large-scale problems, because fast Fourier transform (FFT) is well suitable for parallelized computation. Many software packages have inner FFT subroutines, for example Matlab, so the users can directly call the FFT subroutine no need to program for it by themselves. Even for C-language, there are quite some popular C functions working as FFT transforms. For instance the Center for Wave Phenomena (CWP) at Colorado School of Mines developed a set of Seismic Unix (SU) subroutines which included the FFT. Currently, the SU FFT has gained a wide attention in oil and gas industry. PSTD method can also be easily utilized with the absorbing boundary conditions (ABC) to make PSTD method realistic in the numerical simulations.

Comparing the PSTD method and the FDTD method, we can find that the PSTD scheme makes the modeling much more efficient than Yee's FDTD scheme: the former can produce higher quality synthetic data. Moreover, the PSTD method uses collocated grids rather than staggered grids, so the programming becomes more straightforward and the formulizations become more convenient to understand. However, the PSTD method works most efficiently when the each dimension size of computational domain is power of 2 (usually) so that the FFT algorithm can

take advantage of it. PSTD method requires double memory volume as that traditional Yee's FDTD algorithm does, given same grid density, and in a 2-D problem the PSTD scheme would need operations (1+log2(mn)) times as much as that FDTD costs, where m and n are the grid numbers for the two dimensions respectively. Moreover, most operations that cost by PSTD algorithm are multiplications, which are much more expensive than most operations for FDTD, i.e., substations. Therefore, PSTD method needs more computation time and memory than FDTD does when solving a same problem especially large-scale problem.

2.5 Staggered-grid and non Staggered-grid PSTD Method

The staggered grid scheme was first proposed by Yee (Yee, 1966) for achieving better accuracy and higher stability in modeling the elecgtromagnetic (EM) wave propagation using the finite difference time domain (FDTD) method. It is an approved algorithm for its robustness and has been widely used in the EM research community. Meanwhile, in the development of the pseudospectral time domain (PSTD) method which theoretically only needs two grids per wavelength (Liu QH PSTD using only 2 grids) for EM wave simulations the parameters are collocated at the same nodes and the parameters are essentially non-staggered for take the advantage of algorithm simplicity. Great success of the staggered grid scheme for the FDTD method made some researchers turn their attention on trying to apply the staggered grid scheme for the PSTD method and applied to seismic wave propagations. It has been demonstrated that using staggered grid to the PSTD scheme made the time marching more stable and the numerical dispersion much suppressed for models with large contrast in material properties. In this paper, detailed discussion on the application of the staggered grid PSTD to model the electromagnetic wave propagations is presented.

The staggered grid scheme is realized by shifting and makes the Nyquist wave number a non-zero pure real value of $-\pi/\Delta x$ [7]. By doing this the Nyquist information of the original spatial function is preserved and makes the differentiation operator more stable. In the Fourier domain, adding trigonometric factors in the classic Fourier coefficients is equivalent to the staggered grid approach in the original space domain. The PSTD algorithm development using the staggered grid approach has been associated with the use of the recursively integrated (RI) perfectly matched layers (PML) based on the PML scheme.

2.6 Maxwell's Equations

The electromagnetic (EM) wave propagation in isotropic, inhomogeneous media is governed by the Maxwell's equations,

$$\begin{aligned} \nabla \times \mathbf{H} &= \varepsilon \frac{\partial \mathbf{E}}{\partial t} + \sigma \mathbf{E} + \mathbf{J} \\ \nabla \times \mathbf{E} &= -\mu \frac{\partial \mathbf{H}}{\partial t} \end{aligned} \tag{2.7}$$

Where E is the electric field and H is the magnetic field. J is the electric current density. The dielectric permittivity ε, magnetic permeability μ, and electric conductivity σ are all spatial dependent. When the electric current density J can be ignored, the Maxwell's equations can be extended to the component equations,

$$
\begin{aligned}
&\frac{\partial E_z}{\partial y}-\frac{\partial E_y}{\partial z}=-\mu\frac{\partial H_x}{\partial t}\\
&\frac{\partial E_x}{\partial z}-\frac{\partial E_z}{\partial x}=-\mu\frac{\partial H_y}{\partial t}\\
&\frac{\partial E_y}{\partial x}-\frac{\partial E_x}{\partial y}=-\mu\frac{\partial H_z}{\partial t}\\
&\frac{\partial H_z}{\partial y}-\frac{\partial H_y}{\partial z}=\sigma E_x+\varepsilon\frac{\partial E_x}{\partial t}\\
&\frac{\partial H_x}{\partial z}-\frac{\partial H_z}{\partial x}=\sigma E_y+\varepsilon\frac{\partial E_y}{\partial t}\\
&\frac{\partial H_y}{\partial x}-\frac{\partial H_x}{\partial y}=\sigma E_z+\varepsilon\frac{\partial E_z}{\partial t}
\end{aligned}
\qquad (2.8)
$$

Where E is the electric field and H is the magnetic field. Ex, Ey, Ez and Hx, Hy, Hz denote their components in x, y and z directions respectively

2.7 Absorbing Boundary Condition (ABC) and Perfectly Matched Layer (PML)

Yee's FDTD scheme uses truncated computational domain, actually all numerical modeling method deal with only finite domain rather than an infinite one. The wave advances from the domain will be reflected back if there is no effective boundary condition that wraps around the computational domain. Some scholars have worked on building some absorbing conditions (ABCs) for FDTD method, for instance, C. Cerjan *et al*. (1985). However his method works not efficiently and usually needs about very thick absorbing layer for each side of boundary to attenuate the incident wave energy. Moreover, Cerjan's absorbing boundary condition has not systematically solved the boundary condition problem, i.e., it did not give any mathematical proof that his method is efficient for the incident wave that with any angle and/or frequency. In the last decade, some important research work on ABC has been published. J.P. Berenger (1994) created

a kind of novel ABC, which is referred to Perfectly Matched Layer (PML). In his PML, he created a magnetic conductivity (σ*), and when in a medium if it satisfies the condition

$$\frac{\sigma}{\varepsilon} = \frac{\sigma^*}{\mu} \tag{2.9}$$

the reflection coefficient will be zero. The incident wave will not be reflected back. In equation (2.9), σ is electric conductivity, μ is magnetic permeability, μ is electric permittivity, and σ* the named as magnetic conductivity, which is not a real physical property. Berenger created such a virtual physical property as a controllable parameter that will make the boundary condition to work as wave energy absorber zone.

Since the publication of Berenger's papers (1994), PML has been paid much attention in last decade (Chew and Weedon, 1994; Taflove, 1995; Festa and Nielsen, 2003; Tang and Liu, 2003, Drossaert and Giannopoulos, 2007). Indeed, his PML has gained good reputation due to the proposed a virtual "magnetic conductivity" σ* which is the controllable variable for making the reflection coefficient to be zero. And his method usually only requires about 10 grids for each side of PML, so it is efficient.

Unfortunately, Berenger's PML has its shortcomings: (1) it is not easy to code the algorithm, and nearly 50% code is for constructing the PML function, so the coding work is not very efficient; (2) the method relatively is not suitable for parallel computing compared to other PML algorithms, for example, Drossaert and Giannopoulos's PML (2007). Thus this method is not good at handling with the big scale modeling projects, which usually run on parallel computers or clusters. Therefore, in this dissertation, another better PML is chosen as ABC.

2.8 Recursive Integrated PML (RIPML) and Modified Maxell's Equations

In PSTD modeling of the acoustic, electro-magnetic and elastic waves, absorbing boundary conditions (ABC) are used to mitigate undesired wrap around effects that can arise at the model's truncation boundaries. In an FDTD scheme, ABC is used to mitigate the undesired reflections caused by the model's truncation boundaries. The quest for an ABC that produces negligible reflections and/or wrap around effects has been, and continues to be, one of the most active areas of numerical modeling research (Engquist and Majda, 1977; Reynolds, 1978; Katz et al., 1983; Liao et al., 1984; Cerjan et al., 1985; Higdon, 1987). Most of the popular ABC's can be grouped into those that are derived from differential equations or those that employ a material absorber (Taflove, 1995). The perfectly matched layer (PML) technique which was first put forward by Berenger (1994), can be considered a material absorber.

However, its formulation was a radical departure from that of all previously proposed grid termination techniques. In application, the PML approach has shown to provide significantly better accuracy than most other ABC's and, thus, the PML technique has become a standard to which other techniques must be compared. Because of the quality afforded by the PML scheme, many of the previous literatures on ABC's, which was sizable, was made obsolete (Taflove, 1995). Thus in the following section almost all the other well-known ABCs are neglected and mainly the PML ABCs are discussed. Unfortunately, Berenger's PML has its shortcomings: (1) it is not easy to code the algorithm, and nearly 50% code is for constructing the PML function, so the coding work is not very efficient; (2) the method relatively is not suitable for parallel computing compared to Drossaert and Giannopoulos's PML (2007). This method is not good at handling with the big scale modeling projects, which usually run on parallel computers or clusters.

In this dissertation, another better PML, a non-split frequency-shifted recursive integration PML (RIPML) is use as the absorbing boundary conditions. To obtain absorbing properties in the PML, the electro-magnetic equations are transformed into a stretched-coordinate domain with a complex stretching function (Chew and Liu, 1994). In the frequency domain the 3D stretching functions can be written as

$$\begin{aligned} \tilde{x} &= (1 + i\frac{\omega_x}{\omega})x \\ \tilde{y} &= (1 + i\frac{\omega_y}{\omega})y \\ \tilde{z} &= (1 + i\frac{\omega_z}{\omega})z \end{aligned} \tag{2.10}$$

Where ω_x, ω_y and ω_z represent the loss in the PML. If we define

$$\begin{aligned} \tau_x &= 1 + i\frac{\omega_x}{\omega} \\ \tau_y &= 1 + i\frac{\omega_y}{\omega} \\ \tau_z &= 1 + i\frac{\omega_z}{\omega} \end{aligned} \tag{2.11}$$

The spatial derivatives in the stretched-coordinate PML space can then be written as

$$\begin{aligned} \frac{\partial}{\partial \tilde{x}} &= \frac{1}{\tau_x}\frac{\partial}{\partial x} \\ \frac{\partial}{\partial \tilde{y}} &= \frac{1}{\tau_y}\frac{\partial}{\partial y} \\ \frac{\partial}{\partial \tilde{z}} &= \frac{1}{\tau_z}\frac{\partial}{\partial z} \end{aligned} \tag{2.12}$$

Using the equations, the first-order electric and magnetic equations in the stretched-coordinate space can now be written as the following set of coupled equations,

$$\begin{aligned}
&\frac{1}{\tau_y}\frac{\partial \tilde{E}_z}{\partial y} - \frac{1}{\tau_z}\frac{\partial \tilde{E}_y}{\partial z} = -i\omega\mu\tilde{H}_x \\
&\frac{1}{\tau_z}\frac{\partial E_x}{\partial z} - \frac{1}{\tau_x}\frac{\partial E_z}{\partial x} = -i\omega\mu\tilde{H}_y \\
&\frac{1}{\tau_x}\frac{\partial E_y}{\partial x} - \frac{1}{\tau_y}\frac{\partial E_x}{\partial y} = -i\omega\mu\tilde{H}_z \\
&\frac{1}{\tau_y}\frac{\partial \tilde{H}_z}{\partial y} - \frac{1}{\tau_z}\frac{\partial \tilde{H}_y}{\partial z} = \sigma\tilde{E}_x + i\omega\varepsilon\tilde{E}_x \\
&\frac{1}{\tau_z}\frac{\partial \tilde{H}_x}{\partial z} - \frac{1}{\tau_x}\frac{\partial \tilde{H}_z}{\partial x} = \sigma\tilde{E}_y + i\omega\varepsilon\tilde{E}_y \\
&\frac{1}{\tau_x}\frac{\partial \tilde{H}_y}{\partial x} - \frac{1}{\tau_y}\frac{\partial \tilde{H}_x}{\partial y} = \sigma\tilde{E}_z + i\omega\varepsilon\tilde{E}_z
\end{aligned} \tag{2.13}$$

Where a time dependence of $e^{i\omega t}$ is assumed. The electric and magnetic fields are denoted as E and H respectively. The tilde denotes their frequency domain counterpart.

The basic principle of RIPML is to rewrite the electro-magnetic equations by introducing two new auxiliary vectors, the electric rate vector S and magnetic rate vector T. Their components are denoted as

$$\tilde{S}_{xy} = \frac{1}{\tau_y}\frac{\partial \tilde{E}_x}{\partial y}$$
$$\tilde{S}_{xz} = \frac{1}{\tau_z}\frac{\partial \tilde{E}_x}{\partial z}$$
$$\tilde{S}_{yx} = \frac{1}{\tau_x}\frac{\partial \tilde{E}_y}{\partial x}$$
$$\tilde{S}_{yz} = \frac{1}{\tau_z}\frac{\partial \tilde{E}_y}{\partial z} \qquad (2.14)$$
$$\tilde{S}_{zx} = \frac{1}{\tau_x}\frac{\partial \tilde{E}_z}{\partial x}$$
$$\tilde{S}_{zy} = \frac{1}{\tau_y}\frac{\partial \tilde{E}_z}{\partial y}$$

And

$$\tilde{T}_{xy} = \frac{1}{\tau_y}\frac{\partial \tilde{H}_x}{\partial y}$$
$$\tilde{T}_{xz} = \frac{1}{\tau_z}\frac{\partial \tilde{H}_x}{\partial z}$$
$$\tilde{T}_{yx} = \frac{1}{\tau_x}\frac{\partial \tilde{H}_y}{\partial x}$$
$$\tilde{T}_{yz} = \frac{1}{\tau_z}\frac{\partial \tilde{H}_y}{\partial z} \qquad (2.15)$$
$$\tilde{T}_{zx} = \frac{1}{\tau_x}\frac{\partial \tilde{H}_z}{\partial x}$$
$$\tilde{T}_{zy} = \frac{1}{\tau_y}\frac{\partial \tilde{H}_z}{\partial y}$$

After introducing the electric rate and magnetic rate vectors, it is not necessary to split the electric and magnetic fields into separate components. The electro-magnetic equations become as follows after transforming

$$
\begin{aligned}
S_{zy} - S_{yz} &= -\mu \frac{\partial H_x}{\partial t} \\
S_{xz} - S_{zx} &= -\mu \frac{\partial H_y}{\partial t} \\
S_{yx} - S_{xy} &= -\mu \frac{\partial H_z}{\partial t} \\
T_{zy} - T_{yz} &= \sigma E_x + \varepsilon \frac{\partial E_x}{\partial t} \\
T_{xz} - T_{zx} &= \sigma E_y + \varepsilon \frac{\partial E_y}{\partial t} \\
T_{yx} - T_{xy} &= \sigma E_z + \varepsilon \frac{\partial E_z}{\partial t}
\end{aligned}
\tag{2.16}
$$

The final equations in integration format turn to be

$$
\begin{aligned}
H_x &= \frac{1}{\mu} \int_0^t (S_{yz} - S_{zy}) dt \\
H_y &= \frac{1}{\mu} \int_0^t (S_{zx} - S_{xz}) dt \\
H_z &= \frac{1}{\mu} \int_0^t (S_{xy} - S_{yx}) dt \\
E_x &= \frac{1}{\varepsilon} \int_0^t (T_{zy} - T_{yz} - \sigma E_x) dt \\
E_y &= \frac{1}{\varepsilon} \int_0^t (T_{xz} - T_{zx} - \sigma E_y) dt \\
E_z &= \frac{1}{\varepsilon} \int_0^t (T_{yx} - T_{xy} - \sigma E_z) dt
\end{aligned}
\tag{2.17}
$$

Equations (2.16) and (2.17) completed the RIPML formulas. In this dissertation, RI PML is selected as the ABC.

2.9 The Kirchhoff Integration and Multi-region (MR) Method

Kirchhoff integration, sometimes referred as the Kirchhoff integral theorem, uses Green's function to derive the solution to the homogeneous wave equation at an arbitrary point in terms of the values of the wave equation and its first order derivative at all points on an arbitrary surface which encloses the point. The Schelkunoff surface equivalence theorem states that the electromagnetic sources and/or scatters inside an imaginary volume can be replaced by equivalent magnetic and electric current sources on the surface enclosing the volume resulting in the same fields outside the volume and a zero field inside the volume. The presence of a zero field inside this exclusion volume, in turn, allows its contents sources and scatters. to be replaced by free space. With the entire problem domain now filled by free space, the fields anywhere outside the imaginary volume can be found by integrating the equivalent sources over the surface with the use of the free-space Green's function. Equation (2.18), extended from Fig. 2.1 gives the electric field everywhere in the free-space region outside the exclusion volume in terms of equivalent surface currents on the region surface. Kirchhoff integration has its unique significance because it is the key technique in the MR technique. MR technique, which was proved to be a reputed forward modeling method in improving computational efficiencies of both time and memory cost, was firstly introduced by Johnson and Rahmat-Samii (1997) in 1997. This method is especially suitable for the physical problem where a relatively large space has a uniform background which was embedded with some small scatters. Fig. 2.1 is an illustration of the Kirchhoff integration and MR technique ideas.

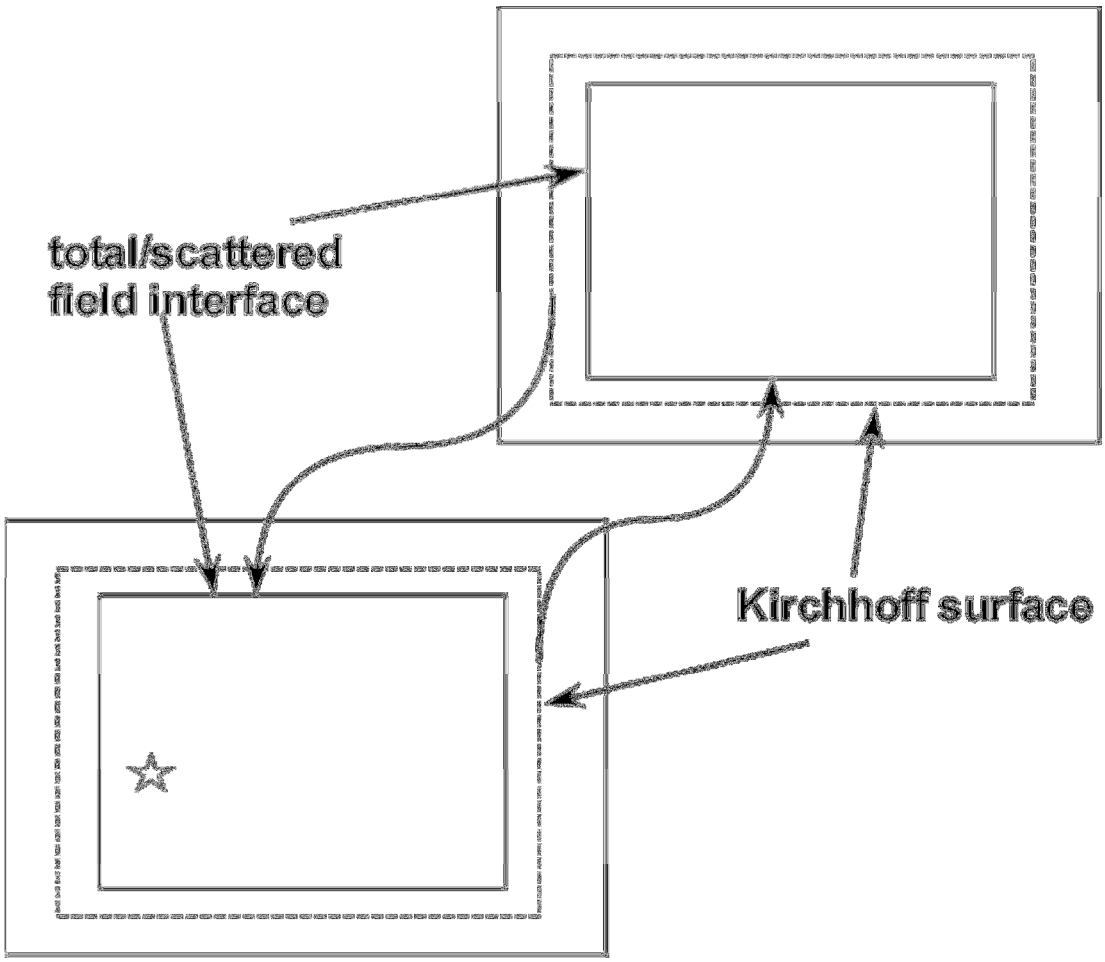

Figure 2.1 Illustration of the Kirchhoff integration and the total/scatter (TS) surfaces setup. One natural source is illustrated in the left-down sub-region, and no natural source exists in the right-up sub-region.

$$\vec{E}(\vec{r},t)=\frac{1}{4\pi}\int_s\{(\frac{\vec{n}\bullet\vec{R}}{R})[\frac{\vec{E}(\vec{r'},t)}{R^2}+\frac{1}{cR}\frac{\partial\vec{E}(\vec{r'},t)}{\partial\tau}]$$
$$-\frac{1}{R}\frac{\partial\vec{E}(\vec{r'},t)}{\partial n}\}ds \qquad (2.18)$$

$$\tau=t-\frac{R}{c}$$

As illustrated in Fig. 2.1, a series of sub-regions are separated from the whole computational domain. In side of each sub-region, one Kirchhoff integration surface is set, and one

total/scattered (TS) field surface is set as the secondary virtual sources. The EM wave field was simulated in the sub-region using the traditional FDTD or PSTD method. While the EM wave reaches the Kirchhoff integration surface, it will be integrated along the Kirchhoff integration surface to the TS surface of another sub-region. Mathematically the TS surface serves as the virtual sources of each sub-region. It generates the EM waves as well as natural sources. The Kirchhoff integration surface and TS surface should be set inside of the PML zone, and the TS surface should be set inside of the Kirchhoff integration surface. Fig. 2.2 is one typical physical problem which is suitable for the MR method.

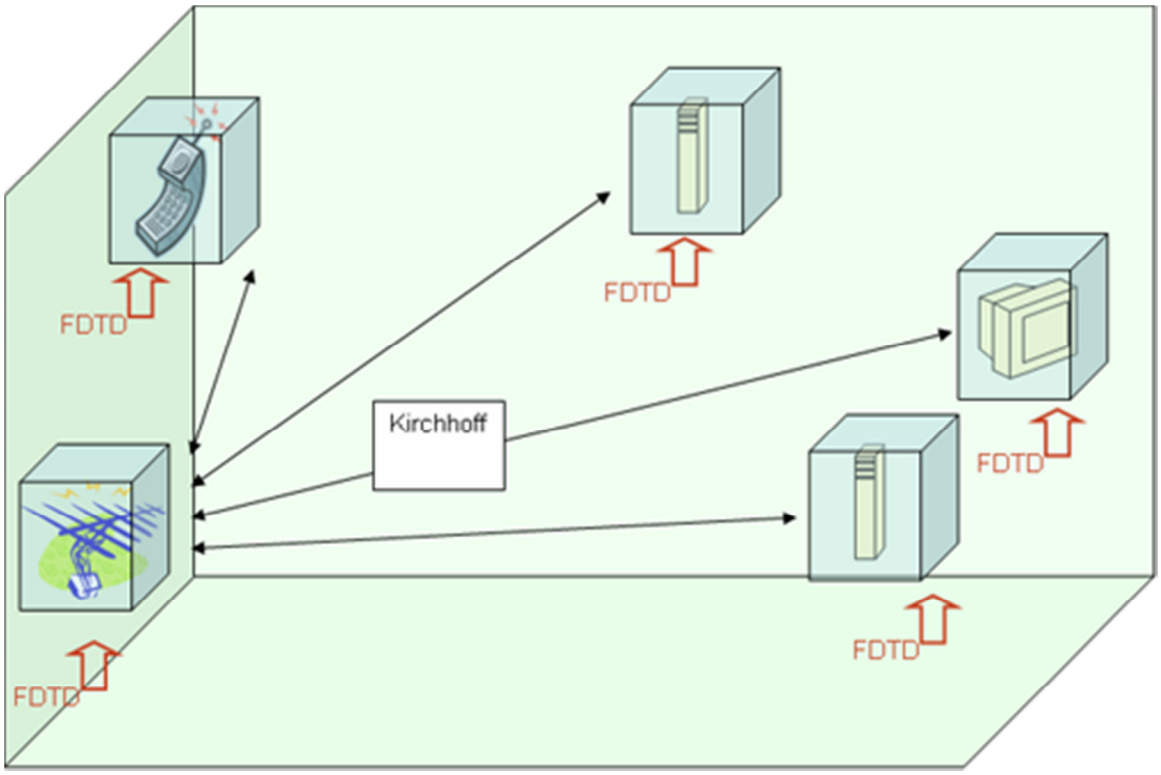

Figure 2.2 An example of the physical problems suitable for the MR method

Fig. 2.2 illustrates a relatively large free space which was embedded with some small scatters. The EM wave propagation can be simulated using the traditional FDTD or PSTD method inside of the whole computational domain, but it will be computational intensive. In order to save the

computational time and memory cost, a series of small sub-regions are separated. In side of each sub-region, a traditional FDTD or PSTD method is used to simulate the EM wave propagation. The EM wave propagation is simulated using the Kirchhoff integration among different sub-regions. As illustrated in Fig. 2.1, a total/scattered field surface is set inside of each sub-region to serve as the secondary virtual sources. The EM wave propagation of the whole computational domain is a hybrid one, traditional FDTD or PSTD used inside of each sub-region, and Kirchhoff integration used among different sub-regions.

Chapter 3. Multi-region and Directional Kirchhoff Integration PSTD Method

3.1 Introduction

In this chapter, a three dimensional (3D) multi-region (MR) pseudospectral time domain (PSTD) method with directional Kirchhoff integration (DKI) surface for numerically simulating electromagnetic (EM) wave propagation in heterogeneous media is presented.

In Many real theoretical and engineering problems which involves electromagnetic wave simulations, Pseudospectral time domain (PSTD) method including the PSTD with the staggered grid real value fast Fourier transform (FFT) differentiation operator, is commonly used for its reputation in efficiency and accuracy. However, PSTD method or other direct time domain techniques can suffer from long computation time and large memory requirement when the computation domain becomes large, especially in a three-dimensional (3D) case. Thus, any wave propagation simulation for a realistic case is computationally intensive. In some cases, especially in some long-distance cases, the 3D simulation using the traditional PSTD method becomes impossible.

In some cases if the whole computation domain only consists of a small number of sparse scatters in a uniform background medium such as air, the computation efficiency in computation accuracy, time and memory usage can be substantially improved by using a multi-region (MR) approach. The multi-region idea is first developed by Johnson and Rahmat-Samii (1997) with FDTD (MR/FDTD) algorithm. Various researches in EM wave propagation simulation using MR method have been proposed since then. However, most research works have been concentrated on

the simulations of the first arrival waveforms. The time window lengths in the previous researches are relatively short. Few multi-region algorithms have been developed to simulate the waveforms after the first arrivals to account for multi-reflections and refractions caused by the scatters. However, high fidelity simulation of multiple reflections is very necessary in many practical problems. In order to simulate not only the first arrivals and the waveforms after the first arrivals, a directional Kirchhoff integration (DKI) MR/PSTD is introduced in this chapter.

3.2 Multi-region PSTD (MR/PSTD) Method

Fig. 3.1a is an illustration of the 3D through-wall detection, a typical MR/PSTD application problem for electromagnetic wave propagation in the multi-region where the two walls, who serve as the scatters, are in the uniform media, air. The volumes of the two walls are same. The size of each wall is 64x64x128 grids. Both wall scatters have dielectric constants of 64. The source generating electromagnetic wave field is located left of the left wall scatter. The receivers are located in and through the right wall. The dielectric constant of air is 1. The electromagnetic wave propagation velocity in the dielectric wall scatters is 1/8 of the velocity in vacuum. The velocity of electromagnetic wave in the air is taken as that in the vacuum approximately. This model is uniform in the z direction. Fig. 1b shows the section of X-Y slice plane at the height of Z = 65 of this model, where the source and receivers are located. The area of deep blue shows air region and the two brown areas represent two dielectric scatter walls. The yellow and white plus signals illustrate the source of and the receivers, respectively. The source spatial coordinate is at the position of (85, 129, 65) in the left side of the left wall. There are 12 receivers are located around the right wall. The spatial coordinates of receivers is arranged from left to right in detail as shown in Fig. 3.1b.

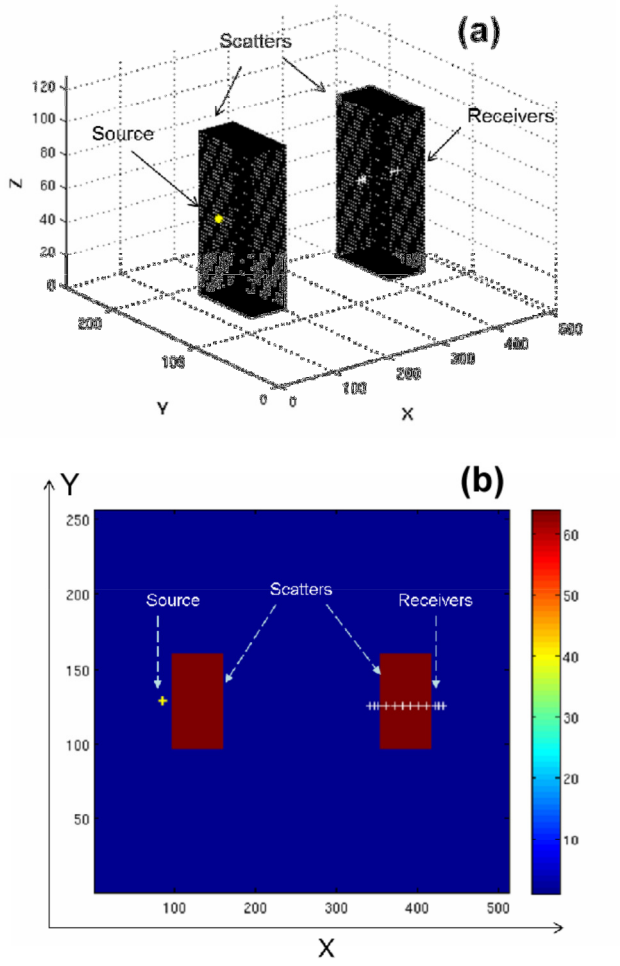

Figure 3.1 (a) Illustration of the multi-region 3D detection. Black cuboid wall： dielectric scatters; other region: air; yellow solid dot: source; white crosses: receivers. (b) A 2D slice in X-Y plane at Z=65 for the 3D model of (a). White crosses: receivers; yellow cross: source; brown solid block: dielectric scatter wall (dielectric constant 64, EM velocity, 1/8 velocity in the vacuum); color bar: dielectric constant scale.

In the model shown in Fig. 3.1, the volume or area occupied by the scatter walls are relative small compared with the entire study region, so an MR/PSTD method is considered to improve the computation efficiency as mentioned above. A number of MR approaches have been introduced to the finite difference technique of time domain (FDTD) method (Johnson, 1997; Coleman, 2005). However, relatively few studies were done in MR/PSTD. Here we present an MR/PSTD

method and apply it into the through-wall detection in three dimensional (3D) case. The Kirchhoff integration method is employed for electromagnetic field calculation from source region to receiving region in the air. The PSTD technique is employed for simulation in both of the entire single region, source and receiver scatter sub-regions as shown in Fig. 3.1. This model is uniform in the Z-direction, the 3-D model is sampled with 512 x 256 x 128 grids in X-, Y- and Z-directions respectively, at 4 mm spacing in all 3 directions in the numerical simulation. The source direction acting in the Z-direction is taken as a spatial point source function and time function of Ricker wavelet shape.

3.3 Kirchhoff Integration and Directional Kirchhoff Integration (DKI)

First, we briefly discuss how the DKI/MR/PSTD method is developed and implemented. Second, we describe the simulation results obtained by DKI/MR/PSTD. The comparison between a DKI surface and a circumferentially enclosed Kirchhoff surface is also presented. A series of single-region PSTD results are also presented for comparison with results from DKI/MR/PSTD. Upon the comparison, the improvements of DKI/MR/PSTD in both computation time and memory usage are discussed.

The first step for EM wave propagation simulation using MR/PSTD is to divide the whole domain into a number of sub-regions. Fig. 3.2 shows the sub-region separation technique for the model in Fig. 3.1 and the directional Kirchhoff integration surface for EM wave propagation simulation.

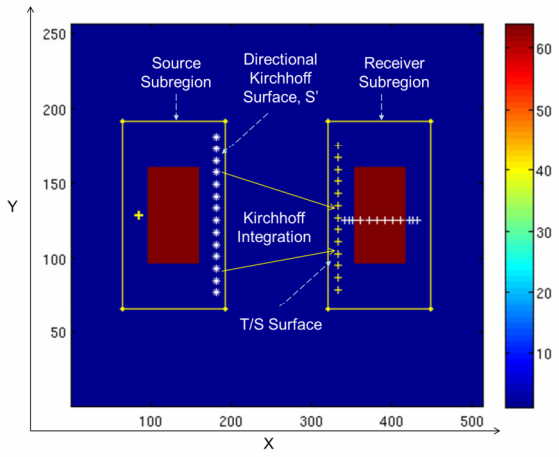

Figure 3.2 Sub-region setup as for the model in Fig. 3.1b (X-Y plane at Z = 65). Left yellow rectangular frame: source sub-region; right yellow rectangular frame: receiver sub-region; white asterisks:DKI surface; yellow crosses: secondary total scatter surface (T/S); yellow arrow line: Kirchhoff integration path; other symbols with same meaning as in Fig. 3.1b.

For the case discussed in detail in the following sections the whole computational domain is separated into two independent sub-regions, as shown in Fig. 2. The left sub-region, which includes the source, free area, and a scatter block, is called the source sub-region hereafter. The right sub-region, which includes free area, a scatter block, and all the receivers, is called the receiver sub-region hereafter. The boundaries of the two sub-regions are illustrated by solid yellow lines. The source in the source sub-region is located at the position of (85, 129, 65). In the receiver sub-region, a total scatter (T/S) surface is introduced as the secondary sources.

In most of the previous multi-region studies, Kirchhoff surface is set to circumferentially enclose all the sources and scatters in one sub-region. In order to distinguish the new Kirchhoff surface introduced in the present analysis, the Kirchhoff surface which circumferentially encloses the sources and scatters is called circumferentially enclosed Kirchhoff surface hereafter. However, in this study, only the Kirchhoff surface whose direction is pointing the receiver sub-region is selected to do the Kirchhoff integration calculation as shown in Fig. 3.2. The selected Kirchhoff

integration surface is called the directional Kirchhoff integration (DKI) surface hereafter. In Fig. 3.2, the white asterisks in the source sub-region represent the directional Kirchhoff surface in the Y-Z plane. The grid numbers of both sub-regions are 128 in all three directions.

The following MR/PSTD calculation procedures of EM wave field are used in each time step. The natural source in the source sub-region generates EM wave. The EM wave field is calculated by employing simulation with PSTD method in the source sub-region. When the EM wave field in the directional Kirchhoff interface as shown in Fig. 3.2 is obtained, Kirchhoff Integration along internal lines is used to evaluate the EM wave of the T/S field interface in the receiver sub-region. The T/S field interface in the receiver sub-region is used as the virtual source to simulate the EM wave propagation in the receiver sub-region using the discrete numerical PSTD method. Although the setup of Kirchhoff surface and T/S interface can be arbitrarily provided in the study region, the medium between Kirchhoff surface and T/S surface, however must be uniform, being air in this study. It should be noted that the procedures mentioned above can be iterated according to the interested time window length and the scattered wave phases related to study.

3.4 Simulation using MR PSTD with DKI Surface (DKI MR/PSTD) Method

We calculate electromagnetic (EM) wave field propagation in the model shown in Fig. 3.1 using the MR/PSTD with a directional Kirchhoff surface as shown in Fig. 3.2. The simulated results are shown in Fig. 3.3. In order to check the validity of the MR/PSTD method with directional Kirchhoff integration surface (DKI/MR/PSTD), we also calculate electromagnetic (EM) wave propagation in the model shown in Fig. 3.1 using the classical PSTD of whole study region. The time source function used in this study is the Ricker wavelet with an advantage frequency 1.0 GHz, and its lasting time is 2.4ns. The spatial source function is a point one locating at (85, 129, 65). The time step interval in this simulation is 0.002 ns. A total time window of 60 ns, which

equals to a total time step of 30000, is calculated. In each sub-region in Fig. 2, a recursive integration perfectly matched layer (RIPML) is used as the absorbing boundary conditions [14]. In order to identify the validity of the DKI/MR/PSTD method introduced by the present analysis Fig. 3.3 shows the Ez waveform obtained using PSTD of whole study region and DKI/MR/PSTD lasting 60 ns at Receiver 12 (431, 125, 65), which is locating at the right side of the scatter wall in the receiver sub-region as shown in Fig. 3.3. At this location, the Receiver 12 only records the EM waves penetrating scatters and propagating to the right air region in Fig. 3.1. The four large wave phases clearly displays the physical characteristics of EM wave propagation (Fig. 3.3). The wave series results simulated from DKI/MR/PSTD are coincided with those from the PSTD simulation in whole study region, completely. The arrival times and the shapes of the various wave phases, direct arrival wave, refraction wave simulated from DKI/MR/PSTD were coincided with the corresponding wave phases from the classic PSTD in whole region well. Such coincidences and the clear physical characteristics of the wave propagation analyzed above show that the DKI/MR/PSTD in the present analysis is valid for simulation of EM wave propagation.

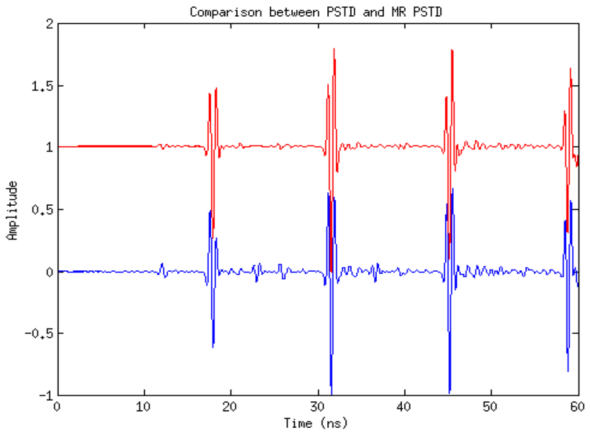

Figure 3.3 Comparison of Ez wave series from single-region PSTD (blue curve) and DKI/MR/PSTD (red curve) at (431, 125, 65).

Similarly Fig. 3.4 compares the normalized Ez waveforms obtained from the PSTD of the whole computational region and DKI/MR/PSTD method at Receiver 1 (341, 125, 65) in Fig. 3.2. The

receiver is placed on the left side of the scatter wall in the receiver sub-region. The four large wave phases exist in the waveform lasting 60 ns in Fig. 3.4. The first wave phase recorded in this receiver includes both the EM waves propagating from the source region and reflected by the scatter wall in the receiver sub-region in about 10 ns. The second, third and fourth waves include EM wave refracted out from right scatter wall in receiver sub-region, besides both the EM waves propagating from the source region and reflected by the scatter wall in receiver sub-region as mentioned in the first direct wave. The amplitudes of four wave phases got small with the time.

Very similar to the comparison result shown in Fig. 3.4 the results in Fig. 3.5 display the arrival times and the waveforms of the direct arrivals and refraction wave simulated from DKI/MR/PSTD were in agreement with those from single-region PSTD.

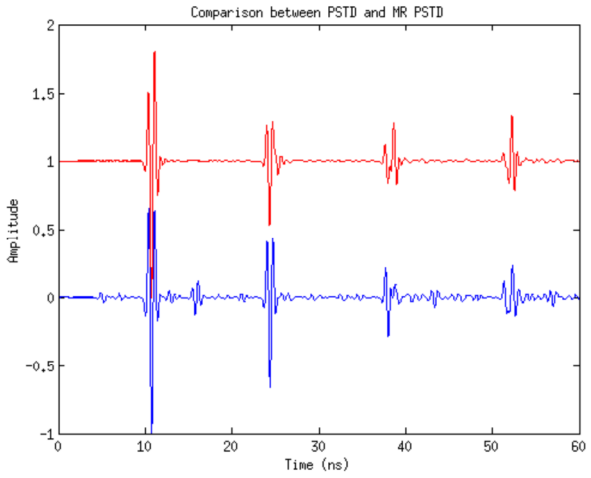

Figure 3.4 Comparing Ez waveforms from sing-region PSTD (blue curve) to that from DKI/MR/PSTD (red curve) at (341, 125, 65).

Clearly, for both cases in Figs. 3.3 and 3.4, not only the first direct EM wave arrivals, but also the EM waves reflected and refracted by the scatter boundaries in the receiver sub-region are successfully simulated by DKI/MR/PSTD method using a directional Kirchhoff surface. In order to verify the accuracy and the validity of the new method, Fig. 3.5 shows a comparison of waveforms of 60 ns for all the 12 receivers between the classical single-region PSTD and

DKI/MR/PSTD. In order to quantify the difference, the normalized root mean square deviation (RMSD) values are also provided. Let P(t) denotes the time series of PSTD result and M(t) denotes the MR/PSTD result. The normalized RMSD (NRMSD) of the PSTD result can be obtained by

$$RMSD(P) = \sqrt{\frac{\sum_{n=1}^{nt} (\bar{P} - P(t))^2}{nt}}$$
$$NRMSD(P) = \frac{RMSD(P)}{P(t)_{\max} - P(t)_{\min}} \tag{3.1}$$

And the NRMSD can be obtained in the same equations. Based on equation (3.1), the difference of NRMSD from the PSTD result to MR/PSTD can be determined by

$$NRMSD(P - M) = NRMSD(P) - NRMSD(M) \tag{3.2}$$

Figure 3.5 shows the PSTD result, DKI/MR/PSTD result and the NRMSD differences of all 12 receivers.

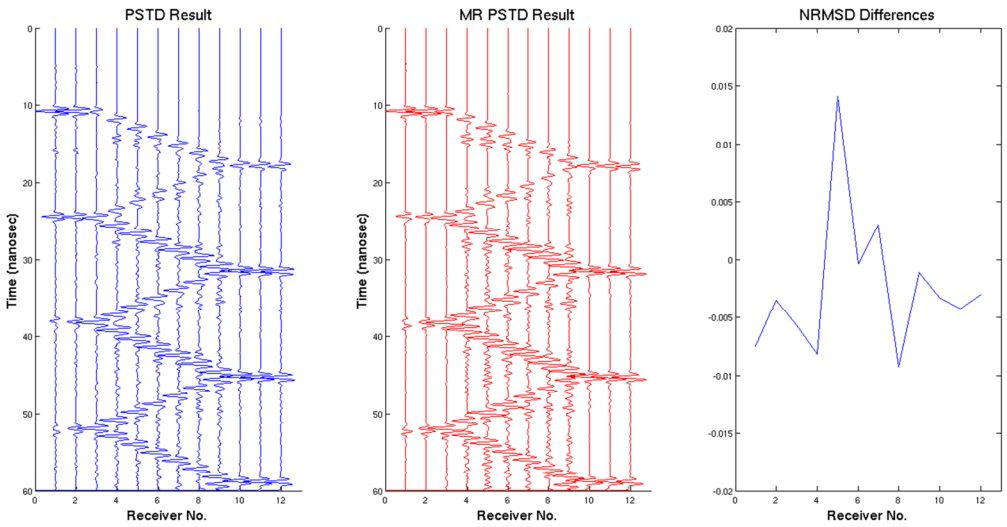

Figure 3.5 Comparison of time traces of EM wave from single-region PSTD and DKI/MR/PSTD method for all receivers. Left: PSTD results; center: DKI/MR/PSTD results; right: NRMSD differences.

It is clearly seen that both methods show clear multiple reflection and refraction series originated from the scatter boundaries. Receivers 1, 2, and 3 are located in the air region left of the scatter wall in the receiver region as shown in Figs.1 and 2. Receivers 10, 11 and 12 are located in the air region right of the wall in the receiver region. Other Receivers (4-9) are located in the right scatter wall where electromagnetic wave propagation velocity is taken as 1/8 (one eighth) of the velocity in vacuum. The dielectric constant is 64. The physical characteristics of electromagnetic wave propagation can evidently be seen from the results of DKI/MR/PSTD in Fig. 3.4. The first electromagnetic wave phase arrived in Receiver 1 at about 10.5 ns. The wave arrived rapidly in Receivers 2 and 3 because of the high speed of electromagnetic wave in the air. The arrival time difference between Receivers 1 and 3 can hardly be seen from the travel time curve in Fig. 3.5. The first reflection and refraction occurred as the wave propagated in the left boundary surface of the right wall in the receiver sub-region. The wave amplitude in Receivers 3 and 4 near both sides of the right boundary of wall was evidently weaker than the incidence at Receiver 1. Then the wave refracted into the right dielectric wall and passed through Receivers 4-9 sequentially. The

slope of arrival phase from Receivers 4 to 9 in the right dielectric wall got greater. Physical material property may be deduced from this phenomenon. Namely, the velocity from receivers 4 to 9 in the right dielectric wall is slower than that from 1 to 3 in the free region.

The electromagnetic wave amplitude also got gradually decayed from Receivers 1 to 9. The second multiple reflection and refraction occurred as the wave propagated in the right boundary surface of the right wall. It is noticeable that the two wave phases at Receiver 9 near the right boundary of the wall in the receiver sub-region occurred as time approaching 20 ns. The first one is the refraction wave from the left free region. The second one may be the reflection wave back into the dielectric block at the right boundary of the right wall. The interval between the two waves is very short because Receiver 9 is close to the right boundary of the right wall. At the same time, the wave penetrated the right boundary of the right wall and refracted into the air. The wave arrived in the Receiver 10 to 12. It is interesting that the penetrating refraction wave in Receiver 10 in the free region looks stronger than the corresponding reflected wave from Receiver 9 in the right dielectric wall. Seeing the wave propagation through the left boundary of the right wall, it is observed that the refraction wave amplitude appears to be weaker than the incidence one when the wave refracts into the dielectric block from the air. In contrast, the refraction wave amplitude looks greater than the incidence wave when the wave refracts into the air from the right dielectric block.

The first reflection wave occurring in the right boundary of the right wall propagated in the dielectric medium wall and passed through Receivers 9 to 4 sequentially in Fig. 3.4. When the first reflected wave arrived at the left boundary surface of the right wall the second refraction and reflection occurred again, similar to the first occurrence in the right boundary surface of right wall as motioned above. The multiple reflection and refraction occurred in the boundary surfaces of the right wall, totally six times as shown in Fig. 3.5. The wave series clearly display the physical

characteristics of EM wave propagation.

In order to assess the validity of DKI/MR/PSTD the simulation results for the wave propagation of the same model in Fig. 3.1 using single-region PSTD is also shown in Fig. 3.5. The waveforms simulated from DKI/MR/PSTD are completely superimposed with those from the classic single-region PSTD. The arrival times of several phases of direct arrival wave, refraction wave simulated from DKI/MR/PSTD were coincided with corresponding phases from the single-region PSTD. The shapes of the various wave phases from the DKI/MR/PSTD are also closely coincided with those from single-region PSTD. Even the wave amplitude variation properties with time from DKI/MR/PSTD in Receivers 1 and/or 2 in Figs. 4 and 5 also coincided with those from single-region PSTD. Such coincidence of physical characteristics of the wave propagation analyzed above shows the DKI/MR/PSTD introduced in the present analysis is valid for simulation of EM wave propagation.

In mathematics, the normalized root mean square (RMS) deviation is a frequently used value to measure the differences between two signals. In this model, the NRMSD differences of all 12 receivers are between -1% and 1.5%. It is a good evidence to prove that the DKI/MR/PSTD method simulated the waveforms with satisfactory accuracy as the traditional PSTD method.

3.5 Memory Cost and the Advantage of MR/PSTD over MR/FDTD

In addition to the calculation time cost, the memory cost is also an important aspect to evaluate the efficiency of MR/PSTD. One big advantage of MR/PSTD is that MR/PSTD has very efficient usage in memory. It is not only superior to the traditional whole domain PSTD method, but also superior to MR/FDTD.

The memory usage in MR/PSTD is different from the memory usage in a pure whole region PSTD code. In a pure whole region PSTD code, the total memory usage is not related with the time window length or the total time step. It is only related to the spatial grid numbers. It means that the memory usage does not increase with the increase of time window length. However in an MR/PSTD code, because the algorithm is related with retardation time, some variables' values have to be restored for later usage in each time step. The increase of time window length can significantly increase the total memory usage.

The variables used in an MR/PSTD code can be classified into 3 types. The first type, which is called three-dimensional (3D) variable thereafter, is three-dimensional variables in each sub-region. For example, Ex, Ey and Ez variables in each sub-region, they require 3D memory storage. The second type, which is called two-dimensional (2D) variable number, is two-dimensional variables in each sub-region. For example the Kirchhoff surface and RIPML element locations, they require 2D memory storage. The memory usage of 3D and 2D variables is purely related with the spatial grid numbers, but not with time window length. The third type variable, which is called time variable thereafter, is related with the time window length. For example the Ez values in the Kirchhoff surface and T/S interface of each sub-region, the values of those variables have to be restored at each time step for later reference. Table 3.1 shows the total number for each variable type in source and receiver sub-regions. As a comparison, the variables in a classical PSTD algorithm of the whole computation domain is also listed in tab. 3.1,

Table 3.1 Variable classification

	nx, ny, nz	3D variable number	2D variable number	Time variable number
Source Sub-region	128, 128, 128	39	4	3
Receiver Sub-	128, 128,	39	4	3

region	128			
Classic PSTD, whole domain	512, 256,128	39	4	None

Fig. 3.6 illustrates the memory cost in different types while the time window length increases.

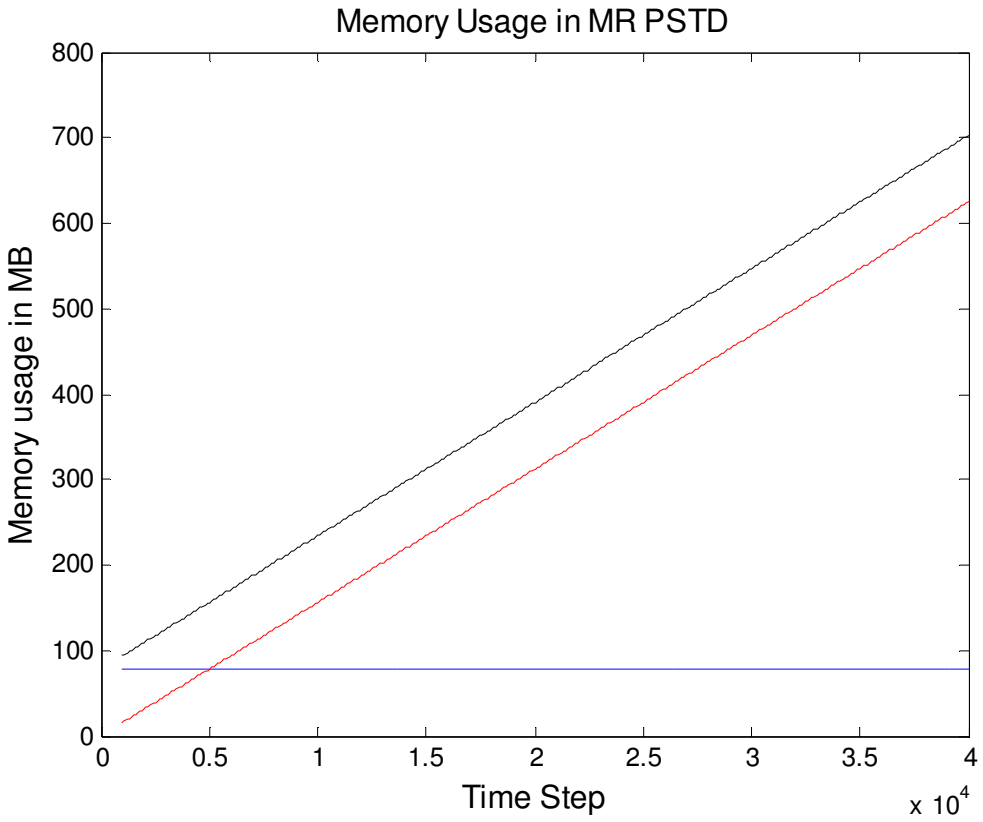

Figure 3.6 Memory usage variation with the calculation time window length according to different variable types in MR/PSTD. Black line： total memory usage; red line ： time variable memory usage; blue line: 3D and 2D memory usage.

Blue line in Fig. 3.6 shows the memory usage variation with the calculation step for 3D and 2D variables. Red line in Fig. 3.6 shows the memory usage of the time variables. The total memory usage is illustrated in Fig. 3.6 using a black line. Fig. 3.6 clearly shows that as the time step increases, the memory usage is dominated by the time variables. In this research, at the time step of 5000 the time variable memory usage becomes larger than the memory usage of 3D and 2D variables. The memory usage of time variable when time step is 30000 is 468 mega bytes(MB),

much greater than the 3D and 2D variable memory usage, 78MB, which is independent of the time step. Although the time window length can significantly influences the memory requirement, it is still much more efficient in memory usage than a classical PSTD method. In the present analysis, the memory usage of a classical PSTD method of the whole computational domain is 2.6GB. Although not increasing with the time window length, the memory cost in the classical PSTD method of the whole computation domain is still much more than the memory usage of an MR/PSTD algorithm.

The time variable memory cost is not only related with the time step, but also with Kirchhoff surface element number. In general the time variable memory cost is proportional to the product of the time step number and the Kirchhoff surface element number. The Kirchhoff surface element number can be classified as a 2D variable. In an MR/PSTD algorithm, the PSTD algorithm inside of each sub-region allows the Kirchhoff surface element number to be much smaller than that of a MR/FDTD algorithm, consequently the MR/PSTD algorithm requires much less memory cost than that of MR/FDTD. In an MR/FDTD algorithm, the grid sizes of a sub-region usually are set to be 5% of the shortest possible wavelength inside of that sub-region. In an MR/PSTD algorithm, the grid sizes of a sub-region can be set to be 25% of the shortest possible wavelength. It means that in a same real physics problem, the FDTD grid numbers in X, Y and Z direction are 5 times greater than the PSTD grid numbers. Consequently the Kirchhoff surface element number in an MR/FDTD algorithm might be 25 times greater than the surface element number in an MR/PSTD algorithm. The memory usage of the 2D variables and time variables in FDTD is also increased at the same scale. In general, the memory usage of 2D variables and time variables in an MR/PSTD algorithm is not more than 20% of that in an MR/FDTD method. Provided that our research interests are focused on the reflected EM waves after the first arrivals, the time window length has to be prolonged. Consequently the memory usage of the time

variables becomes the main part of the memory usage in the whole algorithm. It means that an MR/PSTD can be expected to save 80% memory usage than an MR/FDTD method.

3.6 Conclusions

A technique of 3D MR/PSTD with directional Kirchhoff integration surface (DKI/MR/PSTD) is introduced in this chapter. An application in through-wall detection was performed successfully. The directional Kirchhoff surface is different from the general circumferentially enclosed Kirchhoff integration surface. In general the Kirchhoff integration method is based on the Huygens's principle and the concept of Green's function. Huygens's principle is a widely used physical principle and in any concrete numerical simulation problem. However, in a concrete physical problem, the Kirchhoff integration surface should be selected carefully to satisfy the basic assumption that the integral path must remain in the uniform media. In the study illustrated in this chapter, the Kirchhoff integral path must remain in the air.

The results obtained from the parallel 3-D simulation show a good evidence for the validity of DKI/MR/PSTD in this study on the through-wall detection. The latter EM waveforms and phases can clearly be simulated by employing DKI/MR/PSTD besides the first wave phase. This is difficult for MR/PSTD circumferentially enclosed Kirchhoff integration surface in the source sub-region with the heterogeneous scatter wall. The physical characteristics of the later reflection waves and refraction waves in the multi-refraction and reflection EM wave series were clearly simulated. The EM waveforms simulated from DKI/MR/PSTD coincide well with those from the classical single-region PSTD. The arrival times and amplitudes of various wave phases simulated from DKI/MR/PSTD coincide well with those from the PSTD of whole study region also. Further more the ratio of signal to noise (SNR) in the EM waveform graph simulated by DKI/MR/PSTD

is higher than those by the PSTD of whole study region. It is attributable that the complicated discrete numerical differentiation calculation (e.g., PSTD) is replaced by the Kirchhoff integration calculation in the wide air region. The high ratio of signal to noise of the new DKI/MR/PSTD method introduced by the present analysis imply that the findings of EM wave propagation simulation with further high accuracy and stability will be expected.

With satisfactory results, DKI/MR/PSTD can reduce both the computation time and memory usage substantially. In this study, the computation time of MR/PSTD is less than 1/3 of the classical single-region PSTD and the memory requirement is about one half of the classical PSTD. With a consideration that the two sub-regions are relative large in this study, the efficiencies are satisfactory.

Compared with the DKI/MR/FDTD when computing the same frequency EM wave propagation, the grid size of PSTD can be set larger than FDTD to reduce the grid number of every sub-region. It does not only save the PSTD computation time in sub-regions, but also the total calculation time and memory cost of Kirchhoff Integration because the memory usage of Kirchhoff is directly related with the surface grid numbers. In addition, because PSTD can be easily extended to two and half dimensional (2.5D) problems, DKI/MR/PSTD can also be extended to some 2.5D problems.

Directional Kirchhoff integration and DKI/MR/PSTD method successfully extend the MR/PSTD method to the simulation of the waveforms after the first arrivals with great computational efficiencies in both computation time and memory cost. However, the contribution is not confined in the waveforms. The DKI/MR/PSTD method makes the inner structure study of a certain physical body possible because the inner structure imaging of a certain physical body largely depends on the full waveform simulation. Consequently, it is highly desirable to apply the

DKI and DKI/MR/PSTD methods into a real reflection model because the reflection model is by far the most popular model in inner structure imaging.

Chapter 4. Model Subtraction Method and Human Internal Structure Imaging

4.1 Introduction

Most research works of Multi-region and Kirchhoff integration are concentrated on the transmission model (Johnson, 1997; Bernardi, 2002; Coleman, 2005). However, high fidelity simulation of multiple reflections and refractions is very necessary in many practical reflection problems. Especially when considering a real inner structure imaging problem which often involves migration and/or inversion techniques, the forward modeling of the reflections and refractions for a reflection model is an inevitable step. The purpose of this chapter is to apply the DKI/MR/PSTD method, which was proved to be a very robust weapon in full waveform simulation in Chapter 3, to some real reflection model. By successfully applying the DKI/MR/PSTD the forward modeling of some real, long-distance reflection models could be performed with much better efficiency. In addition DKI/MR/PSTD method can be applied to some extremely long, sometimes astronomical distance reflection simulation problem which was impossible to the traditional PSTD method due to the memory cost in computation.

The biggest problem in the forward modeling of a real 3D reflection model using DKI/MR/PSTD is that the setup of the DKI/TS interfaces naturally introduces strong artifacts, which will be called DKI/TS artifacts hereafter. The DKI/TS artifacts can be both earlier and much stronger than the real reflected wave field. Consequently the true reflected wave field are overwhelmed by the artifacts and become hardly to identify. In order to apply the Multi-region and Kirchhoff

integration methods in to real reflection simulation problems, a model subtraction method is introduced into this research. The basic idea is to introduce a secondary supplementary free space model with the same set up in grid number, grid interval, time interval, time window length, sources and receivers. All computational setup are identical to the original model, the only difference is that the media is a free space without any scatters. A second supplementary free space simulation is performed with this free space model to get the pure DKI/TS artifacts caused by the DKI/TS interfaces in reflection model. Then the DKT/TS artifacts will be subtracted from the traces obtained using the original model to get the true wave field scattered by the physical object. Although one more free space simulation needs to be performed, considering the computation cost in the long-distance, sometimes can be astronomical distance numerical simulation, the computation efficiencies in both time and memory cost can still be drastically improved. In addition, the computational cost of the model subtraction method only depends on the setup of a sub-region. It makes the long distance simulation, sometimes impossible in the traditional PSTD method, not only possible but still accurate enough in the inner structure imaging.

4.2 Model Subtraction Method

Fig. 4.1 is a 2D illustration of the 3D human body reflection model, a typical MR/PSTD application problem for electromagnetic wave reflection. There is one 3D heterogeneous human body who serves as the scatter, and the rest of the whole computation domain is the uniform media, air. The volume of the whole computation domain is 512x128x512 grids in X, Y and Z directions respectively. The spacing intervals in all 3 directions are the same 4 mm in the numerical simulation. The dielectric constant of air is 1, and the human body has a dielectric constant range from 32 to 52. The source generating electromagnetic wave field is located at (256,

64, 256), right of the human body, and the source direction acting in the Z-direction is taken as a spatial point source function and time function of Ricker wavelet shape. All the 15 receivers are also located right side of the human body. The velocity of electromagnetic wave in the air is taken as that in the vacuum approximately, and the electromagnetic wave propagation velocity in the human body is in a range of between 1/7 and 1/5 of the velocity in vacuum approximately. Fig. 4.1 shows the section of X-Z slice plane at Y= 64, All 15 receivers locates along the line of X=375 and Y=64. . The yellow asterisk and white plus signals illustrate the natural source of and the receivers, respectively.

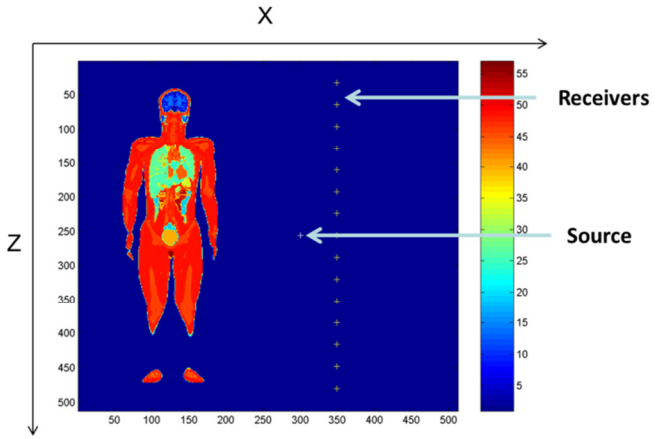

Figure 4.1 A 2D slice of the 3D reflection model in X-Z plane at Y=64. Yellow plus: receivers; white plus: source; color bar: dielectric constant scale.

In the model shown in Fig. 4.1, the volume occupied by the human body is relative small compared with the entire study region. An MR/PSTD method is considered to improve the computation efficiency as mentioned above. Both the source and all the receivers are located at the right of the human body. This is a typical reflection simulation problem. A number of MR/PSTD and multi-region finite difference technique of time domain (MR/FDTD) method have been introduced and extensively used in a variety of real problems, (Bernardi, 2002; Laisne, 2000; Ramahi, 1997). However, relatively few studies were done in the multi-region application in concentrating on the heterogeneous media reflected waveforms simulation after the first

arrivals. Here we present a model subtraction method with MR/PSTD algorithm and apply it into the human body reflection in three dimensional (3D) case. A directional Kirchhoff integration (DKI) method is applied in the electromagnetic field calculation from the sub-region to the receivers in free space. After the model subtraction, a pure and full reflection wave field generated by the human body, with all late wave phases will be obtained. The obtained full reflection wave phases caused by the heterogeneous 3D human model will make the detailed 3D imaging of the human body possible.

4.3 Numerical Reflection Simulation Results

First, we briefly discuss how the model subtraction method is developed and implanted in a DKI/MR/PSTD algorithm. Second, we describe the simulation results obtained from a human body sub-region by DKI/MR/PSTD. The comparison between a free space sub-region waveform and human body sub-region wave form using DKI/MR/PSTD is also presented. Upon the comparison, a model subtraction method is introduced. A human body reflection waveform is presented. Finally why the model subtraction method is necessary in the reflection problem, and the advantages of the model subtraction method using a DKI/MR/PSTD algorithm are discussed.

The first step for EM wave propagation simulation using MR/PSTD is to divide the whole domain into some reasonable sub-regions. Fig. 4.2 shows the sub-region separation technique for the model in Fig. 4.1.

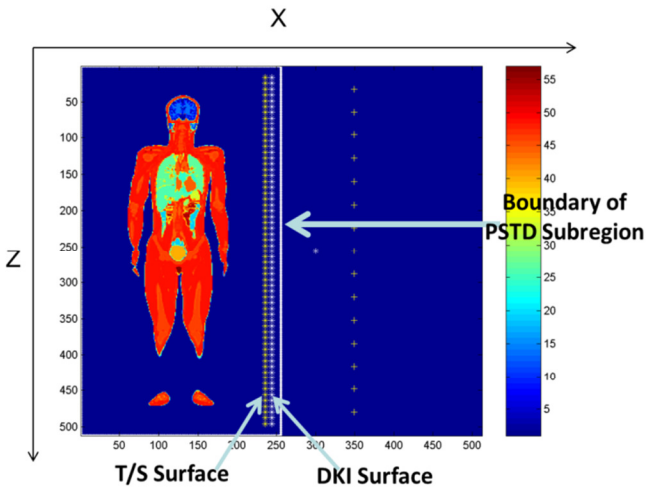

Figure 4.2 Sub-region setup as for the model in Fig. 4.1. A 2D slice of the 3D sub-region setup at Y=64; white rectangular frame: human body sub-region; white crosses:DKI surface; yellow crosses: virtual total scatter surface (T/S).

For the case discussed in detail in the following sections, the left half of the whole computational domain is separated into one independent sub-region, which is called human body sub-region hereafter, as shown in Fig. 4.2. The grid size of the human body sub-region is 256x128x512. The human body sub-region includes a 3-D human body model with no source or receiver. The rest of the computational domain is all air. All source and receivers are located in the air, out of and at the same right side of the human body sub-region. The boundary of the human body sub-region is illustrated by solid white lines. A point source located at (300, 64, 256) is used in this model. A total scatter (T/S) surface is introduced as the virtual sources inside of the human body sub-region at the plane of X= 236, and a directional Kirchhoff integration (DKI) surface is set at the plane of X=240. In Fig. 4.2, the white points in the source sub-region represent the directional Kirchhoff integration (DKI) surface, and the yellow points represent the T/S surface.

The following DKI/MR/PSTD calculation procedures of EM wave field are used in each time step. The natural source in the free space generates EM waves first. The EM wave field is calculated by employing the Kirchhoff integration from the natural source to the virtual T/S

surface in the human body sub-region as shown in Fig. 4.2. Then a staggered-grid parallel 3D PSTD algorithm is used in the human body sub-region with the T/S surface as the virtual sources. When the EM wave simulated by the T/S surface reaches the directional Kirchhoff integration surface either directly or after reflections and refractions by the human body, a Kirchhoff integration is performed along the DKI to the outside receivers. The setup of the DKI surface and the T/S surface can be arbitrary provided in the study region, both the medium between the natural source to the T/S surface, and the medium between the Kirchhoff integration surface and the receivers must be uniform media. In this study, the medium is air.

In a reflection problem using a DKI/MR/PSTD, besides generating the wave propagating to the left, toward the human body sub-region, the virtual sources locating at the T/S surface also generates wave propagating to the right symmetrically. The wave propagating to the right will arrive at the DKI surface directly and be integrated back to the receiver first. Consequently the first arrivals obtained in the receivers are the right-propagating waveforms generated by the T/S surface. The left-propagating EM wave generated by the T/S surface will be reflected and/or refracted by the heterogeneous human body, and only the EM waves reflected back by the human body will arrive at the Kirchhoff integration surface and be integrated to the receiver. Obviously the human body reflection waves reach the DKI surface and the receivers later than the right-propagating EM waves. The waveforms directly obtained in this DKI/MR/PSTD algorithm are a combination of the right propagating wave generated by the T/S surface, and the wave multi-reflected by the human body.

However, the right-propagating waves caused by the T/S surface, which is called the DKI/TS artifacts hereafter, are not physically existing waves and should not be of our research interests. Only the wave left-propagating from the T/S surface and reflected by human body, which is called human body reflection wave field hereafter, is physically correct and of our research

interests. The key point of the reflection model simulation using DKI method is how to remove the DKI/TS artifacts. After removing the DKI/TS artifacts, a pure and full reflection wave field caused by the human body will be available.

In order to remove the DKI/TS artifacts and to obtain the human body reflection wave field, a model subtraction method is introduced in this study. The basic idea is to set a second assistant free space sub-region model. It has the identical grid spatial sizes, grid numbers and identical source and receiver locations. It also has the same sub-region setup as shown in Fig. 4.2. The DKI and T/S surfaces keep exactly the same places as illustrated in Fig. 4.2. The only difference from the human body sub-region model in Fig. 2 is that there is no scatter inside the sub-region. The sub-region is totally a free space. Because there is no scatter inside of this free space sub-region, no human body reflection wave field will exist and be recorded by the receivers after the directional Kirchhoff integration. The only waveform obtained from this free space sub-region model is the right-propagating wave generated by the T/S surface, the DKI/TS artifacts. Because the free space sub-region model is totally identical with the human body sub-region model at the right side of the T/S surface, the DKI/TS artifacts obtained in these two models are also identical to each other. The only wave field difference between the human body sub-region model and the free space sub-region model is the human body reflection wave field. Consequently, the human body reflection wave field can be obtained by subtracting the free space sub-region waveforms from human body sub-region waveforms. After the subtraction, a pure human body reflection wave field is obtained. Fig. 4.3 illustrates the basic ideas of the second assistant free space model and the model subtraction method.

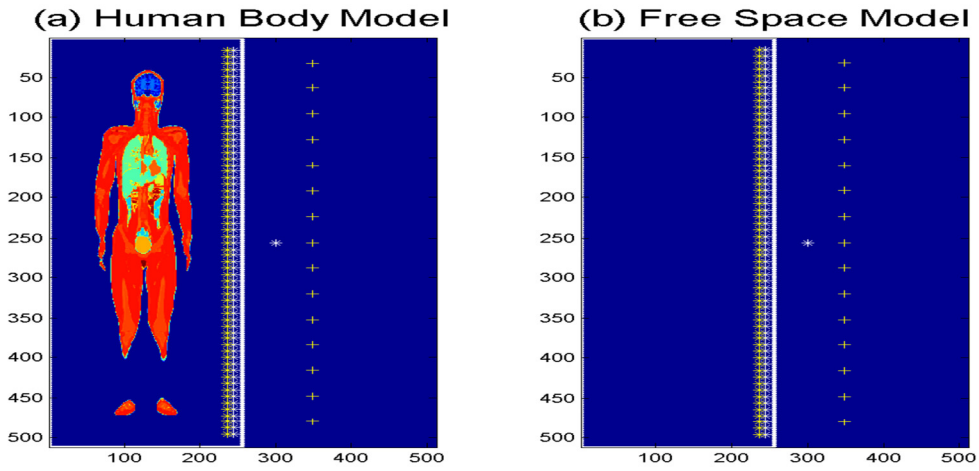

Figure 4.3 Illustration of the basic idea of the model subtraction method. (a) human body model setup; (b): Free space model setup.

Simulations will be performed using both models respectively. Consequently two sets of simulated waveforms will be obtained. After subtracting the free space model waveforms, in fact the DKI/TS artifacts, from the human body model waveforms, the human body reflection wave field will be obtained.

We calculate the electromagnetic (EM) human body reflection wave field of the model shown in Fig. 4.3 using the model subtraction method with a DKI/MR/PSTD algorithm. First, the waveform of the human body sub-region model is obtained using the DKI/MR/PSTD method. This waveform is called human body sub-region waveform hereafter. The human body sub-region waveform is illustrated in Fig. 4.4a. The waveform of the free space sub-region obtained using the DKI/MR/PSTD algorithm, which is called free space sub-region waveform hereafter, is also illustrated in Fig. 4.4b. Free space sub-region waveform in fact is the DKI/TS artifacts. After subtracting the free space sub-region waveform from the human body sub-region waveform, a pure human body reflection waveform is obtained and illustrated in Fig. 4.4c. Fig. 4.4 compares the normalized human body sub-region waveform, normalized free space sub-region waveform

and the normalized pure human body reflection waveform of all receivers illustrated in Fig. 4.3. As a comparison, the waveforms obtained using a single-region PSTD algorithm is illustrated in Fig. 4.4(d).

The time source function used in this study is the Ricker wavelet with an advantage frequency 1.0 GHz, and its lasting time is 2.4ns. The spatial source function is a point one locating at (300, 50, 256). The time step interval in this simulation is 0.002 ns. A total time window of 20 ns, which equals to a total time step of 10000, is calculated. A recursive integration perfectly matched layer (RIPML) is used as the absorbing boundary conditions [15] in human body sub-region, free space sub-region and the single-region PSTD simulation. Although the traces of the human body model obtained using a DKI/MR/PSTD in Fig.4.4 (a) are quite different from the waveforms obtained using a single-region PSTD method in Fig. 4.4(d), the traces after model subtraction in Fig. 4.4(c) look very similar to the forms using a single-region PSTD method in Fig. 4.4(d).

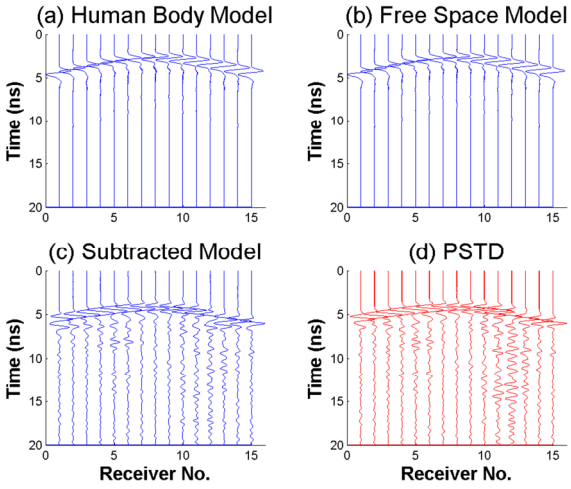

Figure 4.4 Illustration of the traces obtained using the model subtraction method. (a): traces of the human body model setup; (b): traces of the free space model setup, in fact the DKI/TS artifacts; (c): traces after subtracting free space model traces from human body model traces; (d): traces obtained using a single-region PSTD method.

In Fig. 4.4b, the receivers recorded traces even in the free space model. As illustrated in Fig.

4.3(b), there should be no traces recorded back because it is a free space model. Obviously the traces are all DKI/TS artifacts. In addition, the human body waveforms in Fig. 4.4(a) look quite similar to the free space model waveforms, but quite different from traces obtained using the single-region PSTD method in Fig. 4.4(d). They are good evidence to prove that the T/S surface in Fig. 4.2 generating right-propagating DKI/TS artifacts as well as the left-propagating waves. The DKI/TS artifacts generated by the T/S surface reaches the DKI surface first and is integrated back to the receivers earlier than the human body reflection waves. The DKI/TS artifacts have shorter travel distances than the human body reflection wave, and the DKI/TS artifacts do not lose energy due to reflection. Consequently the right-propagating DKI/TS artifacts generated by the T/S surface are integrated back to the receivers earlier and have much greater amplitude. The human body reflection waves are totally overwhelmed and can be almost invisible in Fig. 4.4(a). However, the right-propagating DKI/TS artifacts are totally due to the introduction of the T/S surface as the virtual sources inside of the sub-region. It can be easily simulated with the introduction of a secondary assistant free space model and model subtraction method. After model subtraction, the true waveforms reflected back by the human body itself are precisely obtained.

Fig. 4.4 (c) and Fig. 4.4(d) illustrate the simulation results using DKI/model subtraction method and the single-region PSTD method respectively. Clearly the travel time curves in Fig. 4.4(c) and Fig. 4.4(d) coincide to each other very well. Both results have not only the EM wave reflected by the human body surface, but also the EM wave multi-reflected and/or multi-refracted by the inner structure of the human body. The travel time curve of Fig. 4.4(c) and Fig. 4.4(d) are later than those of Fig. 4.4(a) and Fig 4.4(b) because they are true travel time curve of the human body. The wave fields in Fig. 4.4(c) and 4.4(d) are complicated and suggest that a scatter might be existing. Receiver No. 4, 5, 9, 10 and 11 have more complicated traces because they are facing some parts, arms and legs which have more complicated structures. Consequently the traces of receiver No. 4,

5, 9, 10 and 11 have more late arrivals. The author is using the same linux machine with 8 cores and 64 GB memory to finish the simulations. It takes about 15 hours and 2.5GB memory to finish one DKI sub-region simulation, and 32 hours and 4.8GB memory to finish the single-region PSTD simulation. With the similar results, the DKI/MR/PSTD simulation using model subtraction method has much better efficiencies in computation time and memory cost.

4.4 Plane Wave Reflection Imaging

Reflection model has its unique importance in real physical problems. Most real inner structure imaging problems, usually related to some migration and tomography use reflection model. Various researches have been proposed to get vivid images from reflection model (Shapiro, 1981; Eisenbei, 1999). As the basis of the imaging problem, the simulation of reflection models is also of various research interests.

From this part, the model subtraction method using DKI/MR/PSTD algorithm will be extended to some subsurface imaging discussion. A 3D model is illustrated in Fig. 4.5. The grid size of the whole computation domain is 4mm in all 3 directions. The sub-region size in Fig. 4.5 is 128x256x512 in grid number, and 0.512x1.024x2.048 in meters. A series of sources and receivers are placed at a relatively distant location, at the plane of X=375 in grid number and 1.5 meters. A series of sources generating the same signal to simulate a flat plane incident waves is used. There is one source and one receiver in every 4x4 grids locating at the plane of X=375. Totally 7320 sources and 7320 receivers are used in this simulation. All sources are generating the same Ricker wavelet signal simultaneously with a dominant frequency of 1.0G Hz. The time interval in this simulation is 0.002ns, and a total time window is 24ns. The DKI surface locates at the plane of X=116 in grid number or 0.464m in distance from left, and the T/S surface locates at the plane of X=112 in grid umber or 0.448m in distance from left. A flat block with a relative dielectric

constant of 64 is used in this model. The electromagnetic wave propagation speed is 1/8 of the speed in vacuum. The block has a thickness of 48 in grid number, from X= 33 to X= 80, which means a thickness in 0.192m. This model is uniform in y direction.

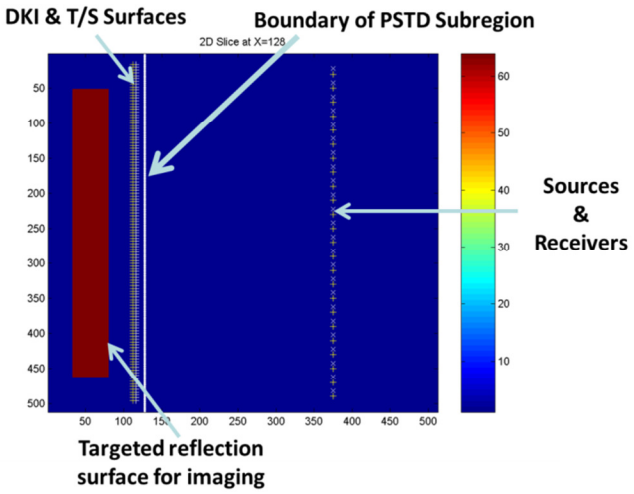

Figure 4.5 Illustration of the 2D slice, of the 3D flat incident wave reflection model. The horizontal direction: x, the vertical direction: z.

The model in Fig. 4.5 is a typical reflection model. It should have a plane wave reflected by the border of the block, and may have other multi-reflected waves caused by the block. Fig. 4.6 illustrates the simulated reflected waveforms obtained at location of (375,128,256), (1.5m, 0.512m, 1.024m) after normalization. As a simulation of flat-plane incident wave reflected by a flat plane, all receivers have similar waveforms.

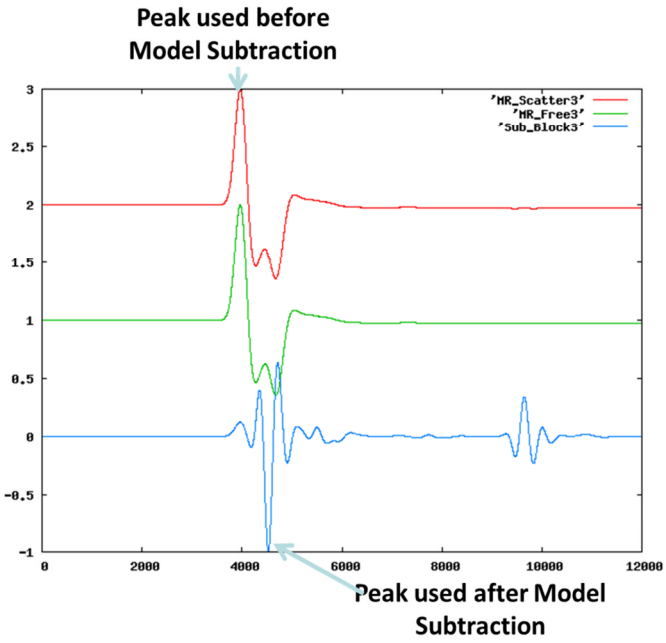

Figure 4.6 Illustration of the waveform obtained at (375, 128, 256). Red line: waveform obtained using the block model; Green line: waveform obtained using the free space model, in fact the DKI/TS artifacts; Blue line: waveform obtained after the model subtraction.

It is clearly that in Fig. 4.6, two wavelets can be found in the trace after model subtraction. The two wavelets are caused by the front and back surfaces of the block in Fig. 4.5 respectively. Only one wavelet can be found in Fig. 4.6 before model subtraction because the DKI/TS artifacts have much stronger amplitude than the wave reflected by the block. The block reflection waves are totally overwhelmed. The amplitude peaks of traces before model subtraction and after model subtraction are used to determine the reflection surface. As a simple plane incident wave simulation, the reflection surface can be determined easily. Fig. 4.7 compares the imaged surface using peaks before and after model subtraction.

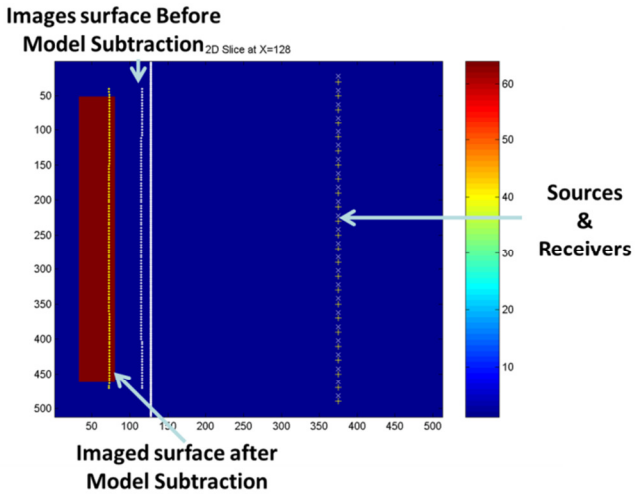

Figure 4.7 Illustration of the 2D slice of determined reflection plane at the plane of Y=128.

Clearly the imaged surface after model subtraction gives the satisfactory location of the reflection surface. The targeted reflection surface of the block locates at X=80, and the imaged reflection surface after model subtraction is at X=74. The difference between the original model and the imaged surface is 6 in grid number and 0.024m in distance. This difference is reasonable because the peak was used for imaging in Fig. 4.6, and the waveform has a clear phase change compared with the original Ricker wavelet. The difference might be caused by the phase change during the wave propagation and is expected to be mitigated with a zero-phase filter. However, before model subtraction the imaged surface is at X = 114. It is approximately the location of the T/S surface of X = 112 but far from the true location of the block surface at X=80. Clearly the main phases before model subtraction are the DKI/TS artifacts. In addition, the amplitude peaks of the two wavelets after subtraction in Fig. 4.6 are used to determine the thickness of the block. The amplitude peaks of the two wavelets after subtraction in Fig. 4.6 locate at nt = 4526 and 9646 respectively. The time difference between these two peaks gives a block thickness of 0.192m or 48 in grid number, which is perfectly matching the model setup. However, there is only one peak could be found in Fig. 4.6 before model subtraction because the DKI/TS artifacts are much stronger than the true reflected wave field. The true reflected wave field is overwhelmed and can

hardly be identified. This reflection model is very simple, but it successfully suggested that after the model subtraction, the DKI/MR/PSTD method might be extended to some real imaging problems.

One more 3D model is used to test the possibilities of extending the model subtraction method to real imaging reflection model. As illustrated in Fig. 4.8, a heterogeneous 3D human body model is used. This model is complicated and more realistic. It has same grid setup as Fig. 4.5. The locations of all sources and receivers, DKI and TS interfaces are all identical to the setup of Fig. 4.5. The only difference is that inside of the sub-region, a complicated 3D human body model is used. Fig. 4.8 is the illustration of the plane at y=116, a little apart from the central part of the human body.

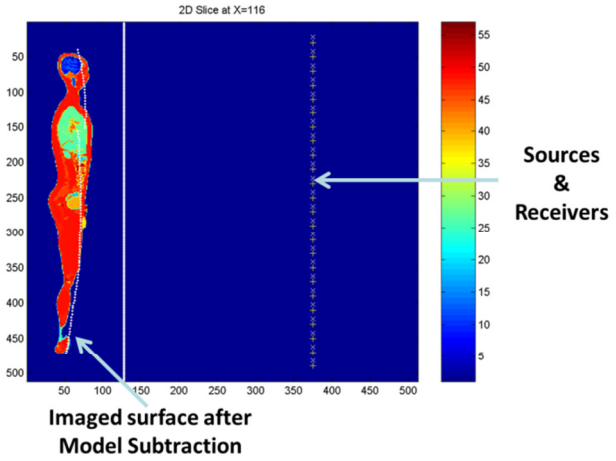

Figure 4.8 Illustration of the 3D heterogeneous human body model and the imaged surface after model subtraction at Y=116.

The imaged surface before model subtraction is omitted because the wave field has strong DKI/TS artifacts. The imaged surface before model subtraction has exactly the same results as that illustrated in Fig. 4.7. Not only the determined surface using the peak before subtraction in

Fig. 4.5 is away from the human body, but also is a plane – which obviously is not natural. However, the imaged surface after model subtraction gives an approximated curve of the human body. The imaged surface after model subtraction offers both the approximately correct location and human body curve. It can be expected to have more accurate results if the model subtraction method could be combined with better imaging techniques, for example, the stack and/or migration techniques.

4.5 Multi-offset Simulation and Kirchoff Migration Results

In this part, the model subtraction method using DKI/MR/PSTD algorithm will be extended to the Kirchhoff time migration discussions. The Kirchhoff pre-stack time migration (Margrave, 2003), is used to verify that the simulated traces obatined by model subtraction method using DKI/MRI/PSTD algorithm can be successfully imaged to determine the humanbody subsurfaces. Migration is an extensively used techinique in subsurface imaging. It removes the dipping reflections to there true subsurface positions. Migration also collapses diffractions and increases the spactial resolution to create the subsurface image. Migration techiniques are more extensively used in seismic subsurface image, but it can also be used in the EM wave subsurface imaging. There are a lot of migration techinques. Among the different migration techniques Kirchhoff migration (KM) and reverse time migration (RTM) are the most extensively used. Migration techniques can also be applied into the time domain or depth domain, and are called as time migration or depth migration respectively. In most cases migration techniques are related to stack. If the trace gather are migrated before migration, it is called a pre-stack migration. If the trace gathers are migrated after migration, it is called a post-stack migration. Pre-stack migration has better result in final image, but it requires much more computational resources. Post-stack migration can save a lot of computational resources because it needs only one migration, but it

does not offer so accurate images as pre-stack migration. Nowadays as the computational resources are improved essentially than before, pre-stack migration becomes more popular.

In this research, a Kirchhoff pre-stack time migration (PSTM) technique are used in the EM wave subsurface imaging. Kirchoff migration has a good reputation in that it can provide a good image with reasonable requirements on computational resources. Among all migration techniques, RTM has the best image results but it makes the numerical computation much more intensive. A 3D human body model illustrated in Fig. 4.8 is used to perform the Kirchhoff PSTM research. Fig. 4.9 shows the same 3D human body model in meters. In order to verify that the model subtraction method is correct and necessary, both the traces before model subtraction and after model subtraction are migrated and compared.

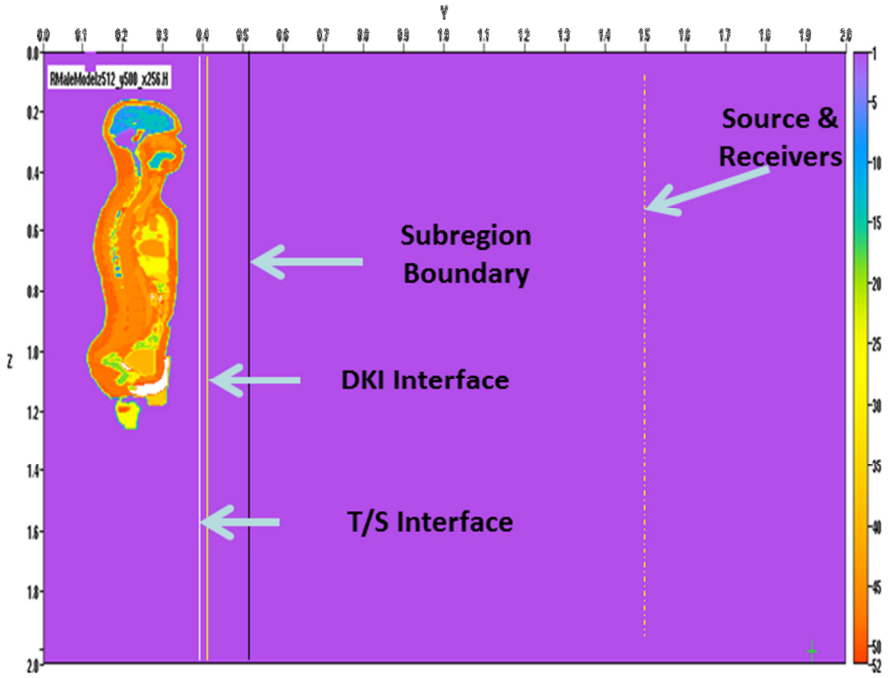

Figure 4.9 A 2D slice of the 3D Human body model in meters. At the plane of y=128 in grid number and 0.512m in meters.

The steps to perform the Kirchhoff PSTM test are as follows,

1 In order to perform the Kirchhoff PSTM, a multi-offset simulation is performed using the model subtraction method using DKI/MR/PSTD algorithm. Fig. 4.9 is the setup of the simulation, a series line of sources and receivers along the line of x=0.512m and y=1.5m are placed. Totally 64 sources are placed along the line of x=0.512m and y=1.5m. The first source locates at z=0.032m, and the last source locates at z=2.048m. The space interval of the sources is 0.032m. Totally 125 receivers are placed along the line of x=0.512m and y=1.5m. The first receiver locates at z=0.016m, and the last receiver locates at z=2m. The space interval of the receivers is 0.016m.

2 One forward modeling using model subtraction method with 3D DKI/MR/PSTD is performed for each source with all 125 receivers. One trace gather after model subtraction (model subtracted trace gather, hereafter) is obtained for each source. Totally 64 model subtracted trace gathers are obtained. During the procedure, 64 trace gathers using the human body model without model subtraction are also obtained. These trace gathers will be called as DKI trace gathers hereafter.

3 For each model subtracted trace gather, a Kirchhoff PSTM was applied. Totally 64 migrated gathers (model subtracted migration gathers, hereafter) are obtained after the pre-stack time migration. Fig. 4.10 and Fig. 4.11 are two comparison examples with source No. 7 and No. 40. The model subtraced trace gathers and model subtracted migration gathers are comprared. It is obvious to see that the model subtracted migration gathers are able to show the human body subsurfaces.

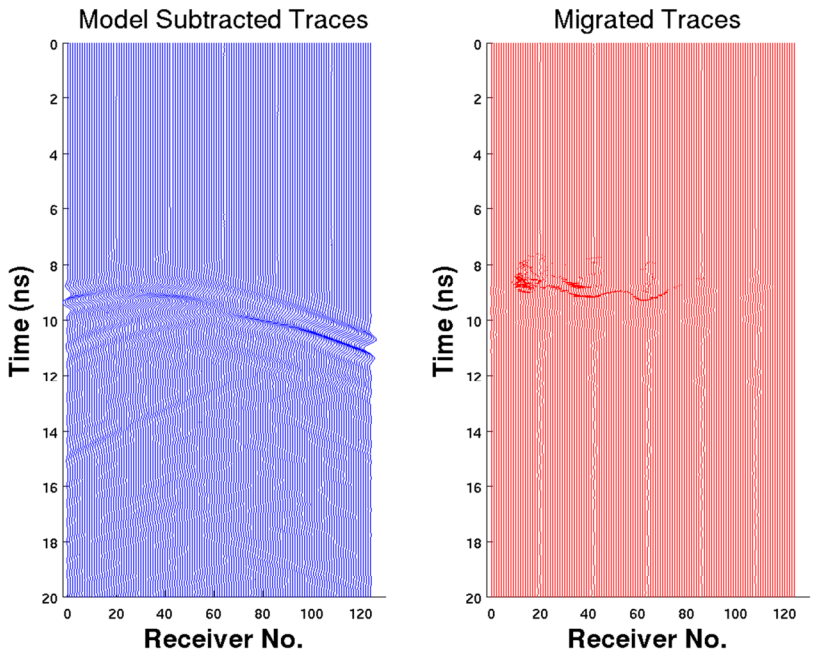

Figure 4.10 Comparisons of the model subtracted trace gather and model subtracted migration gather at the source No. 7. Left: model subtracted trace gather; right: migrated trace gather after Kirchhoff PSTM.

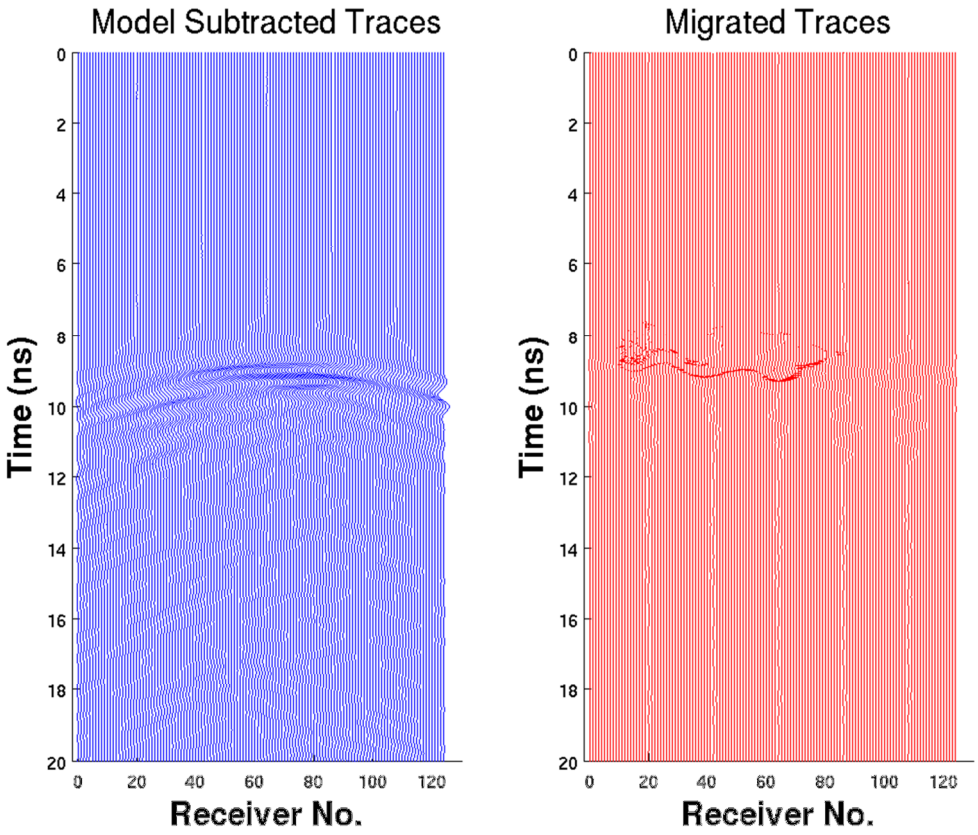

Figure 4.11 Comparisons of the model subtracted trace gather and model subtracted migration gather at the source No. 40. Left: model subtracted trace gather; right: migrated trace gather after Kirchhoff PSTM.

4 Stack all the 64 model subtracted migration gather together, and transfer the image from receiver number and time domain to the offset and depth domain to make a final image (model subtracted image hereafter). Fig. 4.12 is the final model subtracted image with coordinates in meters. Compared with Fig. 4.9, it is obvious that the final model subtracted image succesfully illustrates main subsurfaces of the human body.

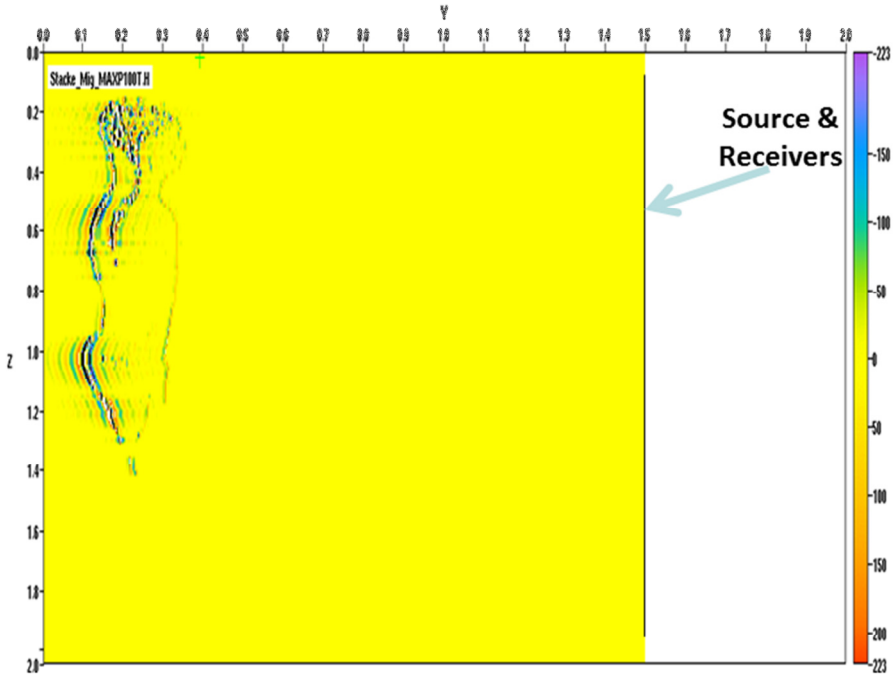

Figure 4.12 The final model subtracted image. As the source and receiver line is put at Y=1.5m, no image right of this line is available.

The same Kirchhoff PSTM and stack process mentioned above can also be performed on the DKI trace gathers without model subtraction. A final image, which will be called as the DKI image hereafter will also be obtained. Fig. 4.13 is the final DKI image which was obtained using the DKI trace gathers without model subtraction.

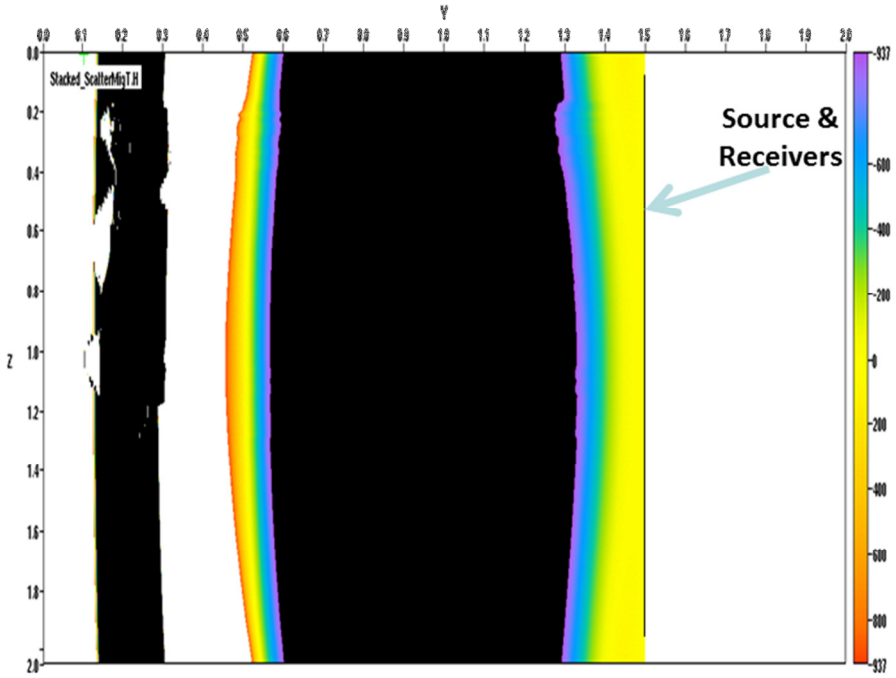

Figure 4.13 DKI image obtained using the DKI trace gathers with out model subtraction. No image is available at the region right to the source and receiver line, Y=1.5m.

Compared with the original model in Fig. 4.9 and the model subtracted image in Fig. 4.12, it is obvious that after the model subtraction, DKI/MR/PSTD method is able to show clear human body subsurface image via Kirchhoff PSTM and stack techniques. However, if the DKI trace gathers obtained by DKI/MR/PSTD method were migrated and stacked directly and without model subtraction, the final DKI image will be overwhelmed by strong artifacts. The humanbody subsurfaces can hardly be seen. This result coincided with the conclusion of the forward modeling. The setup of DKI/TS interfaces naturally causes artifacts which can be both earlier and much stronger than the true wave field scattered by the human body. The introduction of model

subtraction method is the best way to remove the DKI/TS artifacts. The physical meaning is very clear, and the mathematical algorithm is easy to understand and realize.

4.6 Conclusions

A technique of model subtraction method using a 3D DKI/MR/PSTD algorithm is introduced in some theoretical and real 3D heterogeneous scatter reflection waveform simulation problems. An application in a 3D heterogeneous human body reflection was simulated successfully. DKI/MR/PSTD method is reputed as a valid and efficient method in numerical wave form simulation not only in saving computation time and memory cost, but also in successfully offering the later phases after the first arrival. However, the introduction of T/S surface and directional Kirchhoff integration surface can cause some extra waveforms which in fact are artifacts. The DKI/TS artifacts are neither existing physically nor of our research interests especially in the simulation of reflection model. As shown in Fig. 4.4, Fig. 4.6 and Fig. 4.13, the right-propagating DKI/TS artifacts caused by the DKI and T/S surface can be both earlier and much stronger than our targeted heterogeneous media reflection waveforms. The waveforms of research interests can be overwhelmed by the DKI/TS artifacts. A normal move out (NMO) method may be considered to remove the DKI/TS artifacts, but the NMO method requires the T/S and DKI surfaces be far enough from the heterogeneous scatter. It means that the sub-region must be long enough in x direction and must have a large free space inside the sub-region. The efficiencies in both the memory cost and computation time of an MR method will be decreased drastically.

The model subtraction method uses a second assistant free space to simulate the DKI/TS artifacts caused by the T/S and the DKI interfaces. After subtracting the DKI/TS artifacts from the

waveforms of the heterogeneous 3D sub-region, in this study, the block sub-region or the the human body sub-region, a pure targeted reflection wave field is obtained. The model subtraction method has the advantages of computation efficiencies and flexibilities in that, this method does not require any special setup of the sub-region. The sub-region can still keep compact so that the computation efficiencies of the DKI/MR/PSTD method remain unchanged. Except the uniform medium restriction, there is no additional requirement in the locations of the DKI or the T/S surfaces. The locations of the directional Kirchhoff integration surface and the T/S surface can also be arbitrary. Although the DKI/TS artifacts are related to the locations of the DKI and TS interfaces, the DKI/TS artifacts are removed after model subtraction. The true reflection wave field reflected by the 3D heterogeneous scatter is not affected. The model subtraction method is not able to simulate the direct arrivals from the natural source to the natural receivers, but it does not matter because in most cases, what we concern most is the inner structures of heterogeneous 3D scatters. The inner structures are only related to the reflection wave field caused by the physical scatter, the 3D block and the 3D human body in this research. A successful simulation of the reflected and refracted wave field from the 3D heterogeneous scatter is of our most research interests.

Two 3D models are used to extend the model subtraction method to subsurface imaging applications. Multi-sources generating the same source signals are used to simulate a plane incident wave. In both the flat-plane block model and 3D heterogeneous human body model, the model subtraction simulations offer satisfactory location of the physical reflection surface. In the flat-plane block model, the model subtraction simulation offer a perfectly matching block thickness by the two late EM wave phases in Fig. 4.6. Based on the success of incident plane wave imaging results, the 3D human body model is used for the Kirchhoff pre-stack time migration test. The model subtracted trace gathers are able to give accurate human body subsurface after Kirchhoff PSTM and stack. The model subtraction method makes the

DKI/MR/PSTD method possible to be extended to the reflection model imaging problem with its well-reputed efficiencies in computation time and model cost.

The results obtained from the model subtraction method using a 3D DKI/MR/PSTD algorithm show a good evidence for the validity of model subtraction method. The physical characteristics of the late reflection and refraction waves in the multi-refraction and reflection EM wave series were clearly simulated. The human body reflection EM waveforms simulated from the model subtraction method using a DKI/MR/PSTD algorithm coincide well with those from the classical single-region PSTD. The arrival time and amplitudes of the model subtraction method using a DKI/MR/PSTD method matches those of the classical single-region PSTD also. With satisfactory results, the model subtraction method using a DKI/MR/PSTD algorithm can simulated the complex reflected wave field from a 3D heterogeneous scatter. DKI/MR/PSTD with model subtraction method has not only better efficiencies in both computation time and memory cost, but also other advantages in waveform forward modeling.

In a classical 3D single-PSTD simulation problem, generally the memory cost is determined by the whole computation domain grid numbers. In some real simulation which may require extremely long distance in one or more directions, the memory cost could be extremely computational intensive. The memory cost may cause some simulation impossible. However, in the DKI/MR/PSTD with model subtraction algorithm, the memory cost does not depend on the whole computation domain grid numbers. It only depends on the grid numbers of the sub-region. In case of only a relatively small sub-region is necessary, the memory cost will keep low no matter how big the total computation domain is. For example, the memory cost of the models illustrated in Fig. 4.5 or Fig. 4.8 is about 6GB using the DKI/MR/PSTD method. If we try to simulate the same model using a classical single-region PSTD method, the memory cost will be about 25GB. If we need to move the source and receivers further away from the scatter in Fig. 4.5

or Fig. 4.8, the whole computation domain grid numbers has also to be increased. The memory cost can be easily and proportionally increased with the distance. Practically the simulation will be become impossible soon. In a model subtraction method using a DKI/MR/PSTD algorithm, because the sub-region setup keeps unchanged, the computation time and memory cost also keep unchanged. This advantage makes the model subtraction method using a DKI/MR/PSTD algorithm especially suitable for long-distance and high frequency simulation. Model subtraction method using DKI/MR/PSTD can be an ideal algorithm in some real remote sensing researches. The distance could be even astronomical, for example, the radar generating EM radiation from earth and recording the reflected waves from moon. The model subtraction method using DKI/MR/PSTD algorithm not only improve the computational efficiencies in large-scale 3D forward modeling problems, but also suggest a new method in solving some extremely long-distance problem which was impossible before.

Chapter 5. Interferometry and Virtual Reflection

5.1 Introduction

In this chapter, a new technique in virtual reflection simulation and subsurface structure imaging, which includes interferometry and migration, is introduced. The final purpose of this technique is to image some fractures using geophysical method. The basic idea is to transform the transmission wave field into a virtual reflection wave field first, then apply the typical reflection imaging techniques such as migration to get a vivid subsurface image. It is a technique especially useful in geologic fracture detection, characterization using borehole radar.

Characterization of geologic heterogeneity and modeling of hydrologic processes in fractured-rock have been active research fields in the last two decades in both reservoir characterization and groundwater hydrogeology. To address the challenge of identifying complex, three-dimensional fracture-controlled heterogeneity, hydrologists and engineers increasingly are turning to geophysical methods. Advances in technology and data-analysis methods include: 1) borehole televiewer instruments for imaging the borehole well and identifying fracture location and orientation (Williams and Johnson, 2003), 2) flow-meter logging to identify the flow rate, transmissivity, and far-field hydraulic head of discrete fractures (Paillet 1998, 2000), and 3) radar methods for both transmission tomography and reflection analysis (Olsson 1992; Liu, 2006; Zhou *et al*., 2001; Day-Lewis *et al*., 2003; Lane *et al*., 2000).

In contrast to GPR imaging for single large-scale fractures, imaging and characterization of fractured rocks containing dense, micro-opening zones by radar still poses a great challenge. Meanwhile, estimation of scattering loss of electromagnetic (EM) wave energy due to fractures is

of great concern. The reason is in two folds. First, the scattering loss of EM wave energy is an interesting topic from wave propagation point of view and bears the importance for GPR system design for subsurface imaging. Second, robust scattering loss may provide a realistic way to characterize the fracture zones.

Borehole reflection-mode radar is a powerful tool that allows for identification of planar features (Olsson 1992; Lane *et al*., 2000) such as fractures; these features need not intersect a borehole in order to be identified. Both omni-directional and directional antennas are commercially available; the latter can be used to determine the location, orientation, and extent of discrete fractures. The resolving power of reflection-mode data is 1/4 of a wavelength. In a typical granite with an EM velocity of 130 m/micro-second, a 100 MHz radar system might provide resolution of 0.3 m; although larger than the aperture of a fracture, the measurements are sensitive to variations related to chemical alteration and weathering of rock bounding fractures, and has been used successfully to identify discrete fractures at several sites (Olsson 1992; Gregoire and Halleux 2002).

Previous studies (e.g., Liu and He, 2007) showed that fractures in the formations can be better characterized through wave interferometric virtual source (WIVS) approach to convert cross-hole transmission mode radar data to single-hole, multi-offset reflection representation. This thesis \expands the WIVS approach to consider multi-hole, multi-polarization borehole sources. A case study using synthetic data set with five boreholes and vertically and horizontally polarized radar wavefield is demonstrated. The WIVS converted in boreholes other than the hole with transmitting sources at difference distance and different receiving polarization are compared to show the efficiency of this approach.

5.2 Interferometry and Virtual Reflection

Geophysical waves (e.g., radar waves) propagating through the Earth traverse a highly reverberant environment, the result of a medium that contains numerous scatters. For numerical modeling purposes, the medium can be bordered by 1) a perfectly reflecting medium (the Dirichlet boundary condition) to form a closed medium; 2) a perfectly transparent medium (the absorption boundary condition) to form an open medium; or 3) some combination of 1) and 2) on different sides of the model. In this chapter, a 3-D and open medium case is considered.

The idea of interferometry utilizes the cross correlation of signal pairs, which is considered to be the key point of this technique, to reconstruct the impulse responses of a given media. Interferometry provides the possibility to reconstruct the subsurface reflection response. Interferometry can be applied to the traces recorded by either passive sources or active sources, and can also be applied to the simulated traces in forward modeling. Interferometry technique consists of simple cross correlation and stacking of actual receiver responses to approximate the impulse response as if a virtual source was placed at the location of the applicable receiver. Most interferometry research has been concentrated in passive sources to reconstruct the subsurface structure images, and relatively few researches have been done in the fracture imaging using the active sources. From this chapter, a synthetic model is studied to show the possibility to apply the interferometry technique in fracture imaging using active sources. Fig. 5.1 shows the 3D model setup used in this research,

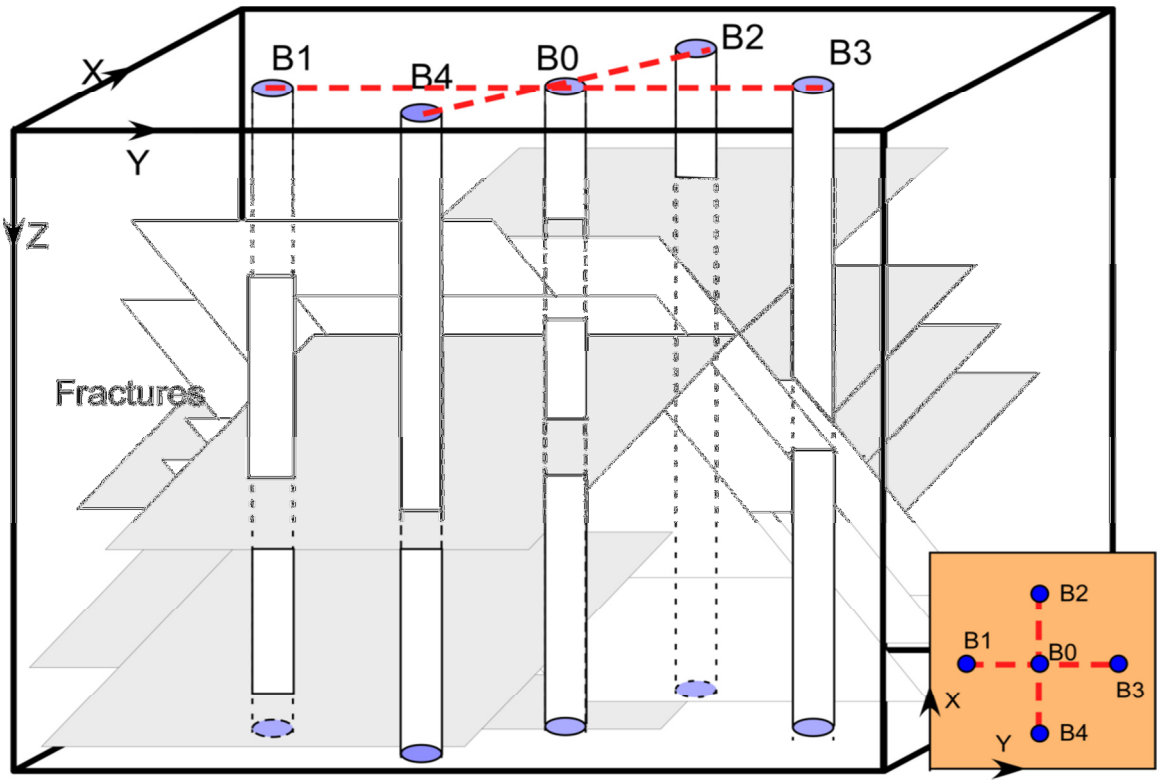

Figure 5.1 A 3D model used in this thesis. A family of fractures is embedded into a uniform media. B0 – B5 are holes for borehole radar.

Fig. 5.1 is a 3D model used in this research. A fractured rock model (Figure 5.1) was constructed to mimic the borehole radar survey environment. The fracture network is generated by the discrete fracture network (DFN) model. Two sets of large permeable fractures are considered, with orientations of 30 and −30 degrees from the vertical direction. Two more sets of smaller, impermeable fractures are considered with orientations of 0 and 90 degrees from the vertical. The material property parameters for rock grain and fracture fluids have been chosen to be representative for a typical fractured rock aquifer. These fractures are embedded into the uniform background. There are two representative fundamental elements in the fractured rock model: background rock matrix with a dielectric constant of 6.25, and the permeable fractures networks with an elevated dielectric constant of 16 to mimic saturated sands filled facture apertures. We set a model with size of 512x256x512 grids in x-y-z directions, respectively. Using a source having a

Ricker wavelet with a central frequency of 100 MHz, the grid size is set to be 0.1 m for satisfying the stability condition of the staggered-grid 3D PSTD algorithm. The time marching step satisfying the stability condition is 0.3 ns. This will give the maximum transmission distance of 57 m. The total simulation time window is 900ns, which means the time step of this simulation is 3000. This time window is long enough to include all possible wave phases of research interests. The structure is uniform in y, B1-B0-B3 direction. B0 is set as the source line. A series of sources are arranged along B0. B2 and B4 are the receiver line, a series of receivers are arranged along B2 and B4 lines.

Totally 44 sources are set along the B0 line. The first source locates at the starting depth of 5 meters, and the last source is placed at the depth of 48 meters. The sources are placed at the interval of 1m between the depths of 5 meters to 48 meters. In borehole lines B2 and B4, the receiver depths are starting from 2 meters with an incremental interval of 0.3m. The receivers ended up at the depth of 48 meters. Totally 158 receivers are placed along each receiver line, B2 and B4.

The first step of the interferometry technique is to make 3D staggered-grid PSTD simulation using each source and all receivers. Totally 44 simulations are performed. Fig. 5.2 shows the 2D illustration along B4-B0-B2 plane at time step of 400. A source at the depth of 20 meters along B0 is illustrated in Fig. 5.2. Two receiver series along B4 and B2 are placed. It is a typical transmission model setup.

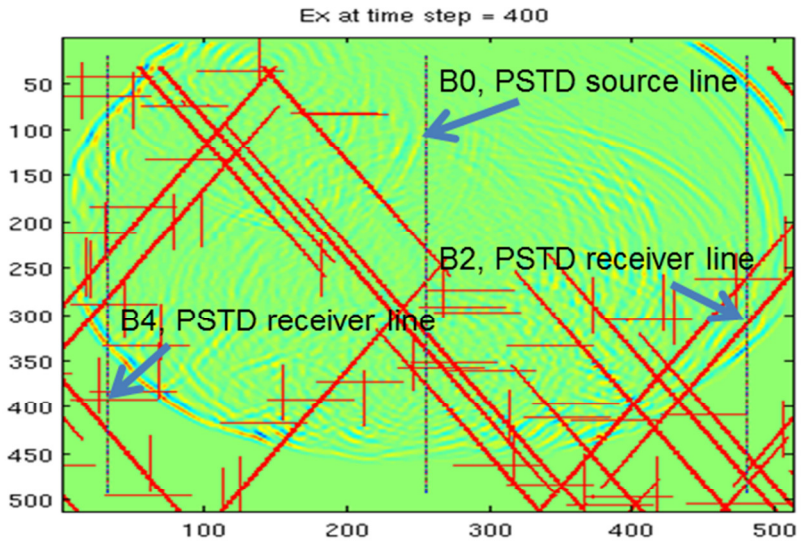

Figure 5.2 2D Illustration of a forward modeling along B4-B0-B2 plane and nt = 400 with the source at the depth of 20m, 200 in the grid number.

Fig 5.3 shows the traces obtained along B4 and B2 line. Although the total simulation time window is 900 ns, the time window up to 700ns is long enough to include all possible wave phases. The time window illustrated in Fig. 5.3 is up to 700ns. The traces obtained using one source and all receivers by the staggered-grid PSTD method will be called as one source transmission simulation gather hereafter.

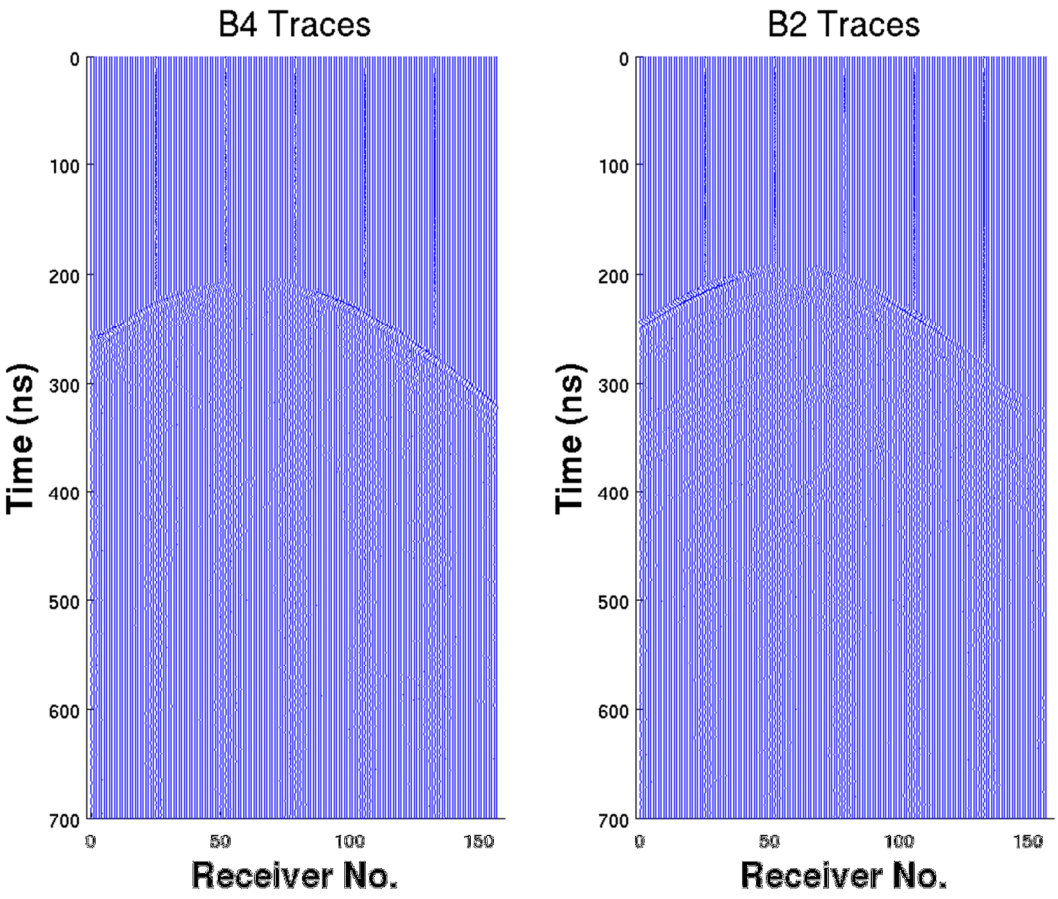

Figure 5.3 B4 and B2 one source transmission simulation gathers obtained using the staggered-grid PSTD method. Source at depth = 20m, and all receivers along B4 and B2 are illustrated.

Fig. 5.3 suggested that the subsurface image could be complicated. Totally 44 source transmission simulation gathers are obtained for both B4 and B2 lines. The source transmission simulation gathers obtained in the transmission simulation are the basis of the further interferometry process.

In the interferometry technique, each receiver line is processed separately with the same technique. In this research, the B4 and B2 lines are processed separately with the same procedure. The purpose of processing B4 receivers is to obtain the subsurface image from B4 to B0, and the purpose of processing B2 receivers is to obtain the subsurface image from B0 to B2. In fact, this

property is one big advantage of interferometry technique in borehole radar. If we set all the sources and receivers along B0 line to get the traditional reflection trace gathers, the trace obtained will be reflected from all possible directions. It will be extremely difficult to separate the wave field to image a specific targeted area. The interferometry technique uses transmission model to create virtual reflection. It makes the imaging of the targeted area possible. The trace gathers obtained along B4 line can be processed and imaged to obtain the subsurface image from B4 to B0, and the trace gathers obtained can be processed and imaged to obtain the subsurface image from B0 to B2. Interferometry technique provides us an ideal method to image our targeted area of research interests in the utilization of borehole radar.

The processing procedures for B4 and B2 lines are identical. In Chapter 5 and 6, B4 line will be processed as the example hereafter. Finally the subsurface image obtained from B4 to B0 and B0 to B2 will be merged together to have a comprehensive subsurface image.

The key technique in the interferometry is cross correlation. As illustrated in Fig. 5.4, a signal at receiver B can be cross correlated with a signal at receiver C to produce a virtual source – receiver propagation.

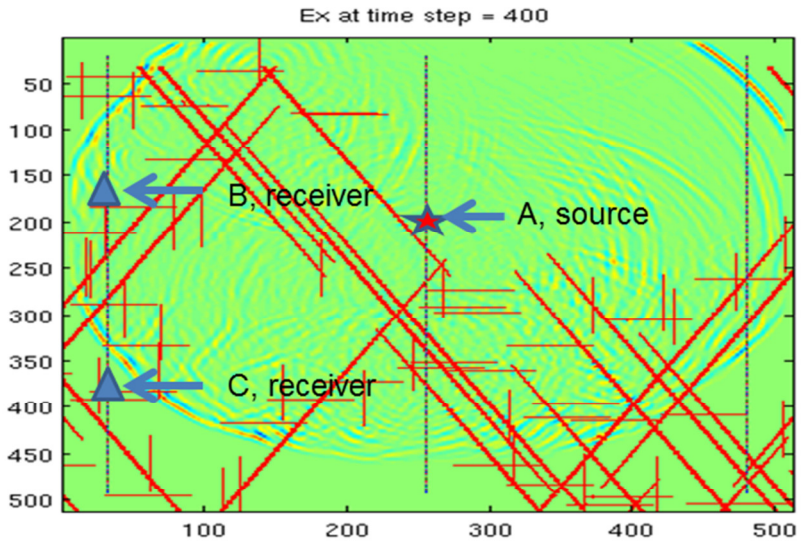

Figure 5.4 Illustration of the natural sources of the simulation. The source signal is Ez, and receiver signal recorded in Ex.

Consider one source A and two receiver points B, C as illustrated in Fig. 5.4. The source A is excited with a time function f(t). The two receivers B and C can be randomly selected. In this research, B and C are selected along the B4 line. Let T(B, A, t) denote the wave field recorded at receiver B due to source A, and T(C, A, t) denote the wave field recorded at receiver C due to source A. The response at B caused by a virtual source C can be denoted as R(B, C, t). R(B, C, t) can be expressed as

$$R(B,C,t) = -\int_{s} T(B,t) * T(C,-t) \tag{5.1}$$

S is the integration surface. In this research, S is the B0 line. Consequently the equation can be expressed as

$$R(B,C,t) = -\sum_{B0} T(B,t) * T(C,-t)$$
$$R(B,C,t) = -\sum_{B0} T(B,\mathrm{A},t) * T(C,\mathrm{A},-t) \tag{5.2}$$

Equation (5.2) states that the virtual reflection wavefield R(B,C, t) between two points B and C in the same borehole can be achieved by the summation of cross correlations of two transmission wavefields of T(B, A, t) and T(C, A, t) with the source A going through all source points available along B0 line. The receiver B turns into the virtual source of the virtual reflection. After the transmission, a 44-source transmission simulation gathers, with source along B0 line and receiver along B4 line, turn into a 158 virtual reflection trace gathers, with one virtual source and all 158 receivers all along the B4 line. In order to illustrate the validity and accuracy of the WIVS approach, a comparison of simulated reflection and virtual reflection is illustrated in Fig. 5.5. Both images have the same source at the depth of 20.1m.

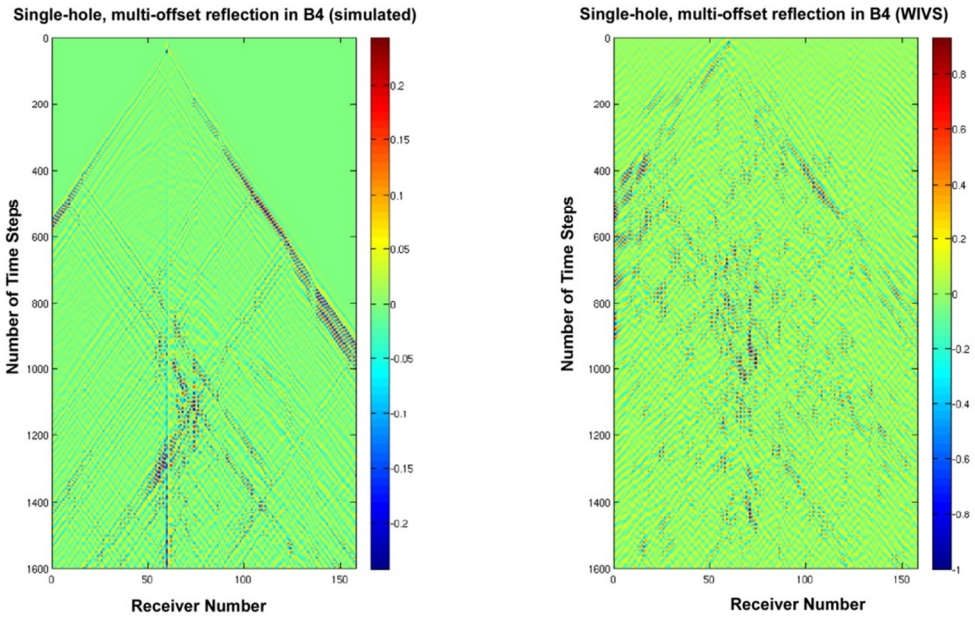

Figure 5.5 The comparison of the simulated single-hole, multi-offset reflection in B4 for the source at depth of 20.1m (left) and the virtual reflection by interferometry with the virtual source at the depth of 20.1m (right).

Fig. 5.5 clearly suggests that interferometry technique is able to give a satisfactory virtual reflection image. The technique transforming the transmission wave field to the virtual reflection wave field is called the wave interferometric virtual source (WIVS) approach. After the WIVS approach, a series of 158 virtual sources are generated. Each virtual source has a virtual reflection trace gather of 158 receivers. Totally a series of 158 virtual reflection trace gathers are created. The transmission wave field with 44 true sources and 158 receivers illustrated in Fig. 5.2 are totally transferred to the virtual reflection wave field of 158 virtual sources and 158 receivers. The natural sources illustrated in Fig. 5.2 become the virtual reflection point along B0 line. Theoretically the more natural sources we can have along B0 line, the more virtual reflection points we will have in the WIVS approach, and the better virtual reflection wave field will be.

5.3 Conclusions

The wave interferometry virtual source (WIVS) approach provides a new angle to process and visualize the data. It is complementary to the raw cross-hole transmission data and shows formation features in a more convenient way. From the examples presented above we can conclude

1. WIVS is a data-based redatuming or transformation process. It is advantageous for characterizing thin features such as fractures or thin beds using borehole radar;

2. WIVS transforming the waveforms obtained using a transmission model into a virtual reflection wave field. Its combination with the commonly used imaging techniques such as stack, migration and tomography are expected to provide a vivid geological structure image.

Transmission model is convenient in the borehole radar setting because it is easy to target the area of research interests. However, transmission model is not easy to be combined into the modern subsurface imaging techniques such as migration and tomography, which are based on the reflection model. The interferometry and WIVS provides the novel possibility in subsurface imaging in that, after transforming the transmission model into a virtual reflection model, the traditional reflection imaging techniques such as Kirchhoff PSTM can be applied to make a vivid subsurface imaging. Breakthroughs in understanding of the fractures can be expected.

Chapter 6 Virtual Reflection and Subsurface Fracture Imaging

6.1 Introduction

In contrast to GPR imaging for single large-scale fractures, imaging and characterization of fractured rocks containing dense, micro-opening zones by radar still poses a great challenge. Meanwhile, estimation of scattering loss of electromagnetic (EM) wave energy due to fractures is of great concern. The reason is in two aspects. First, the scattering loss of EM wave energy is an interesting topic from wave propagation point of view and bears the importance for GPR system design for subsurface imaging. Second, robust scattering loss may provide a realistic way to characterize the fracture zones.

Chapter 5 and previous studies (Liu and He, 2007) showed that fractures can be clearly characterized through WIVS approach. WIVS transforms the radar data from cross-hole transmission mode into a single hole, multi-offset virtual reflection representation. After the transmission, the virtual reflection data become ready to be imaged using migration techniques. This chapter applies the Kirchhoff PSTM technique to the virtual reflection data obtained in Chapter 5 with consideration on the multi-polarization imaging. A case study using synthetic data with boreholes and vertically or horizontally polarized radar wave field is demonstrated in this thesis. Fracture images obtained with transmitting sources at difference distance and different receiving polarization are compared to show the efficiency of this approach.

6.2 Kirchhoff PSTM Technique

In this chapter, a Kirchhoff pre-stack time migration (PSTM) technique is applied to the synthetic virtual reflection trace gathers after WIVS approach to test the validity and effectiveness in imaging the subsurface geological structures, especially to test the sensitivity in detecting and characterizing the fracture. Migration is reputed as one of the most robust weapons in the geological imaging. Although more commonly applied in the seismic reflection research, this technique can also be applied to the electromagnetic reflection subsurface structure imaging. The WIVS technique has successfully offered 158 virtual reflection gathers in Chapter 5. The virtual reflection trace gathers are applied with a Kirchhoff PSTM first to get the migrated trace gathers. Fig. 6.1 illustrates one example of the virtual reflection trace gather after Kirchhoff PSTM.

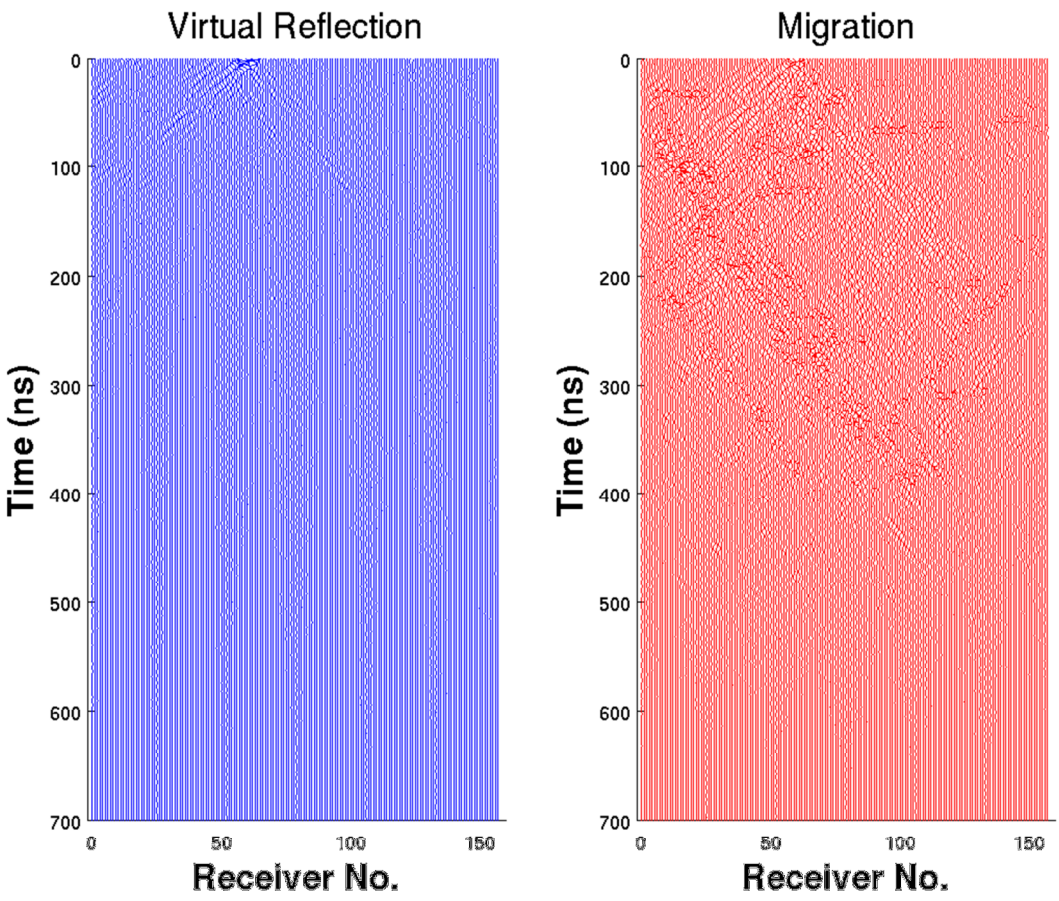

Figure 6.1 Comparisons of the virtual reflection and the Kirchhoff PSTM results. Left: virtual reflection trace gather; right: migrated trace gather after a Kirchhoff PSTM.

Compared with the model illustrated in Fig. 5.4, obviously the migrated trace gather suggests a more obvious geological image then the virtual reflection trace gather. In Chapter 5 we have obtained 158 virtual reflection trace gathers, consequently 158 migration trace gathers can be obtained if the Kirchhoff PSTM is applied to each virtual reflection trace gather. After all the 158 migration trace gathers are obtained, they are stacked to have a final vivid image to illustrate the subsurface structure image. Fig. 6.2 shows the trace gather after stacking all the 158 pre-stack migration trace gathers. This trace gather is called the stacked migration trace gather hereafter. In order to prove the effectiveness of the WIVS approach in fracture subsurface imaging, a stacked migration trace gather using the true reflection simulation is compared in Fig. 6.2.

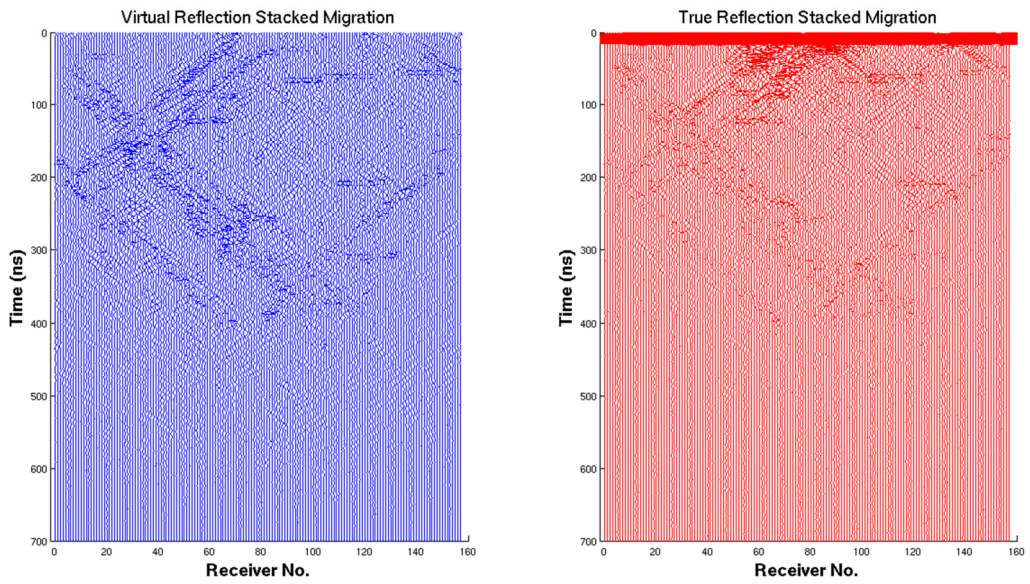

Figure 6.2 B4-B0 stacked migration trace gather, stacked migration trace gather of B4 to show the image between B0 to B4. Left: B4-B0 stacked migration using the WIVS approach; right: B4-B0 stacked migration using the true reflection model.

Fig. 6.2 clearly shows that the stacked migration using the WIVS gives the satisfactory fracture image with little direct arrivals. It is another advantage of WIVS approach because in most cases the direct arrivals are not desired in subsurface imaging. Because the stacked migration trace gather in Fig. 6.2 only shows the image between B4 line and B0 line in Fig. 5.1 and Fig. 5.2, it will be referred as B4-B0 stacked migration trace gather hereafter. Compared with the original model in Fig. 5.2 and the image illustrated in Fig. 6.1, obviously the B4-B0 stacked migration trace gather illustrated a much better image of the subsurface structure. The fracture is easy to see. The pre-stack migration and stack techniques successfully give a vivid image of the geological structure to reflect the fracture is existing using the virtual reflection trace gather obtained in Chapter 5.

6.3 Multi-Borehole Imaging Combination

The processing and imaging procedures mentioned above are for the WIVS with the virtual sources along B4 line, the virtual reflection surface along B0 line and the virtual receivers along B4 line. The B4-B0 stacked pre-stack migration image illustrated in Fig 6.2 suggests the subsurface geological structure between B4 and B0. The same techniques, including the WIVS approach mentioned in Chapter 5 and the Kirchhoff PSTM mentioned in Chapter 6 can be applied to B2 line also. The purpose is to obtain the subsurface image between B2 and B0 lines. Fig 6.3 shows the stacked migration trace gather after we applied WIVS to get the virtual reflection trace gathers, Kirchhoff PSTM to get the migrated trace gathers, and stack to get the stacked migration trace gather. The trace gather obtained using B2 line will be referred as B2-B0 stacked migration trace gather hereafter. Fig. 6.3 shows both the final results of both B4-B0 and B2-B0 stacked migration trace gathers.

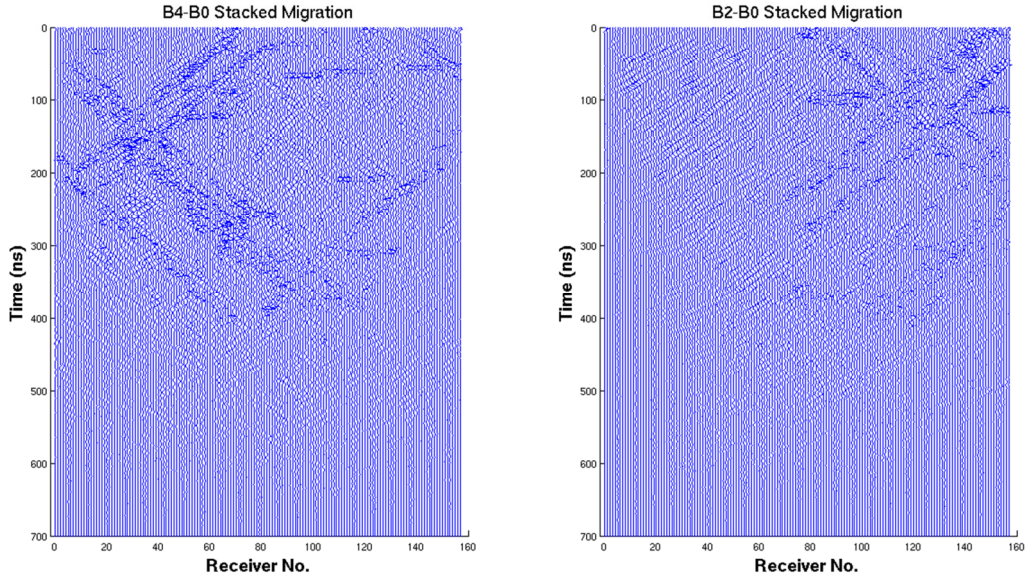

Figure 6.3 Left: B4-B0 stacked migration trace gather; right: B2-B0 stacked migration trace gather, stacked migration trace gather of B2 to show the image between B0 to B2.

Both of the B4-B0 and B2-B0 stacked migration trace gathers clearly illustrates that the fractures exist. Although the B4-B0 and B2-B0 stacked time migration trace gathers are obtained separately, they can be transferred to depth-offset images and merged together. Fig 6.4 shows the merged B4-B0 and B2-B0 image after a depth-offset transfer. The left part of Fig. 6.4 is the 2D slice of the original 3D model along B4-B0-B2 line, and the right part is the merged image using B4-B0 and B2-B0 stacked migration trace gathers. The right part of Fig. 6.4 will be called as merged B4-B0-B2 migration image hereafter.

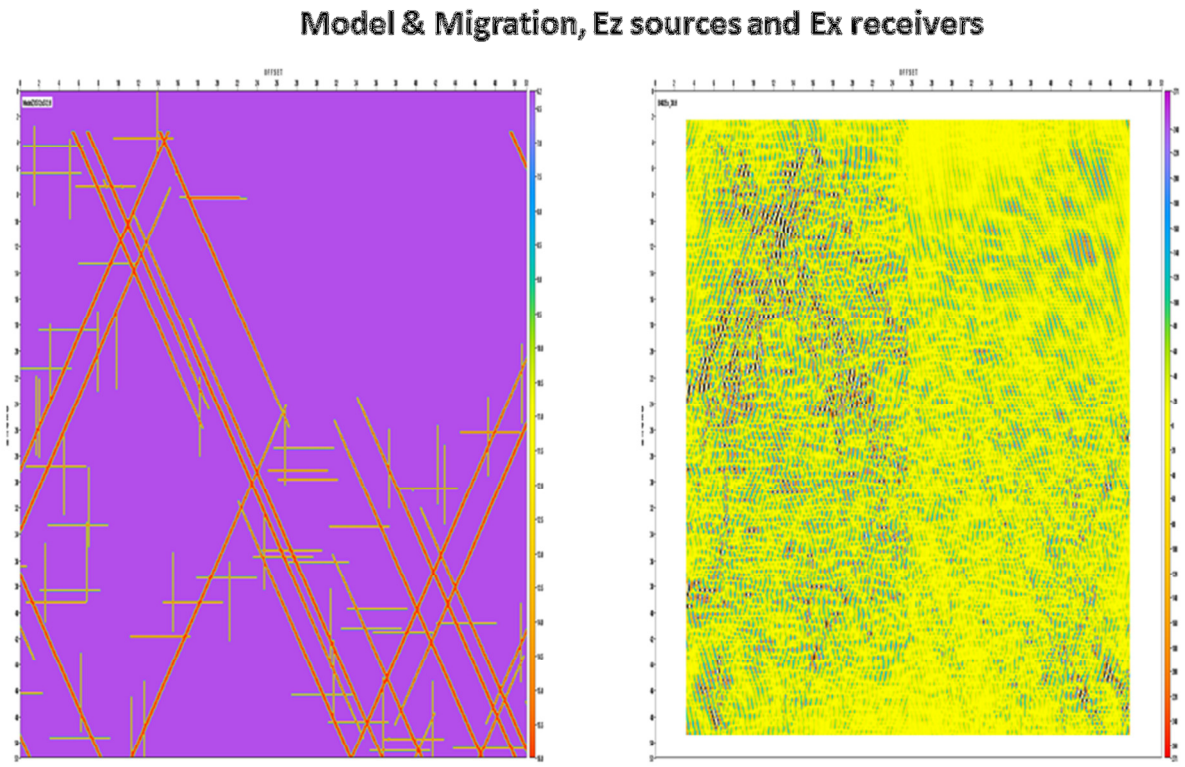

Figure 6.4 A 2D slice of the original model and merged migrated image comparison. 100 MHz Ricker wavelet in Ez along the B0 source line, and Ex component recorded along B4 and B2 in receivers.

Fig 6.4 is a 2D illustration of the comparison between the 3D synthetic model and the final migration result. We can clearly see that the merged B4-B0-B2 migration image successfully show the main fracture in both the orientation and the location. Especially for the fractures in 30 and -30 degrees from the vertical direction, the merged B4-B0-B2 migration image gives a vivid illustration. The left part and the right part of Fig. 6.4 are obtained separately using B4 and B2 receivers respectively, so the amplitude are not uniform in the merged B4-B0-B2 migration image. However, we can still see that in both part the fractures are easy to identify, and the connection along B0 line, the natural source line and border of both B4-B0 and B2-B0 stacked migration trace gathers is good enough in the common sense. Some low frequency noises appear at the merged B4-B0-B2 migration image because the Kirchhoff PSTM sometimes can cause the low frequency noises. Compared with the 2D slice of the original model, we know that the right-upper part should be uniform media. However the corresponding right-upper part of the merged B4-B0-B2 migration image is overwhelmed by the low frequency noises. It is a good estimation that how strong the low frequency noise could be when we applied the WIVS, Kirchhoff PSMT and the stack to some data obtained using true ground penetrating radars in boreholes.

6.4 Multi-Polarized Migration Images

All the work finished above is using Ez component as the natural source along B0 line, and Ex component as the data recorded at the receivers along B4 and B2 lines. EM wave has three components in Ex, Ey and Ez. As a multi-polarization research, all the components, Ex, Ey and Ez signals in both sources and receivers can be tested to verify the sensitivity in subsurface fracture imaging. Fig. 6.5 – 6.12 illustrate the final merged B4-B0-B2 migration images obtained using different electromagnetic wave components in sources along B0 and receivers along B4 and B2 lines. Exactly the same techniques mentioned in Chapter 5 and Chapter6, including the WIVS approach, the Kirchhoff PSTM and the stack are applied to each of the polarization combination.

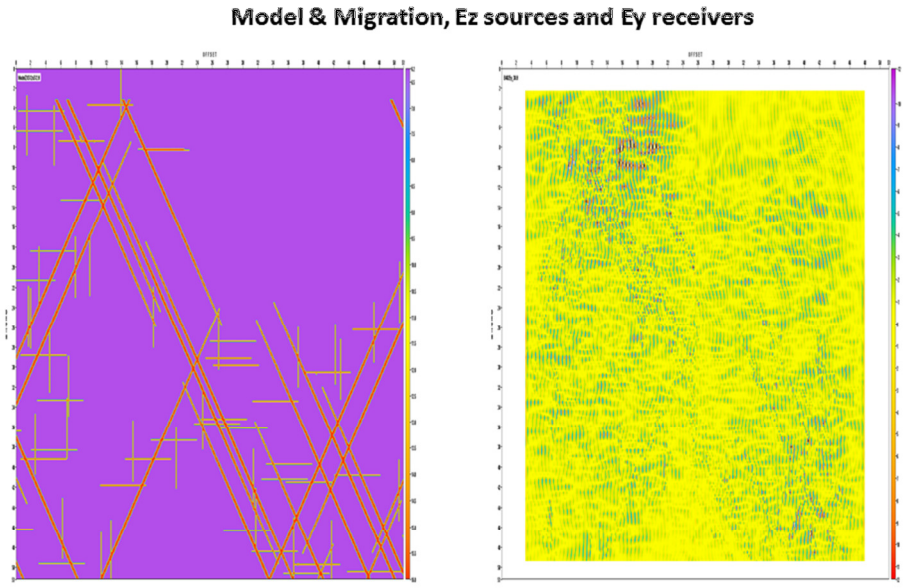

Figure 6.5 Original model and Merged migrated image comparison. 100 MHz Ricker wavelet in Ez as sources along B0 line, and Ey data recorded in receivers along B4 and B2 lines.

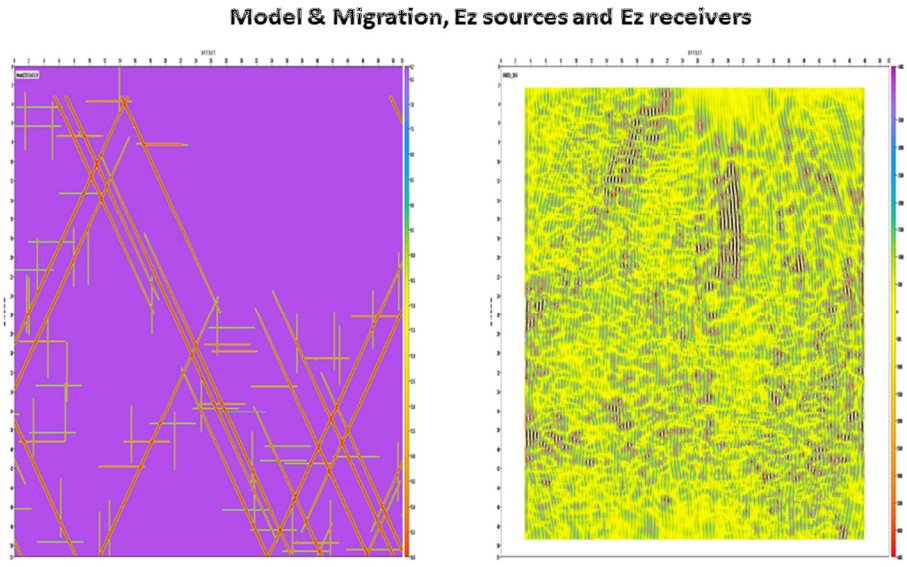

Figure 6.6 Original model and Merged migrated image comparison. 100 MHz Ricker wavelet in Ez as sources along B0 line, and Ez data recorded in receivers along B4 and B2 lines.

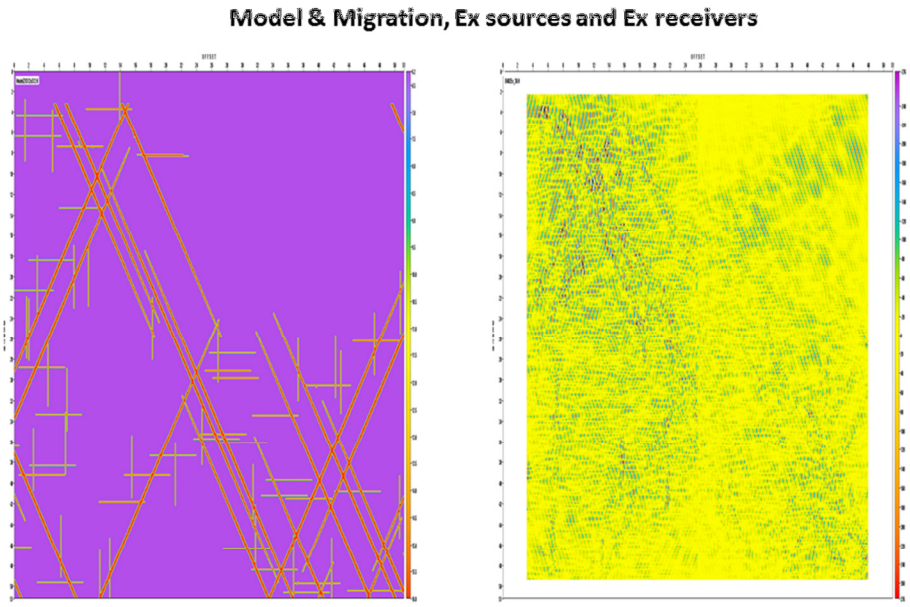

Figure 6.7 Original model and Merged migrated image comparison. 100 MHz Ricker wavelet in Ex as sources along B0 line, and Ex data recorded in receivers along B4 and B2 lines.

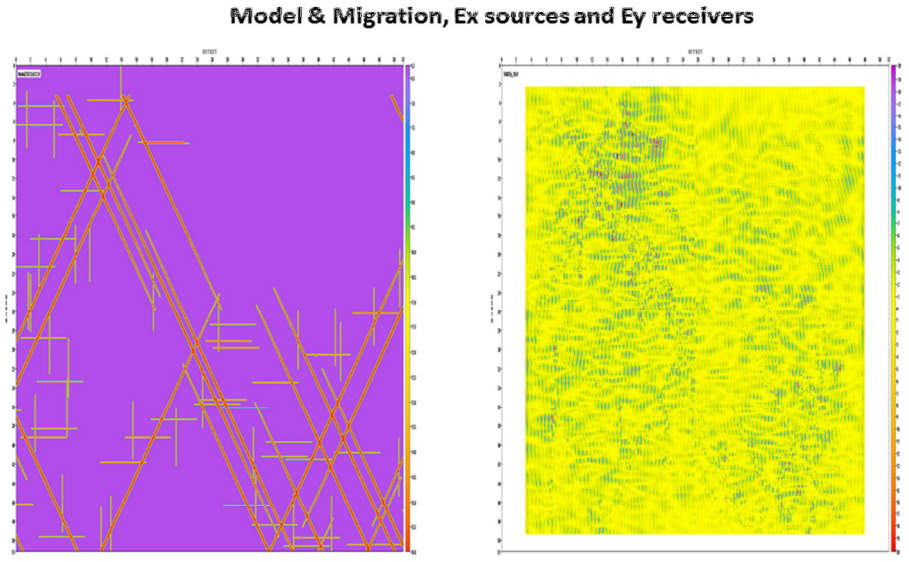

Figure 6.8 Original model and Merged migrated image comparison. 100 MHz Ricker wavelet in Ex as sources along B0 line, and Ey data recorded in receivers along B4 and B2 lines.

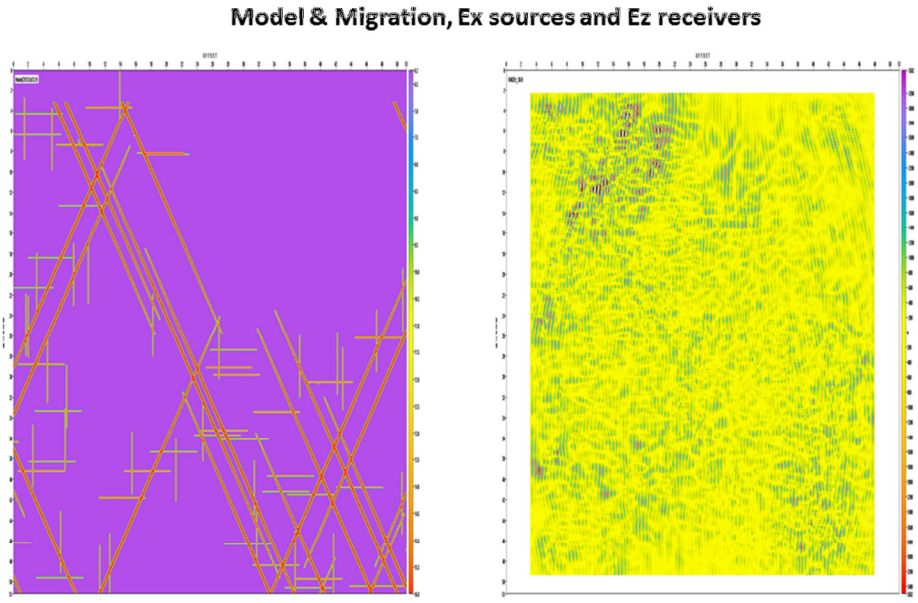

Figure 6.9 Original model and Merged migrated image comparison. 100 MHz Ricker wavelet in Ex as sources along B0 line, and Ez data recorded in receivers along B4 and B2 lines.

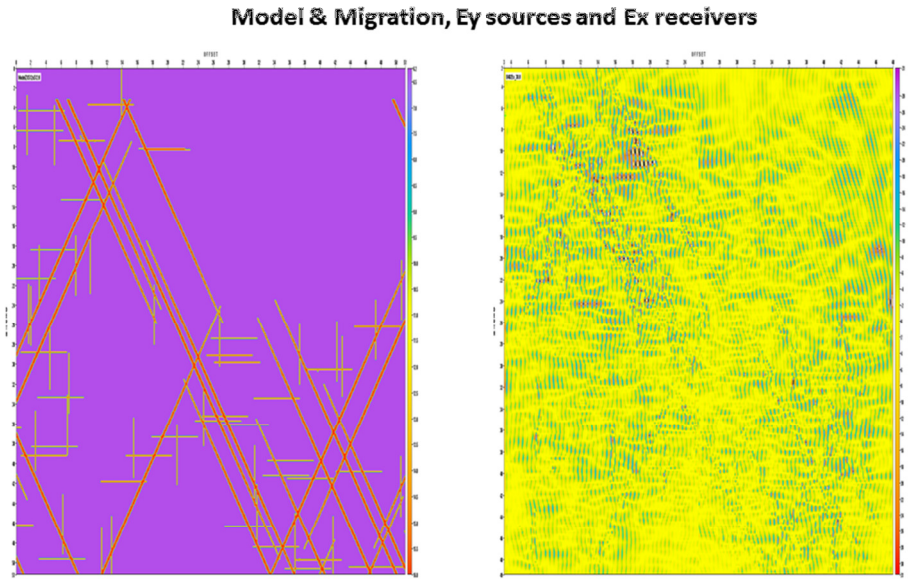

Figure 6.10 Original model and Merged migrated image comparison. 100 MHz Ricker wavelet in Ey as sources along B0 line, and Ex data recorded in receivers along B4 and B2 lines.

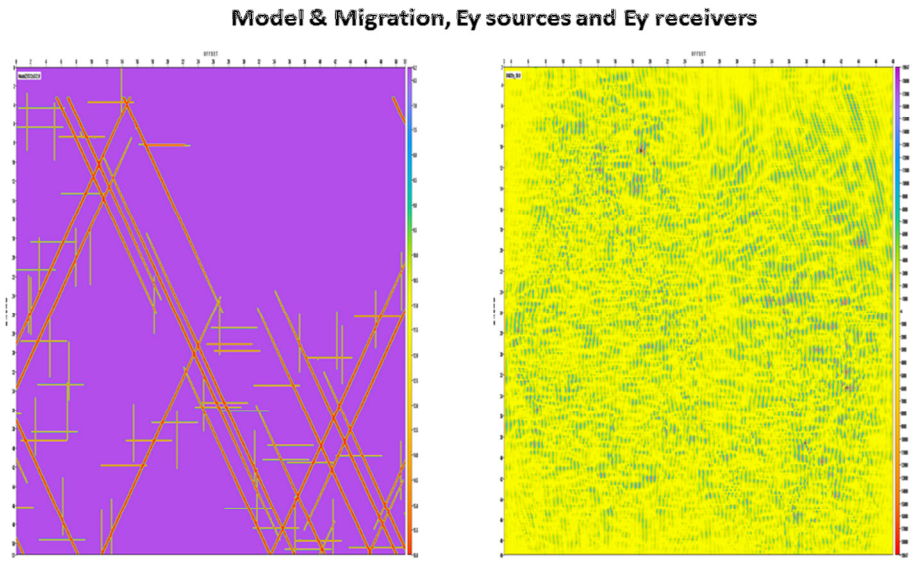

Figure 6.11 Original model and Merged migrated image comparison. 100 MHz Ricker wavelet in Ey as sources along B0 line, and Ey data recorded in receivers along B4 and B2 lines

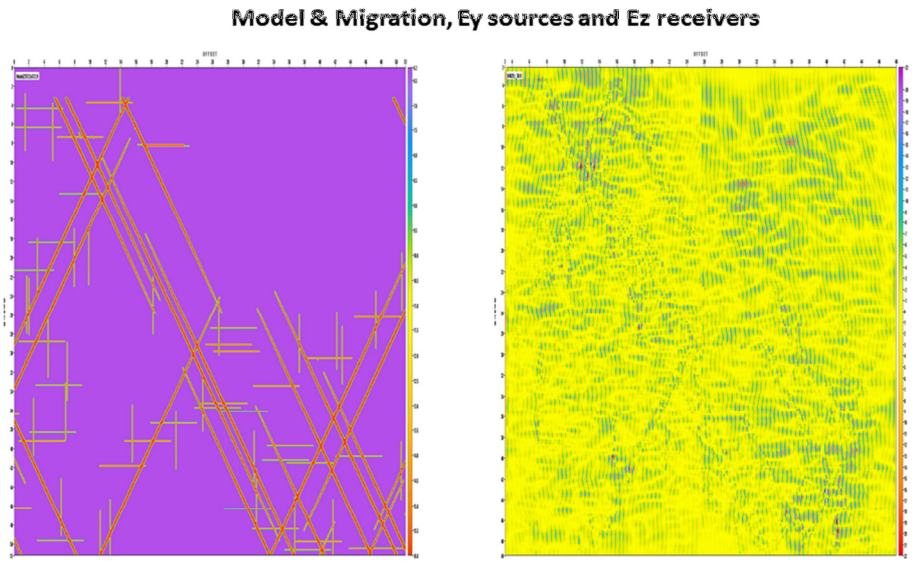

Figure 6.12 Original model and Merged migrated B4-B0-B2 image comparison. 1MHz Ricker wavelet in Ey as sources along B0 line, and Ez data recorded in receivers along B4 and B2 lines.

Fig. 6.4 – 6.12 give us a full set of the merged B4-B0-B2 migration images using different polarization combinations of the EM waves in sources and receivers. Totally 9 merged B4-B0-B2 migration images are available. In general, as illustrated in Fig. 6.4, Fig. 6.7 and Fig. 6.10, for the sources using Ez, Ex or Ey as the signal, the Ex component gives the best result in merged B4-B0-B2 migration images after Kirchhoff PSTM and the stack, especially in showing the fractures in 30 or -30 degrees from the vertical direction. Considering that the original model illustrated in Fig. 5.1, the fractures are along the X and B4-B0-B2 direction and uniform in Y direction, it suggests that Ex component in receiver might be the most sensitive in detecting the fractures in degrees from the vertical direction. Fig. 6.7, Ex in source and Ex in receiver; Fig. 6.8, Ex in source and Ey in receiver; and Fig. 6.10, Ey in source and Ex in receiver give the best images of the fractures which are parallel in the vertical direction. Fig. 6.12, Ey in source and Ez in receiver gives us the best contrast of the area with and without fractures. The right-upper part of the merged B4-B0-B2 migration image, which is without any fractures, is obviously different from the rest part of the figure which is embedded with fractures.

As illustrated in this chapter, multi-polarization approach has great benefits in imaging thin fractures. The different polarizations of the EM wave propagation might be coherent and/or incoherent to the fracture directions. In general, as illustrated form Fig. 6.4 to Fig. 6.12, the coherent polarization gives the best fracture image. It is especially useful in real field data in that, the directions of geological fractures can be determined by examining the image quality of different polarization images. Multi-polarization imaging by borehole radar is expected to a robust tool in geological fracture detection and characterization.

6.5 WIVS and PSTM of a Field Dataset

WIVS approach is also applied to a read world cross-hole transmission dataset obtained from a bedrock well field which consists of two wells (SIMA1 and SIMA2) as illustrated in Fig. 6.13 (Liu and He, 2007).

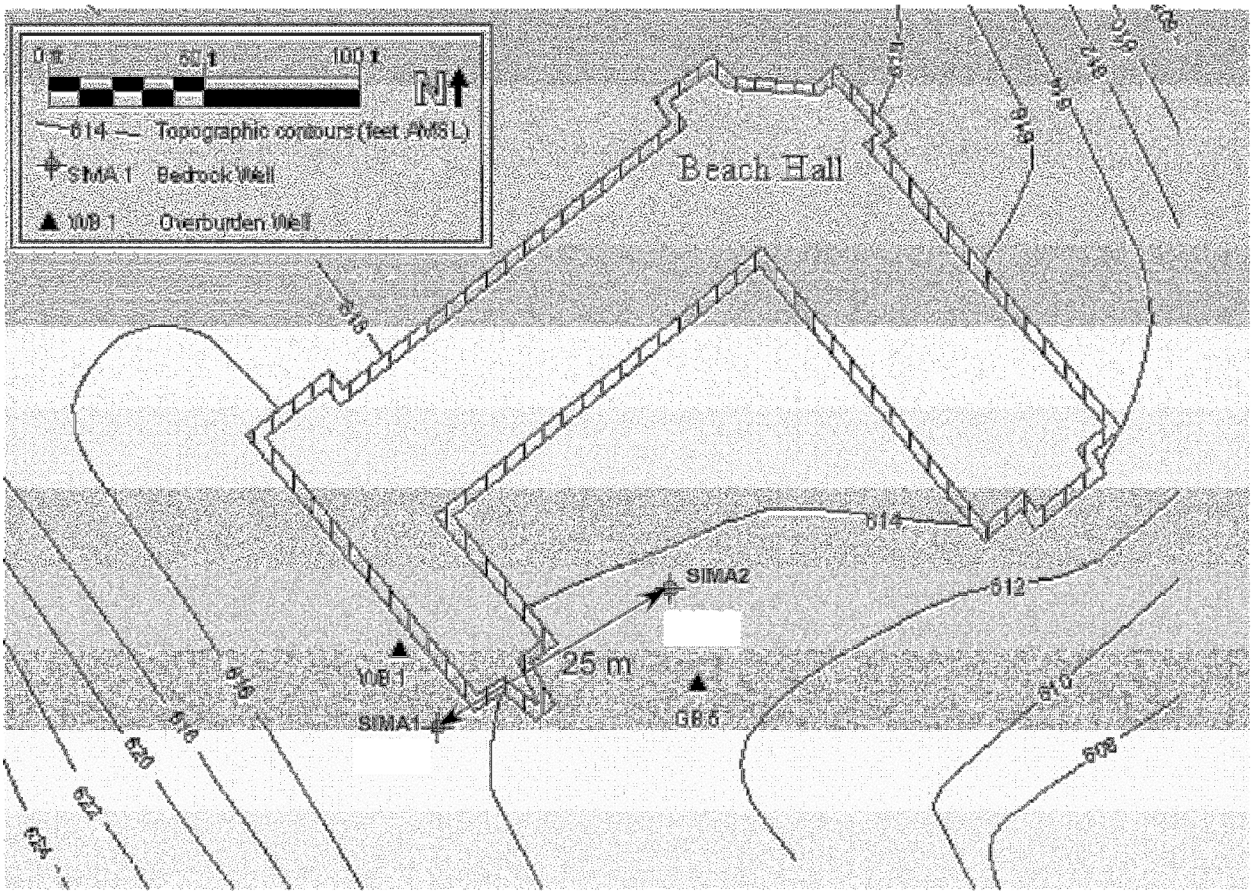

Figure 6.13 Sketch of the bedrock well field on the Storrs campus of Univ. of Connecticut to show the relative positions of two wells (SIMA1 and SIMA2) in which bore hold radar data were collected.

Both wells penetrating 90 into crystalline igneous bedrock, mostly gneiss and schist, on the Storrs campus of University of Connecticut. The distance between the two holes is 25 m. Constant-

offset reflection surveys are conducted in both SIMA1 and SIMA2. The cross-hole transmission survey was conducted with the transmitting antenna in SIMA2, and the antenna in SIMA1 served as the receivers. Fig. 6.14 illustrates the comparison of the mono-static data of SIMA1 and stacked migration image after WIVS approach with virtual sources in SIMA1.

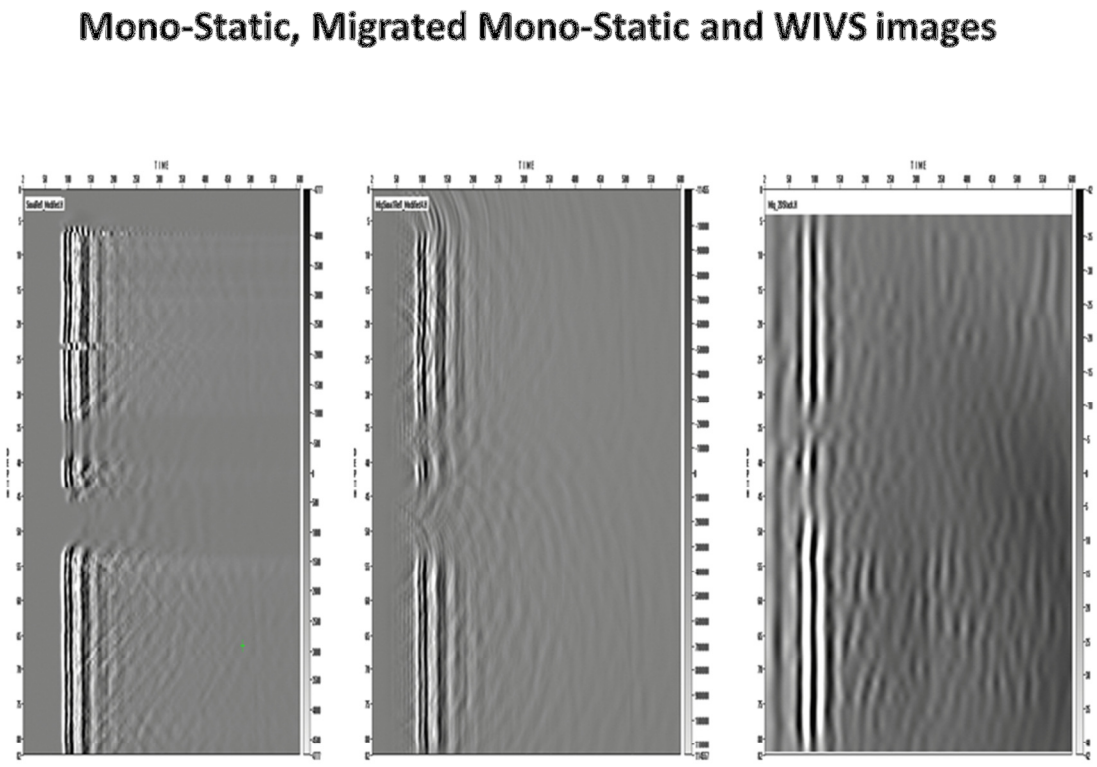

Figure 6.14 Comparisons of fracture images using mono-static, migrated mono-static and stacked migration image of WIVS approach. Left: mono-static data; center: migrated mono-static data; right: stacked migration image of WIVS approach.

The migrated mono-static and stacked migration WIVS images of Fig. 6.14 were obtained using a constant velocity assumption. The dielectric constant used is 7.27, which means the velocity of the EM wave is 1.12e8 m/s. The measured mono-static profile is contaminated by the scattering hyperbolas caused by the tips of opening and fractures. Both migrated images show better vertical profiles to indicate that the site at the depth of radar survey may be dominated by the vertical and

horizontal fractures and cracks. The stacked migration image using WIVS approach, which is the right part of Fig. 6.14, shows a much better profile in vertical fracture profile. It is a good evidence of the existence of the vertical fractures, which are hardly to be observed from the mono-static field data.

6.6 Conclusions

Interferometry and WIVS techniques are valid and efficient in transforming the wave forms obtained using a transmission model into a virtual reflection wave field. After this transmission, it is possible and practical to apply the common reflection imaging techniques to image and characterize the geological image. A 3D model of fractures is tested in this chapter. The Kirchhoff PSTM and stack techniques provided satisfactory subsurface imaging. In addition, as transverse wave, the different polarization combinations can be applied to different source and receiver lines. Fig. 6.4 – 6.12 proved that the different combinations have different sensitivities in characterizing the geological fracture in different directions. The fracture detection and characterization are of more and more importance because the fracture is often related to the shale gas reservoirs, and main source of the micro-seismic activities. The interferometry and WIVS techniques can make great contribution not only in geological fracture detection and characterization, but also in shale gas detection, micro-seismic research and other environmental problems such as ground water resource and contamination.

Ground penetrating radar (GPR) and borehole radar have the advantages in fracture detection and characterization in that, the EM waves are vectorial. Features with strong directionality can change the polarization state of the incident field. GPR and borehole radar can improve the fracture detection and characterization in focusing on the changes in waveforms and polarizations (Sassen and Everett, 2009; Zhao and Sato, 2006). The fully polarimetric borehole radar has the

potential to provide the polarimetric and vectorial analysis which is superior to the current radar resolution capabilities (Zhao and Sato, 2006). A case study from the real field data is provided in this chapter. Although the migration in this chapter is based on constant velocity assumption, the fracture images are already improved drastically. Provided we can have some more reasonable initial velocity structure of fractures, the WIVS approach is expected to offer better fracture subsurface imaging results. We believe that the interferometry and WIVS techniques will be a new robust weapon in fracture subsurface imaging with the advantages in both polarimetric analysis and modern reflection imaging methods.

Chapter 7 Conclusions and Future Applications

7.1 Summary

The numerical forward modeling of the EM wave propagation is always a significant part of physical and geophysical studies. Especially the simulation of a reflection model has its unique importance. In many real physical problems, from both academic research interests and industrial concentrations, the inner structure understanding of certain physical objects is the ultimate purpose. Most real inner structure imaging problems, often related to other techniques like migration and tomography, are based on reflection model. Consequently the study of the numerical forward modeling of a reflection model is of both academic research interests and industrial values.

In general, all numerical simulation methods depend on computation ability as a reality. The computation ability can be promoted with the improvement in hardware, for example, more clusters, robust CPUs and large memories. However the competition of the simulation and the computation facility has no end – Can we try to simulate a real physical problem in larger scale, higher frequency and finer grids base on the current facility? The improvement of the computational efficiencies in both computation time and memory cost are always highly desirable in computational method development. In order to simulate the EM wave propagation provided we have a large scale of uniform media and relatively sparse scatters, the MR method was proposed by Johnson (1997). Two new concepts and methods are introduced in this dissertation to extend the MR method into some real reflection model simulation. Chapter 3 introduced the directional Kirchhoff integration (DKI) method so that the MR method becomes able to simulate

the full wave field. Chapter 4 introduced the model subtraction (MS) method to remove the DKI/TS artifacts. After removing the DKI/TS artifacts, DKI/MR method is able to simulate the reflection model in very long distance. All advantages in computational efficiencies of the MR method remain unchanged, and theoretically there is no distance limitation. The Kirchhoff pre-stack time migration (PSTM) results in Chapter 4 proved that the MS method combined with DKI/MR/PSTD is suitable for inner structure imaging.

As another important topic in reflection model simulation and inner structure imaging, in Chapter 5 the interferometry technique and wave interferometric virtual source (WIVS) approach are applied in this dissertation trying to image the very fractures. Interferometry and the WIVS techniques are especially useful for borehole radar because it is difficult to have the true reflection wave field of the targeted area for borehole radar. Interferometry and WIVS approach transfers the transmission model, which can be realized by several borehole radars, into virtual reflection wave field. After the transmission, the virtual reflection field becomes ready to be imaged using the conventional imaging techniques such as migration and tomography. Based on the virtual reflection trace gather obtained in Chapter 5, Chapter 6 shows the subsurface fracture image using Kirchhoff PSTD method and stack. Obviously the virtual reflection wave field is able to provide a satisfactory fracture imaging. In addition, As a transverse wave, the different polarization combinations of the EM wave in source and receiver are able to show different aspects of geological structure. It suggests that the interferometry and WIVS approach can be expected in fracture detection and characterization under complex environments.

7.2 Suggestions for Future Application

7.2.1 Airborne radar remote sensing

Many active remote sensing problems involve in emitting EM waves from radar and detecting/measuring the radiation reflected back from the topography or subsurface structures. They can be classified to the typical long distance reflection problems. The application of DKI/MR/PSTD method with model subtraction (MS) method is expected to be effective and efficient in remote sensing research. As there is no distance limitation in DKI/MR/PSTD and MS methods, the airborne radar can be set at any flight height without limitations. In addition, the subsurface structure can also be imaged based on the DKI/MR/PSTD and MS methods, and the utilization of other modern imaging techniques such as migration and tomography.

7.2.2 Astronomical EM wave propagation research

As a valid and efficient method in EM full wave field simulation, the DKI/MR/PSTD with model subtraction method is especially suitable for long distance and high frequency EM wave propagation research. Theoretically the distance is not related to the computation and memory cost using DKI/MR/PSTD method. It means practically there is no upper limit in the distance of a real physical problem. The distance could be as remote as astronomical. It makes the DKI/MR/PSTD with model subtraction method an ideal and robust weapon in astronomical radiation research. For example, the DKI/MR/PSTD method could be applied to the research of the solar radiation from the Sun to the Moon or to the Earth Ionosphere, which is the key point of our common communication system and the public health. DKI/MR/PSTD and MS methods can also be applied into other astronomical researches due to its computational efficiencies. We expect that the full astronomical radiation simulation results using DKI/MR/PSTD with MS method be a vital progress of the universe evolution research.

7.2.3 Thin geological fracture detection and characterization

Based on the synthetic analysis in Chapter 5 and 6, interferometry and WIVS techniques are the new aspects to process and visualize data. It facilitates the fracture borehole radar geological structure detection and characterization. It is complementary to the raw cross-hole transmission data and able to show formation features after transforming the data into the virtual reflection data. From the examples presented we may conclude that interferometry and WIVS techniques are good for the common reflection imaging techniques such as migration and tomography. Interferometry and WIVS techniques have advantages in characterizing thin features such fractures or thin beds. The interferometry and WIVS techniques are expected to be helpful in imaging the subsurface structure using borehole radar field data.

Bibliography

Aki, K. and Richard, P.G., 2002, Quantitative Seismology, 2nd edition, University Science Books.

Albert, D.C., 2001, Observations of acoustic surface waves in outdoor sound propagation, J. Acoust. Soc. Am. 113, pp. 2495-2499.

Balanis, C.A., 1989, Advanced Engineering Electromagnetics, Wiley.

Berenger, J.P., 1994, A perfectly matched layer for the absorption of electromagnetic waves, Journal of Computational Physics, Vol. 114, pp. 185-200.

Bernardi, P., M. Cavagnaro, P. DAtanasio, E. Di Palma, S. Pisa and E. Piuzzi, "FDTD, multiple-region/FDTD, raytracing/FDTD," Int. J.Numer. Model. Vol. 15, pp. 579-593, 2002.

Cai, J. and Mcmechan, G.A., 1995, Ray-based synthesis of bistatic groundpenetrating radar profiles, Geophysics, Vol. 60, NO.1, pp. 1727-1734.

Cerjan, C., Kosloff, D., Kosloff, R., and Reshef, M., 1985, A nonreflecting boundary condition for discrete acoustic and elastic wave equations, Geophysics, Vol. 50, No.4, pp. 705-708.

Cerveny, V., Molotkov, I.A., and Psencik, I., 1977, Ray Method In Seismology, Univerzita Karlova, Praha.

Chew W.C., and Weedon, W.H., 1994, A 3D Perfectly Matched Medium From Modified Stretched Coordinates, Microwave and Optical Technology Letters, Vol. 7, pp. 599-604.

Coleman, C. J., A Kirchhoff Integral Approach to Estimating Propagation in an Envrionment With Nonhomogenous Atmosphere and Complex Boundaries, IEEE Trans. On Antennas and Propagation, vol. 53, pp. 3174C3179, 2005.

Cormier, V.F., 1985, Some problems with S, SKS, and ScS observations for the structure of the base of the mantle and outer core, J. Geophys., 57, pp. 14-22.

Cormier, V.F., 2000, Pseudospectral Modeling of the Seismic Wavefield for Constraints On Mantle and Inner Core Heterogeneity, SEISMOLOGICAL SOCIETY OF AMERICA MEETINGS : 2000 PROGRAM .

Cormier, V.F., and Richards, P.G., 1997, Full wave theory applied to a discontinuous velocity increase: the inner core boundary, J. Geophys., 43, pp. 3-31.

Day-Lewis, F.D. , P.A. Hsieh, and S.M. Gorelick, Identifying fracture-zone geometry using simulated annealing and hydraulic-connection data, Water Resources Research, vol. 36, no. 7, pp.1707-1722, 2000.

Drossaert, F. H.,and A. Giannopoulos, A nonsplit complex frequeny-shifted PML based on recursive integration for FDTD modeling of elastic waves, Geophysics vol. 72, pp. T9-T17, 2007.

Eisenbei, W. J. Marotz and J.Shrade, Reflection-optical multispectral imaging method for objective determination of burn depth, Burns vol 25, pp. 697-704, 1999

Engquist, B., and Majda, A., 1977, Absorbing Boundary Conditions for the Numerical Simulation of Waves, Math. Comput., Vol. 31, pp. 629-651.

Festa, G. and Nielsen, S., 2003, PML Absorbing Boundaries, Bull. Seism. Soc. Am., Vol. 93, NO. 2.

Fukao, Y., Akiko To, Masayuki Obayashi, Whole mantle P wave tomography using P and PP-P data, J. Geophys. Res., 108, 14- 2003.

Gazdag, J., Modeling of the acoustic wave equation with transform methods, 1981, Geophysics, Vol. 46, No. 6, pp. 854-859.

Grgoire, C., and Halleux, L., 2002, Characterization of fractures by GPR in a mining environment, First Break, 20, 467-471.

Hecht, E. and Zajac, A., 1973, Optics, Addison-Wesley Publishing.

Higdon, R.L., 1987, Numerical Absorbing Boundary Conditions for the Wave

Johnson, J. M. and R. S. Yahya, MR/FDTD: A multiple-region finite-difference-time-domain method, Microwave and Optical Technology Letters, vol. 14, pp. 101C105, 1997.

Katz, I., Parks, D., Wilson, A., Rotenberg, M., and Harren, J., 1976, Non-Reflective Free Space Boundary Conditions for SGEMP Codes, Syst. Sci. Software, Vol. SSSR-76-2934.

Kosloff, D.D. and Baysal, E., 1982, Forward modeling by a Fourier method, Geophysics, Vol. 47, No. 10, pp. 1402-1412.

Kraus, J., and Fleisch, D.A., 1999, Electromagnetics with Applications, McGraw-Hill.

Kreiss, H.O., and Oliger, J., 1972, Comparison of accurate methods for the integration of hyperbolic equations: Tellus, Vol. 24, pp. 199-215.

Laisne, A., R.Gillard, J. Citerne and G. Piton, A discrete wavelet transform (DWT)-based compression technique for the computation of Kirchhoff integals in MR/FDTD, Microwave and optical technology letters, vol. 27, pp. 312-316, 2000.

Lane, J.W., Jr., Buursink, M.L., Haeni, F.P., and Versteeg, R.J., 2000, Evaluation of Ground-Penetrating Radar to Detect Free-Phase Hydrocarbons in Fractured RocksResults of Numerical Modeling and Physical Experiments, Ground Water, 36(6), 929-938.

Lane, J.W. Jr., Joesten, Peter K., and Savoie, and Jennifer G., 2001, Cross-HoleRadar Scanning of Two Vertical, Permeable, Reactive-Iron Walls at the Massachusetts Military Reservation, Cape Cod, Massachusetts, US Geological Survey Water-Resources Investigations Report 00-4145, 2001.

Lathi, B.P., 1998, Signal Processing & Linear System, Oxford press.

Liao, Z.P., Wong, H.L., Yang, B.P., and Yuan, Y.F., 1984, A Transmitting Boundary for Transient Wave Analysis, Sci. Sin. Ser. A, Vol. 27, NO. 10, pp. 1063-1076.

Liu, L. and Albert, D.G., 2006, Acoustic pulse propagation near a right-angle wall, J. Acoust. Soc. Am. 119, pp. 2073-2083.

Liu, L. and Guo, T., 2003, Determining the Condition of Hot Mix Asphalt Specimens in Dry, Water-Saturated, and Frozen Conditions Using GPR, JEEG, Vol. 8, Issue 2, pp.46-52.

Liu, L., and K. He, Wave interferometry applied to borehole radar: virtual multi-offset reflection profiling, IEEE Transactions on Geoscience and Remote Sensing, Vol. 45, No. 8, 2554-2559, August 2007.

Liu, L. and Li, Y., 2001, Identification of liquefaction and deformation features using ground-penetrating radar in the New Madrid seismic zone, USA, Journal of Applied Geophysics, Vol. 47, pp. 199-215.

Liu, L., Day-Lewis, F.D., and Lane, J.W., Jr., 2004, Fracture characterization using borehole radar: computer simulation and field calibration, in 2004 U.S. EPA/NGWA Fractured Rock Conference: State of the Science and Measuring Success in Remediation, September 13-15, 2004, Portland, Maine. Proceedings: National Ground Water Association, CD-ROM, pp. 523.

Liu, L., Fracture characterization using borehole radar: Numerical modeling, Water, Air, and Soil Pollution, vol. 6, pp. 17-34, 2006.

Liu, L., J.W. Lane, Jr., and Y. Quan, Radar attenuation tomography using the centroid frequency downshift method, J. Applied Geophys. vol. 40, pp. 105-116, 1998.

Liu, Q. H., 1997, "The PSTD algorithm: a time-domain method requiring only two cells per wavelength," Microwave Opt. Tech. Lett., Vol. 15, NO. 3, pp. 158-165.

Margrave, G. F., Numerical Methods of Exploration Seismology with algorithms in Matlab, 2003

Maxwell, J.C., 1873, A Treatise on Electricity and Magnetism, Clarendon Press,Oxford, UK.

Olsson, O., Falk, L., Forslund, O., Lundmark, L., and Sandberg, E., 1992, Borehole radar applied to the characterization of hydraulically conductive fracture zones in crystalline rock, Geophysical Prospecting, 40(2), 109-142.

Orzag, S.A., 1980, Spectral methods for problems in complex geometries, J. Comp. Physics, Vol. 37, pp. 70-92.

Paillet, F. L., 1998, Flow modeling and permeability estimation using borehole flow logs in heterogeneous fractured formations, Water Resources Research, 34(5), 997-1010.

Paillet, F. L., 2000, A field technique for estimating aquifer parameters using flow log data: Ground Water, 38(4), 510-521.

Papadopoulous, A.I. and Don, C.G., 1991, A study of barrier attenuation by using acoustic impulses, J. Acoustic. Soc. Am. 90, 1011-1018.

Porat, B., 1997, Course in Digital Signal Processing, Wiley.

Press, W.H., Flannery, B.P., Teukolsky, S.A., and Vetterling, W.T., 1992, Numerical Recipes in C: The Art of Scientific Computing, Cambridge University Press.

Ramahi, O. M., Near-and Far-Field Calculations in FDTD Simulations Using Kirchhoff Surface Integral Representation, IEEE Trans. on Antennas and Propagation, Vol. AP-45, pp. 753-759, 1997.

Reynolds, A.C., 1978, Boundary conditions for the numerical solution of wave propagation problems, Geophysics, Vol. 43, NO. 6, pp. 1099-1110.

Sassen, D. S. and M. E. Everett, 3D polarimetric GPR coherency attributes and full-waveform inversion of transmission data for characterizing fractured rock, Geophysics, Vol. 74, No. 3, pp. 323-334.

Shapiro, J. H., B. Capron and R. Harney, "Imaging and target detection with a heterodyne reception optical radar", Applied Optics vol. 20, pp. 3292-3313, 1981

Sheriff, R.E. and Geldart, L.P., 1995, Exploration Seismology, 2nd Edition, Cambridge University Press.

Taflove, A., 1995, Computational Electromagnetics-The Finite Difference Time- Domain Method. Norwood, MA: Artech House.

Tang, Z. and Liu, Q.H., 2003, The 2.5D FDTD and Fourier PSTD Methods and Applications, Micro. Optic. Tech. Let., Vol. 36, NO. 6.

Williams, J.H., and C.D. Johnson, 2003, Acoustic and optical borehole-wall imaging for fractured-rock aquifer studies, J. Applied Geophysics, 55, 151-159.

Witte, D. C., The pseudospectral method for simulating wave propagation, Ph.D. dissertation, Columbia University, 1989.

Xiao, L., Liu, L., and Cormier, V.F., 1998, 2-D FDTD Solution for Maxwells Equations using PSTD method, Proceedings of the 7th International Conference on GPR, May 27-30, 1998.

Yee, K.S., 1966, Numerical Solution of Initial Boundary Value Problems Involving Maxwells Equations in Isotropic Media, IEEE Trans. Antennas Propagat., Vol. 14, pp. 302-307.

Zeng, X., McMechan, G.A., Cai, J., and Chen, H., 1995, Comparison of ray and Fourier methods for modeling monostatic ground-penetrating radar profiles, Geophysics, Vol. 60, NO. 6, 1727-1734.

Zeng, Y.Q. and Q. Liu, A multidomain PSTD method for 3D elastic wave equations, Bull. Seism. Soc. Am., vol. 94, pp. 1002-1015, 2004.

J. Zhao and M. Sato, Radar polarimetry analysis applied to single-hole fully polarimetric borehole radar, IEEE Transactions on Geoscience and Remote Sensing, vol. 44, no. 12, 3547-3554, 2006.

Zhou, C., L. Liu, and J. W. Lane, Nonlinear inversion of borehole-radar tomography data to reconstruct velocity and attenuation distribution in earth materials, Journal of Applied Geophysics, Vol. 47, pp. 271-284, 2001.

Author's Bibliography

Papers in Peer-reviewed Journals:

[4] Zhao, Z., and L. Liu, Wave Interferometry and Kirchhoff Migration: Virtual Multi-offset Reflection and Imaging, ready for submission to *IEEE Transactions on Geoscience and Remote Sensing*,

[3] Zhao, Z., L. Liu, and B. Barrowes, Reflected radar wave field simulation and imaging using a model subtraction method with hybrid numerical simulation, ready for submission to *Microwave and Optical Technology Letters*,

[2] Zhao, Z., Z. Zhao, J. Xu and R. Kubota, Synthetic seismograms of ground motion near earthquake fault using simulated Green's function method, *Chinese Science Bulletin 2006, Vol 51 No. 24* 3018-3025,

[1] Zhao, Z., Z. Zhao, J. Xu, R. Kubota, and L. Liu, Strong ground motion simulation for seismic hazard assessment in urban area, *Journal of Geophysics and Engineering*, Vol. 4, No. 3, pp. 308-316, 2007 (impact factor 0.86)

Papers in Conference Proceedings ([G]UConn graduate student):

[5] R. Qian, J. Li, L. Liu, and Z. Zhao[G], Internal structure of sand dunes in the Badain Jaran desert revealed by GPR and its implications to inter-dune lake hydrology, *Proceedings of the 15th International Conference on Ground Penetrating Radar*, Brussels, Belgium, June 30-July 4, 2014.

[4] Liu, L. Z. Zhao[G], and J. Zhao, Characterization of fractures using interferometry techniques with multi-hole, multi-polarization borehole radar, *Expanded Abstracts,* Society of Exploration Geophysicists Annual Meeting, September, 22-27, 2013.

[3] Fu, L., Z. Zhao[G], L. Liu, and S. Liu, Multi-Region Finite Difference Time Domain Simulation for Airborne Radar, *Expanded Abstracts,* Society of Exploration Geophysicists Annual Meeting, September, 22-27, 2013.

[2] Zhao[G], Z., L. Liu, and B. Barrowes, Radar wave simulation using three-dimensional multi-region pseudospectral time domain algorithm with directional Kirchhoff integration surface, *Proceedings of the 14th International Conference on Ground Penetrating Radar*, pp. 248-253, Shanghai, China, June 4-8, 2012.

[1] Liu, L., B. Barrowes, and Z. Zhao[G], Staggered-grid pseudospectral time domain (PSTD) method using real Fourier transform for 2.5D electromagnetic wave

propagation, *Proceedings of the Progress In Electromagnetics Research Symposium (PIERS 2008),* p. 1238-1244, Hangzhou, China, March 24-28, 2008. (ISSN: 1559-9450; ISBN: 978-1-934142-00-4)